2014-08-06

Development of "Turn-On" Fluorescent Nuclobase Mimics as Kiinase Inhibitors

Jyothi Dhuguru
University of Miami, jyothi.dhuguru@gmail.com

UNIVERSITY OF MIAMI

DEVELOPMENT OF "TURN-ON" FLUORESCENT NUCLEOBASE MIMICS AS KINASE INHIBITORS

By

Jyothi Dhuguru

A DISSERTATION

Submitted to the Faculty
of the University of Miami
in partial fulfillment of the requirements for
the degree of Doctor of Philosophy

Coral Gables, Florida

August 2014

UNIVERSITY OF MIAMI

A dissertation submitted in partial fulfillment of
the requirements for the degree of
Doctor of Philosophy

DEVELOPMENT OF "TURN-ON" FLUORESCENT NUCLEOBASE MIMICS AS KINASE INHIBITORS

Jyothi Dhuguru

Approved:

_____ James N. Wilson, Ph.D. Professor of Chemistry	_____ Angel E. Kaifer, Ph.D. Professor of Chemistry
_____ Rajeev Prabhakar, Ph.D. Professor of Chemistry	_____ M. Brian Blake, Ph.D. Dean of the Graduate School

_____
Ralf Landgraf, Ph.D.
Professor of Biochemistry and Molecular Biology

DHUGURU, JYOTHI (Ph.D., Chemistry)
Development of "Turn-on" Nucleobase Mimics as Kinase Inhibitors. (August 2014)

Abstract of a dissertation at the University of Miami.

Dissertation supervised by Professor James N. Wilson.
No. of pages in text. (121)

Fluorescent probes are indispensable tools for biologists owing to the safe and non-invasive method of detection they offer with minimum perturbation of the cell under investigation. Despite all the advatanges they offer, there are certain limitations for the use of fluorescent probes for live cell imaging such as phototoxicity to the cell, photobleaching or photoinstability, etc. Additionally, they require labeling with specific recognition units such as biomolecules like DNA, RNA or an antibody to render them specific to the target cell. In this context, "turn-on" fluorescent probes are advantageous, as they remain silent or inactive and become emissive only under special circumstances or in the event of a biochemical process/reaction. This can overcome the challenges arising from the use of fluorescent probes and more importantly, these probes do not require the additional rinsing steps which prevent the access to the target cell dynamics. Dysregulation of ERBB is encountered in several malignancies including head, neck, breast and ovarian cancers, thereby making it an extensive area of research. In this context, development of novel strategies to study the receptor activation will be very beneficial for designing effective small molecule inhibitors. In this project, we have designed and developed novel fluorescent "turn-on" probes targeting the ATP binding pocket of ERBB receptor which can provide deeper insights into the receptor activation,

receptor conformation at the time of ligand binding, subsequent signaling pathways activated upon ligand binding, etc. DMAQ (6-(4-dimethyl-aminostyryl)-*N*-benzylquinazolin-4-amine) was the first "turn-on" fluorescent probe designed in this direction which was followed by a series of 15 kinase inhibitors with binding affinities comparable to gefitinib, a well-known anti-cancer drug. Further, we also evaluated the effects of extension of conjugation and the presence of electron donating/withdrawing groups at the 6-position of quinazoline core on the optical properties of the probes. We confirmed from our studies that substitution at the 6-position of quinazoline core does not perturb the binding affinity of the probe to the receptor. Overall, our probes can serve as a good platform for designing effective small molecule inhibitors with variable substitution at the 6-position to improve the hydrophilicity and prevent issues arising from aggregation inside the cells besides illuminating the receptor activation and cellular dynamics.

To My Family

Acknowledgements

Firstly, I would like to thank my advisor Dr. Wilson for his guidance, continuous support, patience and sharing his knowledge throughout this journey. I am very grateful to him for sharing his valuable insights that greatly improved my thinking, writing and working skills and helped me grow as a scientist. I would also like to offer my greatest appreciation to Dr. Kaifer and Dr. Prabhakar for their invaluable suggestions, support and assistance during my study.

I take this opportunity to thank our collaborator Dr. Landgraf and his lab members Dr. Renauld and Wenjun for their assistance in our projects and helping me with my research.

I also would like to thank all the faculty and staff members of the department of chemistry for their continuous support especially Dr. Eve who helped me in my teaching assignments and I am thankful to Dr. Hudson for the NMR support and Edward Torres for the Mass spectrometry. I would like to express my gratitude to everyone who helped me in this journey. I also wish to thank Dr. Saleesh for his valuable suggestions and support in the past years.

I am very grateful to the University of Miami and the Department of Chemistry for providing financial support during my study and Richter Library for providing me all the resources needed for my research.

Finally, I would like to thank my parents for their encouragement and support throughout my graduate education.

TABLE OF CONTENTS

LIST OF FIGURES

CHAPTER 1

CHAPTER 2

CHAPTER 3

CHAPTER 4

CHAPTER 5

CHAPTER 6

LIST OF SCHEMES

CHAPTER 2

CHAPTER 3

CHAPTER 4

CHAPTER 5

CHAPTER 6

LIST OF TABLES

CHAPTER 2

CHAPTER 4

CHAPTER 5

Chapter 1

"Turn-on" Fluorescent Probes and ERBB Receptor

1.1. ***Background***:

Fluorescent probes are defined as molecules that interact with biological molecules to induce a simultaneous change in their photochemical and or photophysical properties such as fluorescence intensity, molar absorptivity, quantum yield, emission and excitation wavelength and so forth. In the recent years, there has been an enormous increase in the number of fluorescent probes owing to their promising applications in the chemical, biological and biomedical areas.[1,2,3,4] They are very advantageous over other methods such as MRI, radioisotopic labeling, electrochemical techniques, etc., in providing safe, and non-toxic detection with high sensitivity and great resolution with minimal damage to the cell under investigation. Recent advances in fluorescent probes can be seen in their applications for the study of complex cellular events such as enzyme activation, protein-protein interactions, expression of biomolecules and their localization in live cells.[4,5] Despite all the above advantages, they have certain limitations such as phototoxicity resulting from the continuous excitation of the probe, photobleaching or photoinstability, lack of permeability and target specificity. Moreover, some assays demand additional rinsing steps to remove the unbound probe along with cell fixation which may alter the fluorescence intensity of probes and the lack of target specificity requires tethering of recognition units such as antibody, oligonucleotides to impart specificity to the probe.

1.2. *Turn-on fluorescent probes*:

In this context, turn-on fluorescent probes also called as "activatable probes" offer many benefits and they can overcome most of the challenges of the fluorophores noted above. Turn-on fluorescent probes are fluorescent probes that remain inactive and turn on only in certain special environments or as a result of specific events. The ability of probes to turn-on only under certain special circumstances prevents the problems arising from continuous excitation such as photobleaching, phototoxicity and the production of free radicals which is another serious problem encountered with continuous excitation. As the probe is inherently fluorescent, it eliminates the additional steps of rinsing of the unbound probe facilitating the imaging or detection of intracellular dynamics with greater accuracy.[6] A turn-on emission helps in monitoring the minute changes in the cellular environment without damaging the cell under investigation.

1.3. *Classification of turn-on fluorophores:*

Turn-on (activatable) fluorophores can be broadly classified into three groups based on their mechanism of activation such as 1) High molecular weight probes that are self-quenching but activated upon the disaggregation into smaller components 2) Small molecule turn-on probes linked to large molecule probes and 3) Small organic fluorescent probes with intrinsic activation mechanism.[6,7,8] These probes produce significant changes in the photochemical properties such as fluorescence intensity, emission/excitation wavelength either by binding to the target or undergo specific changes in their structure/conformation in special cellular environments.

1.3.1. *High molecular weight turn-on probes:*

These probes are designed in such a way that they remain silent or inactive until activated by an enzymatic cleavage secreted by the cellular or extracellular membranes leading to the generating a fluorescent signal.[9] In this strategy, one single enzyme has the potential to activate several probes simultaneously thereby enhancing the resolution with high target to background ratio (Figure 1.1). These probes have been used in cancer patients to locate/image tumors and other malignancies.

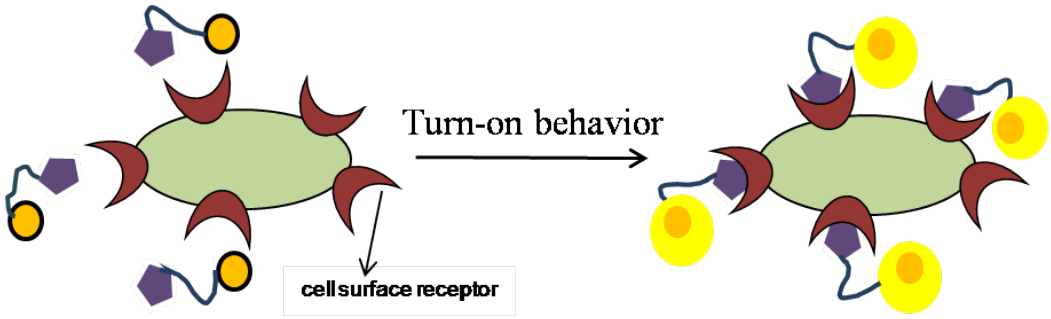

***Figure 1.1.*Turn-on fluorescence on binding of the probe to the cell-surface receptor**

For instance, the near infrared activatable probes (NIRF) developed by Tung and coworkers for cathepsins D, B, E were successfully applied for the detection of *in vivo* tumors.[10,11] In another instance, quencher-fluorophore activatable probes were developed by Piwnica-Worms and coworkers for the detection of apoptosis where Alexafluor647 and QSY 21were conjugated linked via a caspase recognition sequence were cleaved by the action of caspases thereby restoring the fluorescence of the dye.

1.3.2. *Small molecule turn-on probes linked to large molecule probes :*

This is another approach used to design the turn-on probes with high target specificity as the activation mechanism involves the binding of the probe to the target cell followed by

internalization and fluorescence emission from the probe following a specific biochemical reaction. Although this method is highly specific as the emission is turned on only in the target cells, yet signal amplification is not enhanced considerably relative to the previous enzymatic method. For instance short homodimers (H-dimer) of rhodamine derivatives functionalized with transtuzumab bind to ERBB2 receptor were turned on upon the dissociation of the dimers to monomers in cells thereby helping in the detection of tumors overexpressing ERBB (Figure 1.2).[12] These H-dimers are practically inactive outside the cell and are turned on upon internalization and the conformational change of the bound protein thereby detection of the overexpressed receptor.

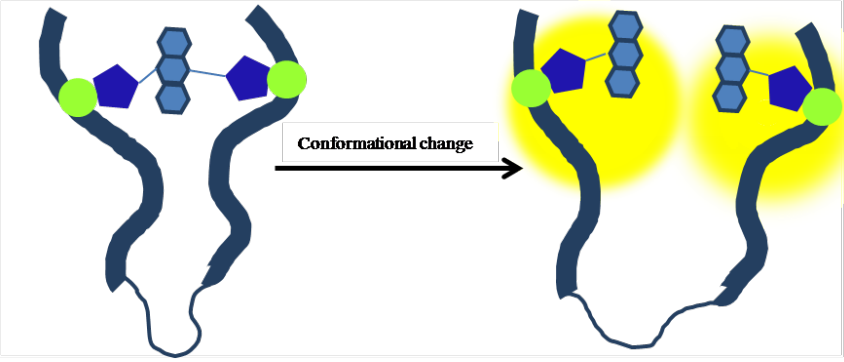

***Figure 1.2*. Activation mechanism involving H-dimer formation after binding to the protein**

1.3.3. ***Small organic fluorescent probes:***

Small molecule fluorescent probes are commonly designed based on the two photochemical mechanisms such as Photoinduced charge transfer (PeT) and intramolecular charge transfer (ICT) and they have been successfully applied for the investigation of cellular events. Several small molecule probes have been developed for the detection of pH, H_2O_2,[13] reactive oxygen,[14] and NO (nitric oxide)[15] species and so on.

1.4. *Photochemical mechanisms underlying turn-on emission:*

Several strategies have been used to design fluorescent probes. The most commonly used mechanisms involve Forster resonance energy transfer (FRET), Photoinduced electron transfer (PeT), Intramolecular spirocyclization and intramolecular charge transfer (ICT).

1.4.1. *Forster resonance energy transfer (FRET):*

Forster resonance energy transfer (FRET) involves a non-radiative energy transfer from the donor to the quencher thereby quenching the emission from the donor (Figure 1.3). FRET is a highly distance dependent phenomena and the emission intensity of the donor decreases with increasing distance between the donor and the acceptor.[16] Therefore it has wide spread applications in cellular studies for reporting specific events such as nucleic-acid-protein interactions and protein-protein interactions. There are well-demonstrated fluorophores that are designed on this strategy such as genetically encoded probe such as GFP protein, BODIPY and cyanine dyes such as Cy3, Cy5, etc.

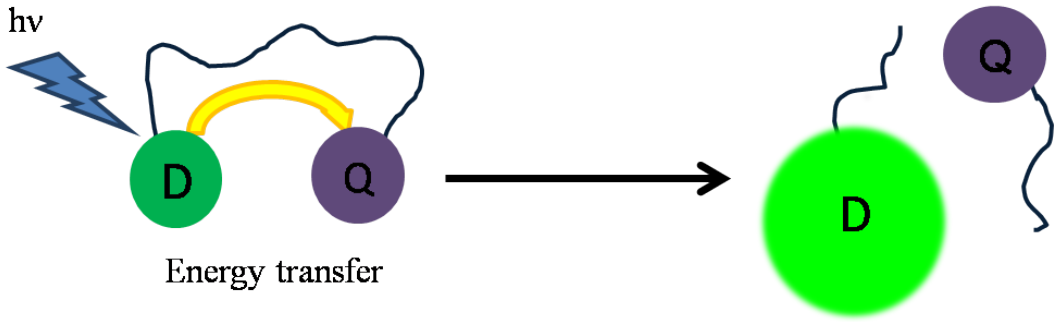

***Figure 1.3*. Turn-on fluorescence based on FRET**

1.4.2. *Photoinduced electron transfer (PeT):*

This is another common method of fluorescence quenching based on the transfer of electron from the PeT donor to the excited fluorophores (Figure 1.4). Nevertheless, upon

substrate or target binding of the donor, the emission of the fluorophore is turned on. A typical PeT system is comprised of a fluorophore, a PeT donor and a spacer linking the donor and the fluorophore. This is a powerful tool for biomedical imaging when compared to other detection techniques such as computer tomography (CT), MRI and X-ray radiography as the fluorescence is turned on only upon receptor binding and the PeT probes provide high spatial resolution in contrast to other imaging techniques.[17,18]

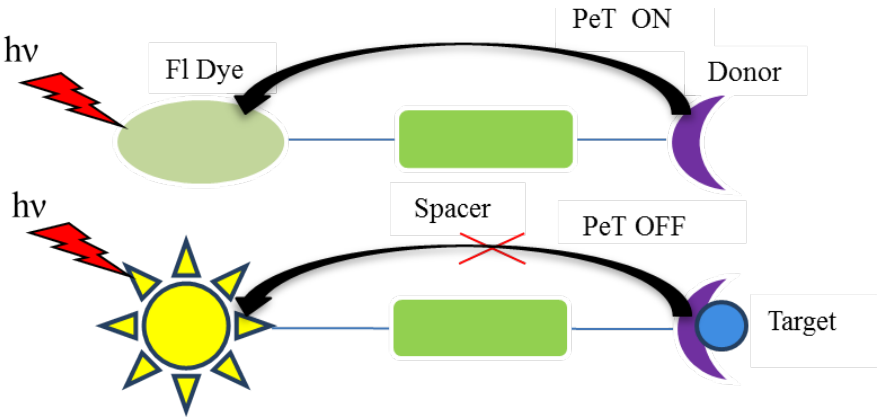

***Figure 1.4*. Turn-on fluorescence based on the electron transfer from the PeT donor to the excited fluorophore**

1.4.3. ***Intramolecular spirocyclization:***

Highly sensitive rhodamine based fluorescent probes have been designed based on this this strategy. They have potential applications in metal sensing, detection of pH, reactive oxygen species, etc. This reaction involves ring-opening of a spirocyclized derivative which is colorless and non-fluorescent but exhibits strong fluorescence on reaction with the analyte as demonstrated by the acetylated derivative of spirocyclization of hydroxymethyl rhodamine green (Ac-HMRG) in the Figure 1.5.[19,20] The disjoint conjugation of the spirocyclized derivatives makes it non-fluorescent while reaction with the analyte regenerates the fluorescence of the probe. This interchangeablity in the closed and open forms and the regulation of fluorescence has been utilized by researchers to

design highly environment sensitive probes(e.g., rhodamine-B thiohydrazide, rhodamine-B hydrazide.[21,22]

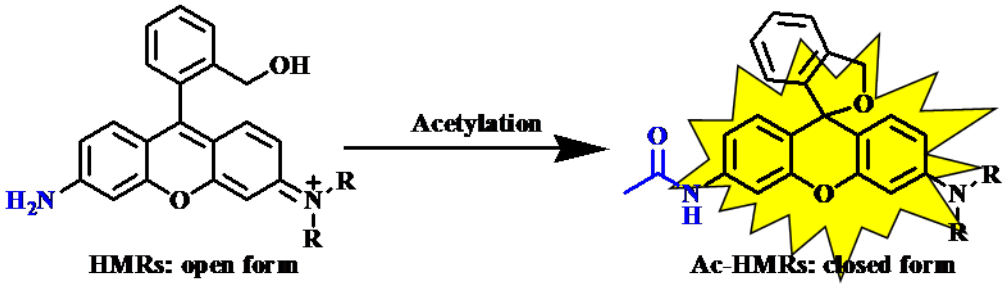

Figure 1.5. **Turn-on fluorescence on intramolecular spirocyclization**

1.4.4. ***Intramolecular charge transfer (ICT):***

This is a typical phenomenon observed in molecules with a strong electron donor and electron withdrawing groups where photoexcitation triggers the electron transfer from donor to the acceptor resulting in an intramolecular charge transfer state.[23] Dimethylaminobenzonitrile and DCS (*trans*-4-(*N,N*-dimethylamino)-4'-cyanostilbene) are the two examples of this category that have been extensively investigated in the past few years.[24] In the non-polar solvents, these D-A systems prefer a planar geometry (PICT) due to the dominating mesomeric interactions while in polar solvents, the twisted intramolecular charge transfer state (TICT) is favored due to the complete charge separation in the excited state.[25] The emission spectra of these D-A molecules typically show one emission peak in the non-polar solvents resulting from the normal excited state (LE: local excited) while in polar solvents a longer wavelength peak corresponding to emission from the TICT is observed.[26,27] Therefore the photophysical properties of the molecules undergoing ICT are very sensitive to the external environments especially the solvent viscosity and polarity. This dependability of the probes on the external

environments makes them fascinating probes with potential applications due to their sensitivity to the micro-environmental changes.

While the dual fluorescence of DMABN was discovered by Lippert et al, the concept of TICT was introduced by Grabowski et al. which explained the excited state behavior of many D-A systems and this novel area provided valuable insights on electron transfer.[28] Several small molecule fluorescent probes have been designed and developed using one or more strategies.

We utilized the concept of intramolecular charge transfer to design several "turn-on" fluorescent probes that that are highly sensitive to external environments such as pH, solvent polarity and viscosity. Our probes show turn-on behavior in non-polar solvents such as toluene, cyclohexane and octanol whereas the fluorescence is quenched upon switching the solvent to highly polar environments such as water or PBS (Figure 1.6).

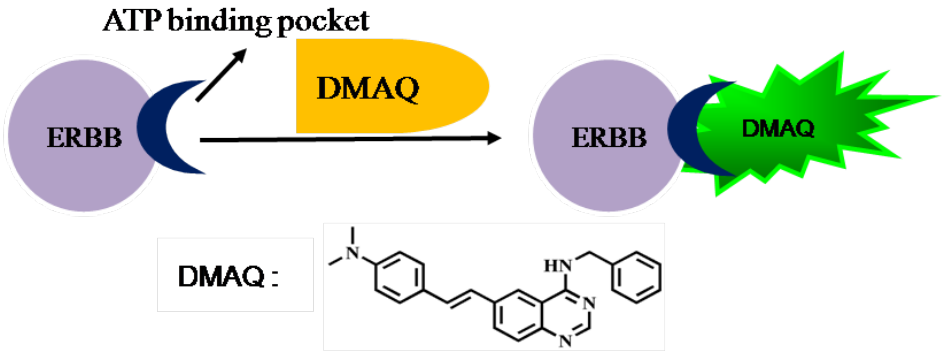

Figure 1.6. **Turn-on fluorescence of DMAQ on binding to the ERBB receptor**

Our research on "turn-on" fluorescent probes begun with arylpyrimidones with attractive photophysical properties. The optical properties of pyrimidones are not well investigated, although their pharmacological significance is well established. We developed a series of single arm and double arm aryl pyrimidone derivatives as highly proton sensitive "turn-

on" probes with excellent solvatochromism (Figure 1.7). Additionally, we also evaluated the effects of the electron donating groups on the optical properties of our derivatives by varying the strength of the electron donating groups on the compounds. These changes were clearly evident in the emission and absorption spectra of our derivatives, the details of which will be described in the second chapter.

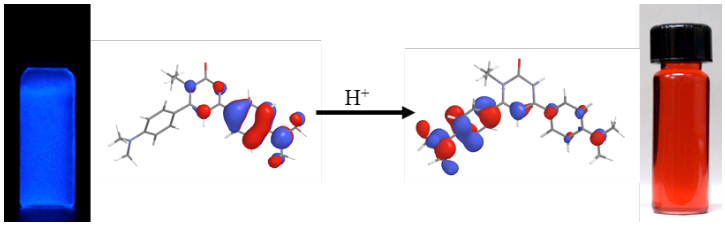

Figure 1.7. Proton-responsiveness of aryl pyrimidones

Our interest in the "turn-on/off" response probes prompted us to extend the research on aryl pyrimidones to other biologically relevant compounds.[29] So, in an attempt to investigate the population dynamics and the activation of ERBB receptor, we developed a series of "turn-on" fluorescent nucleobase mimics. The current assays or labeling technologies under use have some limitations such as the cell fixation, additional rinsing steps and moreover the phosphorylation assays do not give us required information on the receptor activation.

1.5. ***Development of fluorescent turn-on probes targeting ERBB***:

In this direction, DMAQ (4-dimethyl-aminostyryl)-*N*-benzylquinazolin-4-amine) was the first "turn-on" probe successfully designed and synthesized to study the receptor dynamics.[30] The probe showed excellent "turn-on" response when the solvent is changed

from polar to hydrophobic and viscous environment when it is docked in to the catalytic site of ERBB receptor (Figures 1.6 and 1.8).

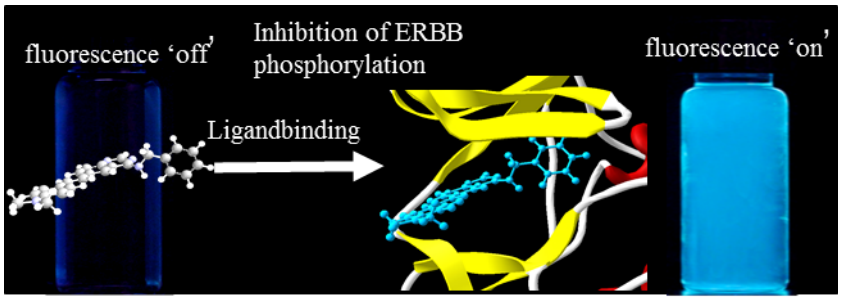

Figure 1.8. **Turn-on emission of DMAQ (shown in blue) on binding to the ERBB receptor**

This behavior is expected from a turn-on probe which is non-emissive in polar environments such as water and PBS but becomes fluorescent in less-polar and hydrophobic environments such as PEG and octanol. The optical properties of the probes in PEG, PBS and octanol coincided well with the behavior of the probe in the bound and unbound states to the ERBB receptor. We evaluated the binding affinity and selectivity of the probe against ERBB receptor by western blotting and the probe was found to bind to the ERBB receptor with high efficiency. DMAQ served as an excellent platform for designing more Type -1 and Type- 2 novel fluorescent quinazoline based probes. We synthesized a series of 15 "turn-on" kinase inhibitors in order to investigate the effect of chemical modification on the 6- position of the quinazoline ring (Figure 1.9). [31] We also evaluated the effects of the electron donating/withdrawing groups and the extension of conjugation on the optical properties of our compounds. The details of the synthesis, photophysical properties and inhibition studies will be reported in the coming chapters.

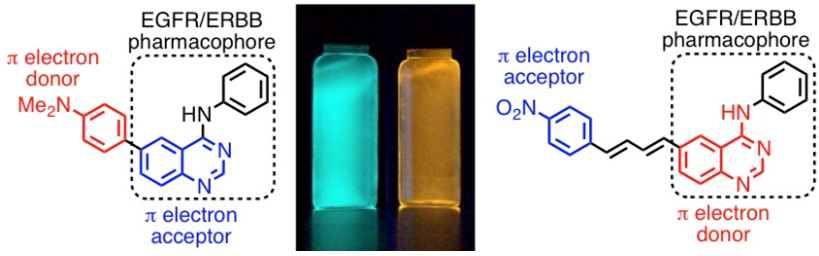

Figure 1.9. **Design of kinase inhibitors**

1.6. ***Tyrosine kinase receptor:***

Among the vast majority of therapeutic targets against cancer, kinases have gained tremendous attention in the recent years. Tyrosine kinases (TKs)[32,33] belong to the huge family of protein kinases involved in the catalytic phosphorylation of tyrosine residues in protein substrates using ATP (Adenosine triphosphate). They are sub-divided into two classes namely receptor tyrosine kinases and non-receptor kinases based on the structure and location of the kinases. While receptor tyrosine kinases are located inside the cell and help in the signal transduction from inside and outside the cell, the non-receptor tyrosine kinases are located in the cytoplasm and they lack the transmembrane domain and remain in the inactive state until activated by intracellular signaling or through trans-phosphosylation by other kinases. They are critical to many vital cellular processes such as cell division, cell differentiation, cell proliferation and so on. Although the TK (tyrosine kinase) activity is strictly regulated in a cell, yet dysregulation of TKs can occur by a combination of one or more of the following mechanisms such as chromosomal translocation that results in the receptor oligomerization in the absence of ligand binding and second reason can be a mutation, small deletion of genes and/or point mutations in the kinase domain and lastly increased TK activity resulting from the impaired TK

activity or lack of TK inhibitor proteins. All the above mentioned mechanism can lead to the aberrant TK activation which is implicated in a number of malignant tumors of head, neck, colon and breast cancers. [34,35]

1.6.1. ***Receptor tyrosine kinases:***

Out of the six hallmarks proposed by Hanahan and Weinberg,[36] receptor tyrosine kinases[37,37b] (RTKs) are involved in at least half of these traits and their signaling pathways. This unambiguously reveals the crucial role of RTKs in the development of cancer resulting from the activating mutations and dysregulation of RTKs and their ligands such as insulin growth factor (IGF), vascular endothelial growth factor (VEGF), fibroblast growth factor (FGF), etc. The analysis of human genome has identified nearly 60 RTKs belonging to ~16 different tyrosine families. They are characterized by the presence of a large extracellular ligand-binding domain, a single transmembrane domain and a cytoplasmic portion with a protein tyrosine kinase domain. Studies indicate that various cellular functions such as cell-division, cell growth/proliferation, apoptosis, etc., are controlled and activated by the binding of the growth factors to the receptor tyrosine kinases. Due to their critical role in various cellular events, RTKs are most extensively investigated in the recent years as one of the most attractive targeted therapies of cancer.[38]

1.6.2. ***ERBB receptors and their ligands:***

Epidermal growth factor receptor[39] (EGFR) belongs to a large family of receptor tyrosine kinases. There are four types of EGFR namely EGFR (HER1), ERBB2 (HER2), ERBB3 (HER3) and ERBB4 (HER4).[40] The EGFR ligands that bind to the receptor

contain EGF-like motif in common and are synthesized by transmembrane precursors. The EGF family of ligands have been classified in to three major groups: The first group contains ligands that specifically bind to the EGFR and it includes EGF, amphiregulin, transforming growth factor-α (TGF-alpha) and the second group shows dual specificity to both ERBB1 and ERBB4 and it includes betacellulin, heparin-binding EGF (HB-EGF) and epiregulin. The third group includes neuregulins that bind to ERBB3 and ERBB4.

1.6.3. ***Structure and functions:***

Their structure is similar to RTK with an extracellular ligand binding domain, hydrophobic transmembrane domain and an intracellular tyrosine kinase domain. Under normal conditions/in normal cells, ligand binding to the ERBB receptor leads to the activation of the receptor resulting in homodimerization (with in the ERBB family: ERBB1:ERBB1, ERBB2:ERBB2, etc.) or heterodimerization between ERBB and other receptors (e.g., ERBB:IGFR) followed by the phosphorylation of the tyrosine kinase residues occurring from the phosphate transfer from ATP. These phosphorylated residues recruit various proteins by serving as docking sites which in turn triggers various signaling pathways involved in different cell functions.

1.6.4. ***EGFR upregulation and cancer:***

Reports indicate that abnormal kinase activity of ERBB receptors from abberant activation of the receptor results in uncontrolled growth stimulation which is implicated in several tumor malignancies including head, neck, brain and breast cancers thereby making it an interesting target for cancer treatment. This abnormal activation of receptor

in cancer can result from the over-expression of ERBB, autocrine ligand-receptor stimulation, point mutations and/or partial deletions of genes. Ligand independent activation of ERBB can occur from the over-expression of the receptor and or mutations resulting in hyperactivation of the receptor.

Various alterations of ERBB receptor are seen in the cancer patients. Overexpression of the receptor in seen in several patients resulting from gene amplification. Studies also reveal the development of somatic mutations in NSCLC patients in a group of patients undergoing combined chemotherapy with gefitinib and erlotinib. Recent advances include the development of antibodies (cetuximab, transtuzumab) that can target the extracellular domain of the receptor and small molecule inhibitors (lapatinib, imatinib) that target the catalytic domain of the receptor. These drugs directly affect the receptor and the subsequent signaling pathways responsible for tumor development and have so far been successful in arresting the growth and progression of the tumor. However, the existence of multiple isoforms with different functions that are sometimes oncogenic and sometimes tumor-suppressive complicate the therapeutic treatment.

1.7. ***ERBB inhibitors as therapeutic agents:***

Several strategies have been developed to target the ERBB receptor including monoclonal antibodies against the extra-cellular domain, anti-sense therapy, conjugation of toxins to ERBB ligands and anti-ERBB antibodies, small molecule inhibitors to block the catalytic domain of the receptor.[41] Among these therapies, monoclonal antibodies and small molecule inhibitors are widely used in ERBB-linked cancers. Although, these

inhibitors have proven to be very useful in arresting the development of cancer, there are some challenges need to be overcome to improve their efficacy.

1.7.1. ***mAntibodies against ERBB***:

These agents block the phosphorylation of the receptor by binding to the extracellular domain of the receptor. This prevents the activation/triggering of the downstream signaling through MAPK and Akt/PI3-kinase pathway. The success of this antibody based therapy was well demonstrated by the transtuzumab which when combined with other chemotherapy agents increased the survival rate in cancer patients which eventually gained FDA approval in 1998 for the treatment of ERBB linked cancers. Other examples include cetuximab and panitumumab which are approved in several countries for the treatment of head, neck and colon cancer. These agents have high affinity towards the specific ERBB receptor close to the natural ligands and competitively bind to the receptor and induce the subsequent internalization and downregulation. In addition to the blocking of ERBB signaling, they also induce an anticancer cytotoxic immune response as these agents have proven to be more efficient *in vivo* than *in vitro* which is attributed to the anti-angiogenic activity of mAB *in vivo.*

1.7.2. ***Small molecule inhibitors against ERBB:***

Several years of research coupled with the crystallization studies revealed that ATP-binding domains of kinases can be the potential targets for therapeutic treatment of cancer.[42,43] These results have proven that the development of small molecule inhibitors targeting the ATP-binding pocket can be an effective strategy of cancer therapy.[43-44]

These molecules can not only block the signaling of one specific ERBB receptor but can also simultaneously target/block the activity of other ERBB receptors through heterodimerization.[45] Crystal studies indicate that these ATP-competent inhibitors form/present three hydrogen bonds to the amino acids located in the hinge region of the receptor kinase similar those formed by the adenine ring of ATP. Most of them do not exploit the ribose binding region or the triphosphate binding site of ATP. Small molecule inhibitors have been classified in to different types based on two factors: Reversibility of binding inhibition to the kinase and the binding site/region of the interaction in the kinase. They are broadly classified in to four types as Type-1, Type-2, Type-3, Type-4 and covalent inhibitors.[46,47]

Type-1 inhibitors: Majority of small molecule inhibitors belong to this category. Type-1inhibitors are defined as those molecules that bind to the ATP binding pocket of the receptor in the active conformation. They are the ATP mimics that bind to the receptor utilizing the hydrogen-bonding interactions with the hinge residues of the kinase that link the N and C terminal domains in a similar fashion to the adenine ring of ATP. The success of these inhibitors is demonstrated by the fact that nearly ten Type-1 inhibitors have been approved by FDA for the cancer treatment.

Type-2 inhibitors: These inhibitors by contrast bind reversibly to the receptor in the inactive conformation facilitated by the DFG-out conformation of the receptor providing an additional interaction to the kinase resulting from the opening of hydrophobic site juxtaposed to the catalytic site of the receptor.[48,49] In addition to the extra interactions

with the activation loop of the kinase (allosteric site), the inhibitor also forms ~3 hydrogen bonds with the kinase in the hinge region. Type-2 inhibitors are known to have high degree of selectivity owing to these hydrophobic interactions in the allosteric site. Some of the Type-2 inhibitors that gained FDA approval include ABL1, imatinib, nilotinib and sorafenib.

Type-3(allosteric)inhibitors: These inhibitors bind outside the ATP binding pocket/catalytic domain at an allosteric site of the receptor.[50,51] They are non-ATP competitive and are known to have high degree of binding selectivity owing to their exploitation of the binding site to the receptor and the modulation of the kinase activity in a unique manner specific to the kinase. They are highly selective as they bind to the less-conserved sites on kinases. Examples include MEK1, MEK2, BMS-345541 and GNF2.

Type-4 inhibitors: They are also called as substrate directed inhibitors. These inhibitors bind reversibly to outside the catalytic domain/ATP pocket of the receptor in the substrate binding site. The interaction is found to be reversible and they are non-ATP competent inhibitors as they do not bind to the ATP binding pocket. Inhibitors of this class exhibit high degree of selectivity as the binding site is unique to a particular substrate. Well-demonstrated example of this class includes ON012380 which is a potent inhibitor of Bcr-Ab1, targeting the Crk substrate of the protein.

Covalent inhibitors: These ATP-competitive inhibitors bind to the active site of the receptor in an irreversible and covalent manner. As they react with the solvent-exposed,

nucleophilic cysteine residues of the kinase, their general design is comprised of an electrophile tethered to a well-demonstrated EGFR pharmacophore such as 4-anilinoquinazoline scaffolds. As the inhibition involves the formation of a covalent bond between the inhibitor and the solvent rich cysteine residues of EGFR, they are known as covalent inhibitors. Examples include hypothemycin, HKI-272, radicicol A and Cmk.

1.8. ***Conclusions:***

Turn-on fluorescent probes are very advantageous over the traditional fluorophore-tethered recognition units. Several strategies have been used to design these activatable probes. ERBB receptor is an attractive target of cancer therapy and many small molecule kinase inhibitors are currently being developed with a few drugs already approved by FDA for cancer treatment. There are several kinds of small molecule inhibitors based on the reversibility and region of binding to the receptor. Turn-on fluorescent probes targeting ERBB receptors can be specifically designed by incorporating an optical element and a pharmacophore. We designed turn-on fluorescent kinase inhibitors based on quinazoline core that target the ATP binding pocket of the receptor. DMAQ was the first fluorescent turn-on probe to be synthesized which was followed by a series of 15 kinase inhibitors. Besides establishing these turn-on probes as kinase inhibitors, we also demonstrated that the substitution on 6-position of quinazoline core does not inhibit the binding affinity of the inhibitor.

Chapter 2

Hyperchromism and Proton-Responsiveness of Phenyl Pyrimidones

2.1. *Background*

Pyrimidine with two sp^2 hybridized nitrogen atoms is the most notable six membered heterocycle and is one of the most prevalent, biologically relevant heterocycle with remarkable pharmacological activity (Figure 2.1).

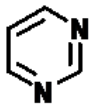

Figure 2.1. **Structure of pyrimidine**

Pyrimidine is an essential component of nucleic acids and many pyrimidone derivatives such as thymine, guanine, uracil and cytosine have been isolated from the hydrolysis of nucleic acids as shown in the Figure 2.2.

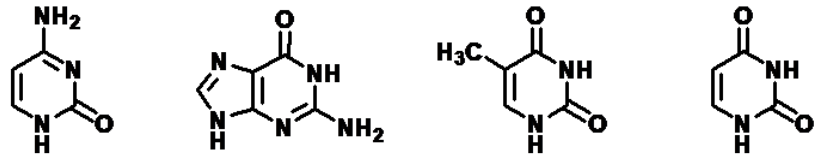

Figure 2.2. **Examples of nucleic acids with pyrimidine motif**

Pyrimidine and its derivatives are involved in a wide variety of biological and pharmacological activities including anticonvulsant,[52] (Phenobarbital) antibacterial,[53] (Trimethoprim, Sulphadiazine) antifungal, antiviral (Idoxuridine) and anticancer properties.[54,55] They are synthetically versatile substrates, which can be used for a

synthesis of a large variety of heterocyclic compounds and as a raw material for drug synthesis. For instance, fused pyrimidine derivatives such as imidazopyrimidines are known for their antimycobacterial properties and triazolopyrimidones are useful as antitumor agents.[56] Pyrimidone motif is also found in Zebularine a nucleoside analog of cytidine, a known DNA methylation inhibitor.[57] In another example, pyrimidone thiazolidonedione derivative (PMT13) has been evaluated to be an effective hypolipidaemic and hypeglycaemic compound.[58] Recently, Schlapbach et al. have also reported a series of pyrrolo-pyrimidone derivatives as potent MK2 inhibitors.[59] Dihydropyrimidinones are widely used in the pharmaceutical industries as calcium channel blockers, antihypertensive agents, and alpha-1-a-antagonist and in another context, aryl substituted pyrimidones have been used as kinase inhibitors, antimicrobials, and analgesics.

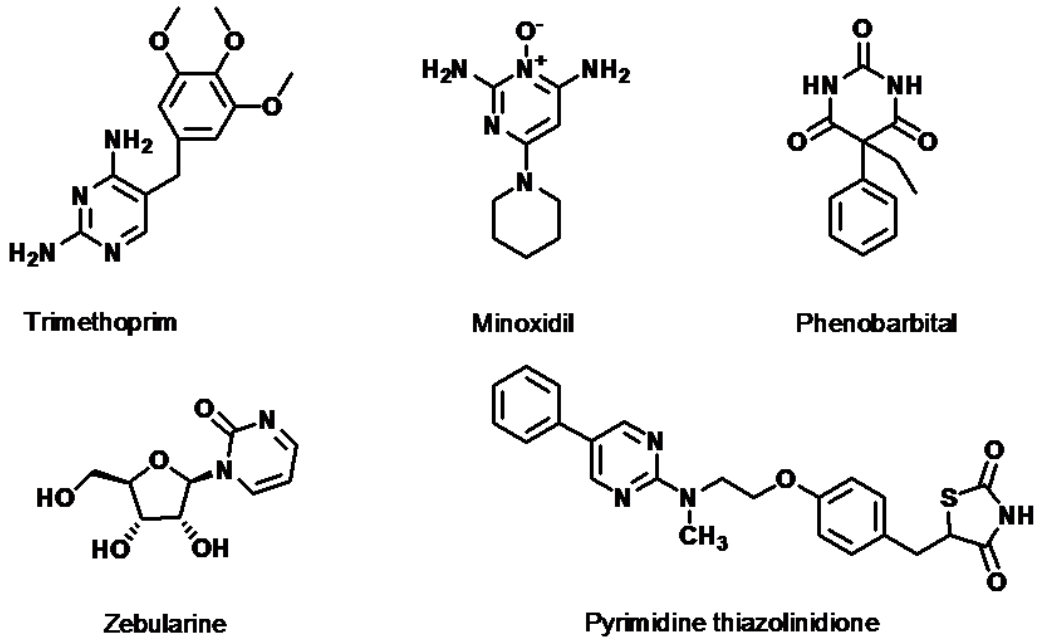

Figure 2.3. **Examples of drugs with pyrimidine motif**

Some examples of drugs/biologically active compounds that contain pyrimidone motif are shown in Figure 2.3.

2.1.1. ***Turn-on emission:***

Fluorescent probes have become indispensible tools for biologists owing to the wealth of information offered by the probes on the intricate cellular processes with high sensitivity and versatility.[4, 60] There has been an enormous increase in the number of novel fluorescent probes discovered in recent years and their remarkable role in unfolding the cellular mysteries cannot be compared with other optical imaging tools available today.[61] Turn-on fluorescent probes are the probes that remain silent until stimulated by any special environment or specific biochemical processes.[62] Turn-on sensors are defined as those compounds whose fluorescence is quenched in the absence of the analyte or target, but become fluorescent on reaching the specific target. In contrast, if the fluorescence of the probe is quenched on reaching the target and turns emissive in the absence of the analyst, such sensors are called as "turn-off" sensors. As the turn-off sensors can deliver false positive results due to the presence of other quenchers in the cellular environments, they are generally not desirable for biomedical applications. During our current investigation of the optical properties of the arylpyrimidones, we discovered that our compounds show "turn-on/off" behavior in response to the addition of trifluoroacetic acid (TFA). Given the pharmacological significance of pyrimidone motifs, we envisaged that the optical evaluation of single arm and double arm aryl pyrimidones (Figure 2.4) would

serve a good platform for the synthesis of turn-on fluorescent probes with great potential in fluorescence imaging and other biological applications including biosensors.

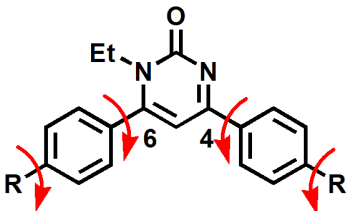

***Figure 2.4*. Pyrimidone with two flexible phenyl rings**

2.1.2. ***Photophysical studies on pyrimidones:***

To date, very few reports exist in literature on the photophysical properties of pyrimidones. Although, their pharmacological significance is well established, the optical properties of these derivatives are not yet unfolded.[63] Liu et al reported three pyrimidone derivatives and studied their spectral characteristics by two photon absorption.[64] Shafer and his group reported a series of 4,6-diarylpyrimidone derivatives as CDC7 serine/threonine kinase inhibitors.[65] Similarly in another example, Wu et al[66] developed a group of 4,6 - diarylpyrimidones as Zn^{+2} responsive ligand where the coordination of the Zn^{+2} ion to the pyrimidone core enhances the fluorescence (Figure 2.5)

CDC7 inhibitor **Fluorogenic Zn^{+2} sensor**

Figure 2.5. Diaryl pyrimidones as kinase inhibitors and metal ion sensors

2.2. Results and Discussion:

2.2.1. *Hyperchromism and isomerism:*

Hyperchromicity refers to the increase in the intensity of the peak resulting from an increased absorption of light by the chromophore. This phenomenon is usually observed in the nucleic acids such as DNA when a double-stranded DNA dissociates into two single stranded chains.[67] Hyperchromicity was the most striking feature shown by our compounds upon the introduction of TFA. While we were able to explain the bathochromic shifts based on the frontier molecular orbital approach, the cause of hyperchromicity could not be rationalized based on the results obtained.

Biginelli reaction for the synthesis of pyrimidones:

We used Biginelli reaction for the synthesis of pyrimidones. [29, 68]

Scheme 2.1. Mechanism of Biginelli reaction for the synthesis of pyrimidones

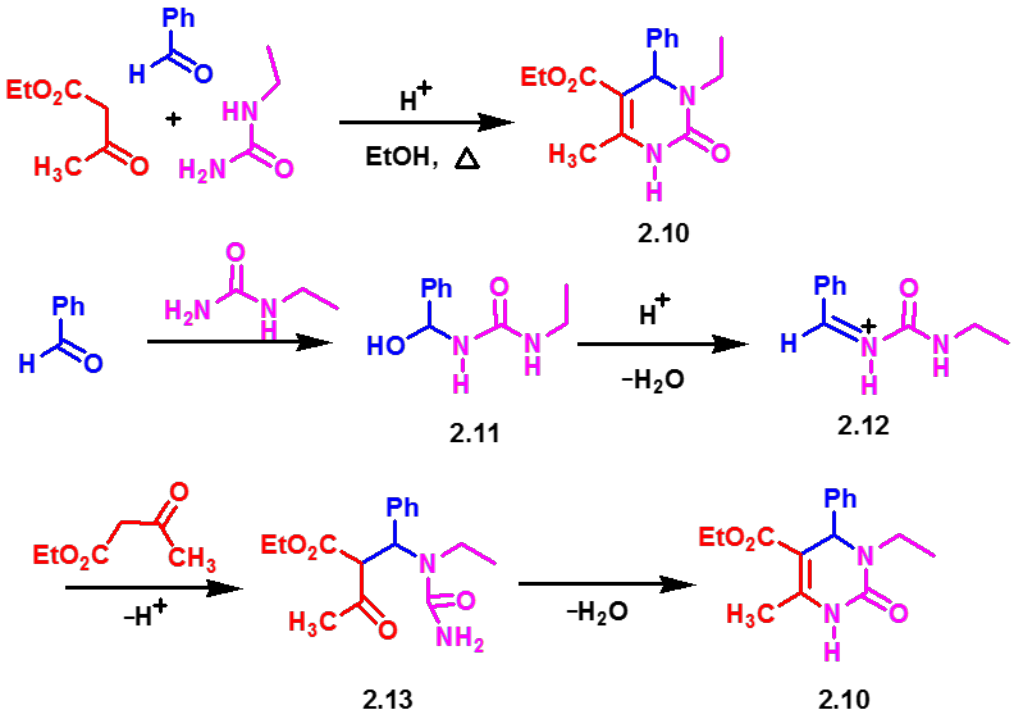

Biginelli reaction is a multi-component reaction developed by Pietro Biginelli in 1893,[69] that generates 3,4-dihydropyrimidin-2(1H)-ones from ethylacetoacetate, an aryl aldehyde (such as benzaldehyde), and urea (Scheme 2.1).

Scheme 2.2. General reaction for the synthesis of phenyl pyrimidones and the structures of single arm and double arm aryl pyrimidones (2.19-2.26).

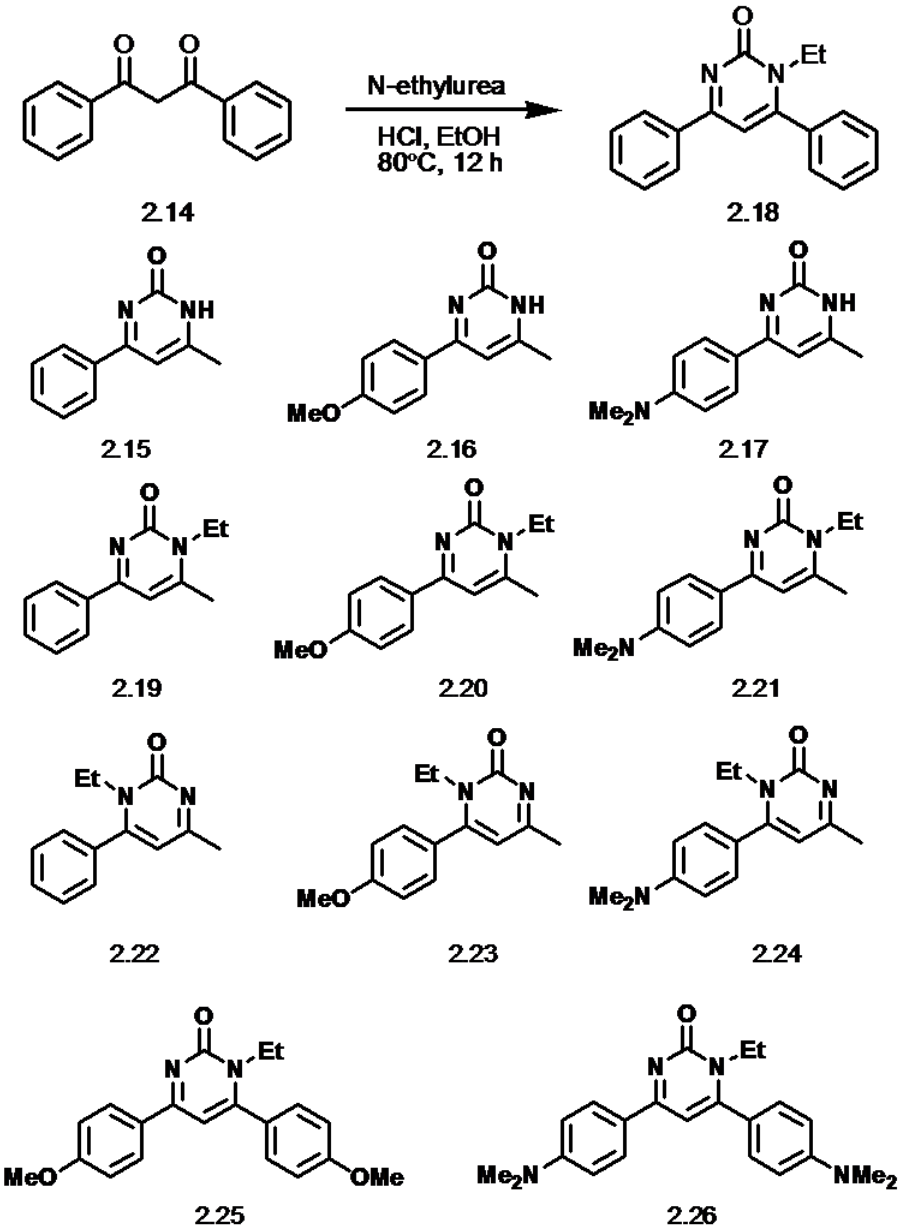

During the synthesis of single arm substituted pyrimidone compounds, we noticed that condensation of the asymmetric diketones with ethyl urea resulted in the formation of isomers. Compounds from **2.19-2.24** were obtained as isomers from the same reaction and were isolated by column chromatography. Purified isomers were characterized by ^{1}H NMR and 1D-NOE spectra as shown in the Figure 2.6. Synthesis of compounds (**2.15-2.17**) was accomplished under the same reaction conditions except that urea was used instead of ethyl urea.

2.2.2. ***Proton and 1D NOE studies:***

From the DFT calculations, we observed that the pendant phenyl substituent is aligned differently in the two isomers of the compounds from **2.19-2.24.**

We found that in the case of 4-phenyl-pyrimidones from **2.19-2.21**, the pendant phenyl substituent and pyrimidone ring were in a planar orientation while in the case of the 6-phenylpyrimidones from **2.22-2.24**, the pendant phenyl substituent was twisted with respect to the pyrimidone ring. This alignment essentially influences the chemical shifts of the aromatic protons of the isomers which were evident from the considerable changes in the chemical shifts in the ^{1}H NMR spectra as demonstrated in Figure 2.6

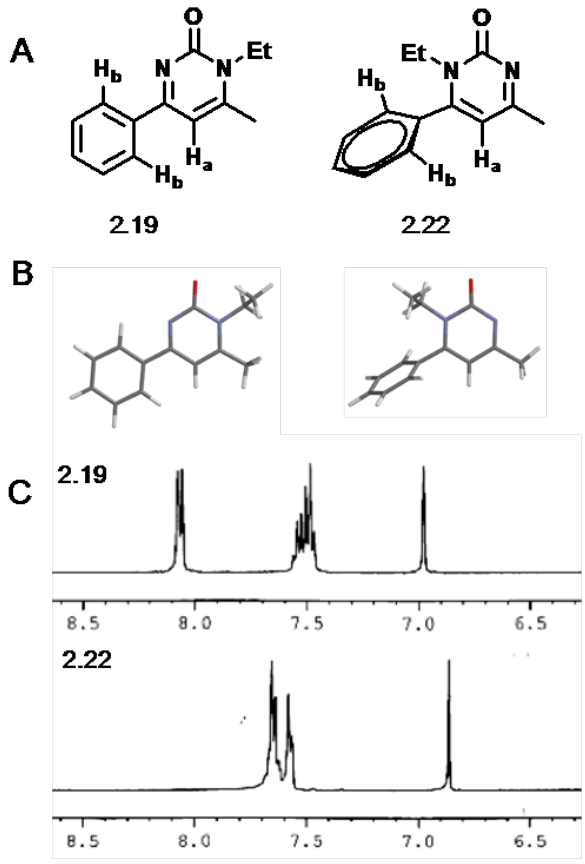

Figure 2.6. **A) Structural isomers (2.19 and 2.22) B) Structural identification based on optimized geometries (DF6-31G*) C) ^{1}H NMR spectral differences of 2.19 and 2.22**

For **2.19**, the H_a protons showed a downfield shift by 0.13 ppm compared to **2.22** and the H_b protons showed a significant change in the chemical shift by 0.6 ppm relative to **2.22**. This marked difference in the chemical shifts was rationalized based on two facts: One reason was attributed to the planar arrangement/orientation of the pyrimidone core and the aromatic ring causes the deshielding of the H_b protons and the second being the electron withdrawing nature of the pyrimidone core contributed to the significant difference in the chemical shifts of H_b protons. Further structural assessment of the isomers was supported by 1D-NOE spectra where specific irradiation of the α-carbon protons of the N-ethyl substituent for the compound **2.19** results in a nuclear overhauser

effect (NOE) on the adjacent 6-methyl group while the irradiation of the same protons for **2.22** resulted in the NOE on the phenyl group in the proximity instead of methyl group thereby confirming the structural assignment for both the isomers.

2.2.3. ***Photophysical studies:***

The UV-Vis and fluorescence studies of these compounds revealed the effects of conjugation between the pendant phenyl arms and the pyrimidone core on the optical properties of these fluorophores. Trifluoroacetic acid (TFA) was used as the protonation source. As the nitrogen atoms on the heterocyclic compounds are sensitive to protonation in general, we were interested to know if a similar protonation of our pyrimidone derivatives can influence their optical properties. We were fascinated to see the results where we observed that the protonation of the nitrogen atom at 3rd position on the pyrimidone ring on the addition of TFA resulted in remarkable changes in the optical properties of our fluorophores.[70] Further evidence obtained from the molecular orbital picture/calculations, explained the reasons for these changes in the optical properties.

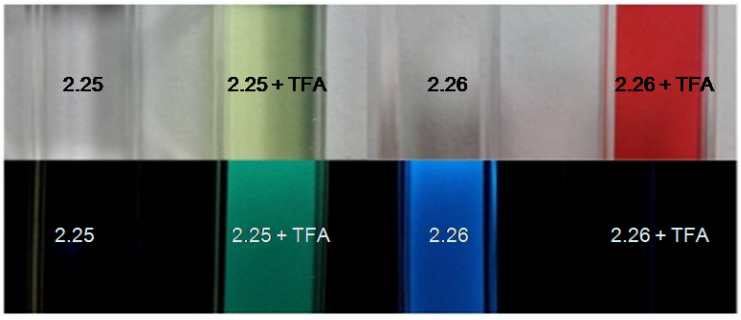

Figure 2.7. **UV-Vis and emission spectra of 2.25 and 2.26 in the presence and absence of TFA**

In the case of **2.19-2.21,** the π-electron framework of pyrimidone and phenyl rings show extended overlap due to the planar orientation while the steric-congestion in the case of **2.22-2.24** does not allow for an extended conjugation. The most striking spectral features observed when TFA was added to these compounds were bathochromic shifts and hyperchromicity (Figure 2.7).

2.2.4. ***Absorption spectroscopy:***

Compound **2.26** which was practically colorless in CH_2Cl_2 turned deep red upon the addition of TFA.

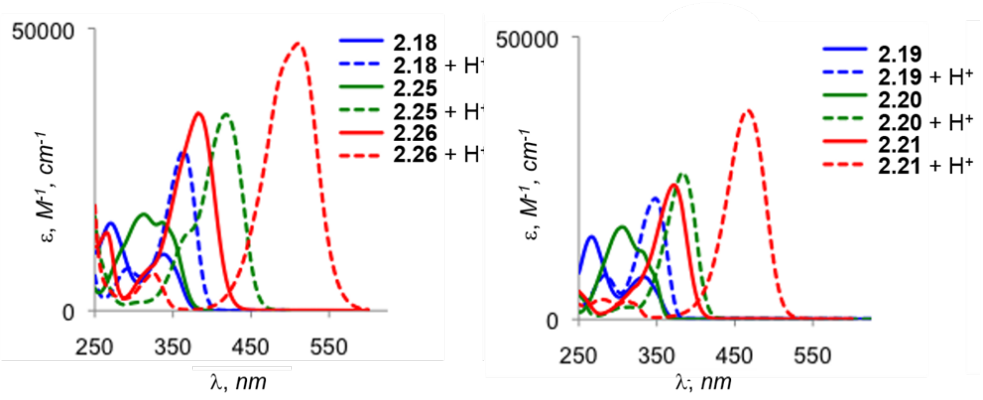

Figure 2.8. **Absorption spectroscopy in the presence and absence of TFA**

For **2.18**, only a slight bathochromic shift was observed, whereas the effect was moderate in **2.25** and most prominent in **2.26** with a shift of 126 nm.

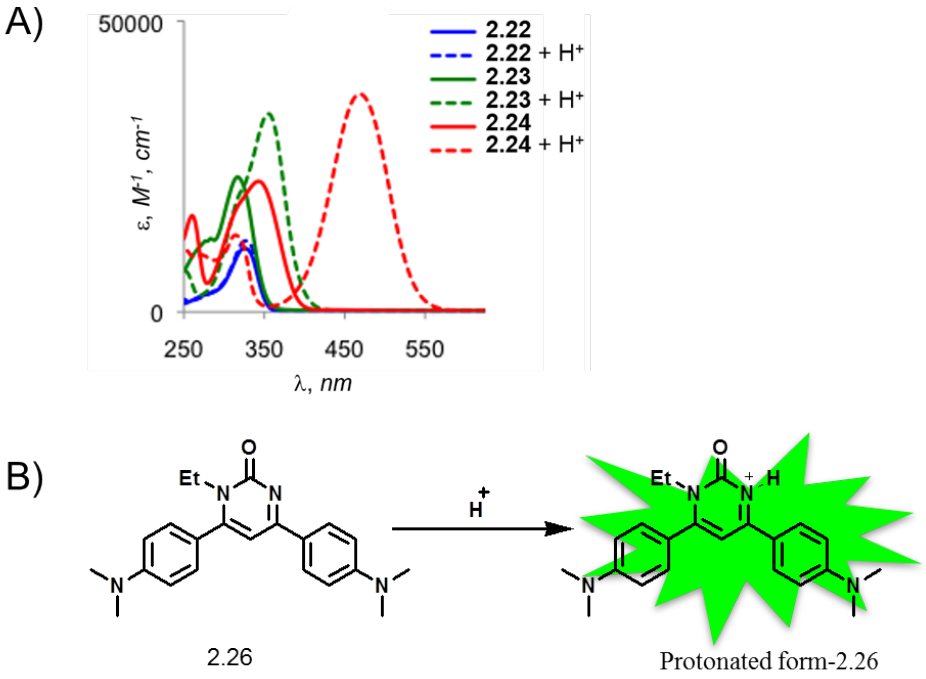

***Figure 2.9*. A) Absorption spectroscopy in the presence and absence of TFA B) Turn - on response of 2.26 upon the addition of TFA.**

This difference in the shifts can be attributed to the strong electron-donating ability of dimethylamino group in **2.26** while the effect being moderate in **2.25** with methoxy substituent (Figure 2.8). On the other hand, this trend was reversed with respect to molar absorptivity ε, where the largest enhancement of three-fold was observed for **2.18** while **2.25** exhibited two-fold and 2.26 exhibited 1.5 fold increases. Compound **2.24** exhibited larger bathochromic shift while **2.22** had the lowest molar absorptivity relative to **2.23** and **2.24** (Figure 2.9).

2.2.5. ***Emission spectroscopy:***

Introduction of TFA also induced significant changes in the emission intensity of these fluorophores. The compounds **2.25** and **2.26** were found to be weakly or non-emissive in CH_2Cl_2 while the addition of TFA resulted in a marked enhancement in the fluorescence.

As shown in the Figure 2.10, for **2.25** the increase was most significant with a 30-fold enhancement in Φ_{em} on the addition of TFA (Table 2.1). In contrast, highly fluorescent compound **2.26** with a Φ_{em} of 0.49 in CH_2Cl_2 was completely quenched upon the introduction of TFA. Another interesting feature we observed from the absorption spectra of our compounds was that the absorption spectra of 4-phenylpyrimidones and diphenyl derivatives closely resemble with each other both in terms of $\lambda_{max,\ abs}$ and the magnitude of the bathochromic and hyperchromic shifts (Table 2.1).

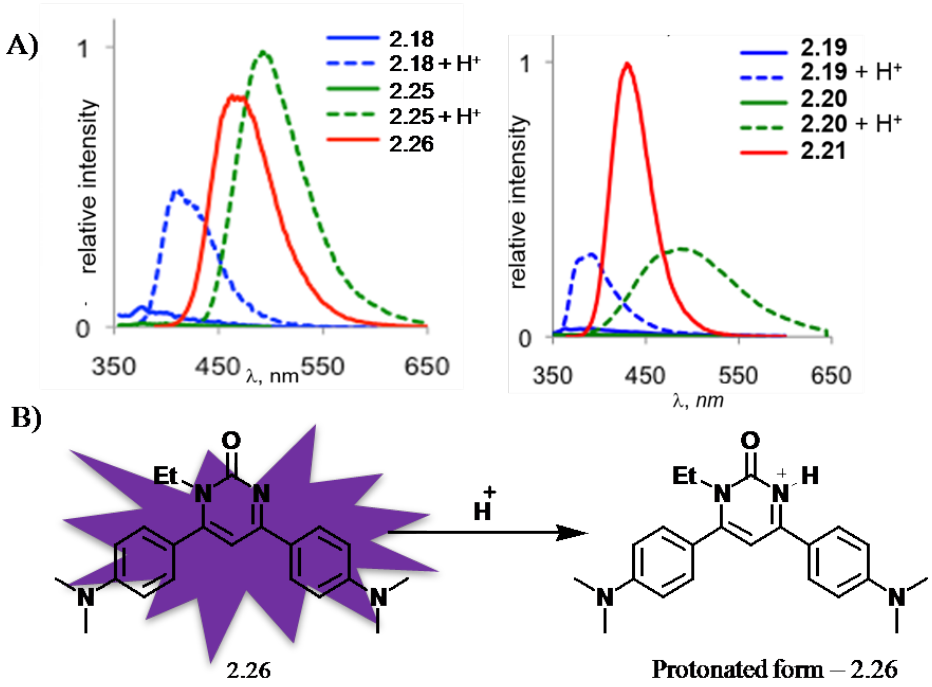

Figure 2.10. **A) Fluorescence spectra in the presence and absence of TFA B) Emission quenching of 2.26 upon the addition of TFA**

This was also reflected in the electronic transitions of these compounds as depicted in the Figure 2.12. Although we could not rationalize the reason for hyperchromicity, yet the observed bathochromic shifts were attributed to the reduced HOMO-LUMO gap of these fluorophores.

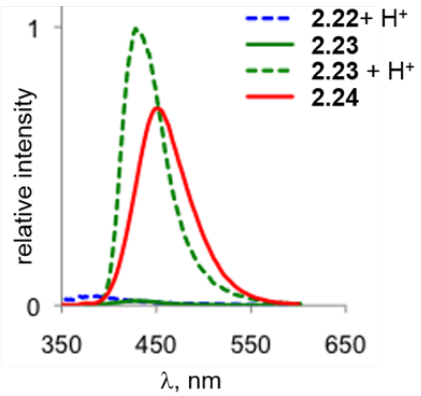

Figure 2.11. **Fluorescence spectra of 2.22-2.24 in the presence and absence of TFA**

From **2.22-2.24**, only compound **2.24** was found to be emissive and the fluorescence of **2.23** was enhanced upon introduction of TFA (Figure 2.11). The above changes have been rationalized on the fact that the electron withdrawing character of the pyrimidone core is enhanced upon protonation which in turn lowers the LUMO and an intramolecular charge transfer state is produced where the phenyl ring is relatively electron rich and the pyrimidone core being the electron withdrawing counterpart.

2.2.6. ***Molecular orbital studies:***

A close inspection of the molecular orbital picture of our compounds in the neutral and protonated forms revealed some interesting facts on the electronic transitions of these chromophores. We used DFT (M06) at the 6-31G* level to study the equilibrium geometry of these compounds in the neutral and the protonated forms. Our experimental values of $\lambda_{max,\ abs}$ coincided well with the energy of the calculated HOMO-LUMO transitions. The LUMO, HOMO, HOMO^{-1}, HOMO^{-2} orbitals for **2.19-2.21** in the neutral and protonated forms are shown in the Figure 2.12.

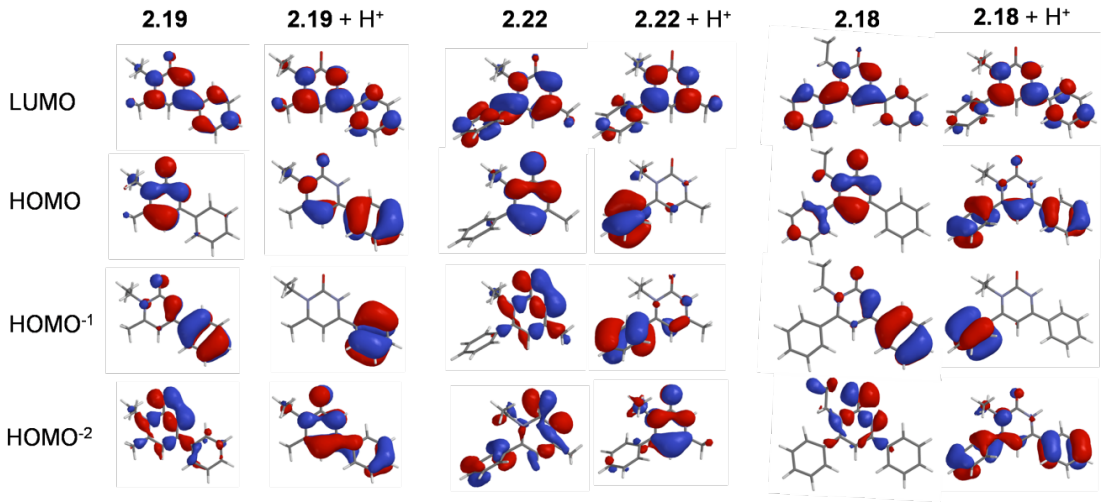

Figure 2.12. **Frontier molecular orbital representations of 2.18, 2.19 and 2.22 before and after protonation**

Similar molecular orbital picture was observed for the rest of the series. For **2.18** and **2.19**, the HOMO of the protonated form was found to be a combination of the HOMO and HOMO^{-1} orbitals for neutral forms. The largest enhancement of ε (3-fold) for **2.18** was attributed to the maximum spatial overlap of HOMO and LUMO for the protonated species. Another likely reason for the increase in ε upon protonation was rationalized based on the electronic transition from HOMO^{-2} to LUMO transition which was calculated to be 0.8 and 0.3 eV respectively. As HOMO^{-2} was mostly σ in character for the unprotonated species and is orthogonal to the π-system, it cannot overlap effectively with LUMO. In contrast, the HOMO^{-2} was π in nature and thereby effectively overlaps with the LUMO for the protonated species, and this maximum spatial overlap between the orbitals results in the larger absorption coeffecients (ε).

Table 2.1. Photophysical characteristics of 2.18 to 2.26

Compd	$\lambda_{max, abs}$,[a] nm	ε,[a,b] M^{-1}, cm^{-1}	E_{calc},[c] eV	$\lambda_{max, abs}$,[d] nm	ε,[b,d] M^{-1}, cm^{-1}	E_{calc},[c,e] eV	$\lambda_{max, em}$,[a] nm	Φ_{em}[a,b]	$\lambda_{max, em}$[d]	Φ_{em}[b,d]
2.18	344	9900	4.3	361	28 000	4.3	374	0.01	408	0.05
2.19	335	7200	5.0	348	21 000	4.5	384	0.009	389	0.14
2.20	335	16 000	5.0	387	25 000	4.0	375	0.01	486	0.40
2.21	376	23 000	4.4	473	37 000	3.5	426	0.57	–	–
2.22	329	10 000	5.3	331	12 000	4.5	–	–	390	0.007
2.23	321	23 000	5.4	358	33 000	3.8	420	0.006	424	0.28
2.24	348	22 000	4.8	474	37 000	3.2	448	0.24	–	–
2.25	337	17 000	4.8	414	34 000	3.7	375	0.02	488	0.62
2.26	378	34 000	4.4	504	47 000	3.1	464	0.49	–	–

[a]CH_2Cl_2;[b]±5%;[c]Energy of the HOMO–LUMO transition; DF MO6 6-31G*; [d]CH_2Cl_2 with 1% TFA; [e]For the N3 protonated species.

The molecular orbital picture of HOMO and $HOMO^{-2}$ for **2.22** in the protonated and unprotonated forms also showed that the electron density was localized either solely in the phenyl arm or the pyrimidine core.A very small enhancement in the ε for **2.22** can likely be attributed to the decreased n→π* transitions and enhanced contribution of π → π* transitions to the absorption band at 330 nm. Of all the compounds in the series from **2.19-2.26**, compounds with dimethylamino group exhibit high quantum yields in the absence of TFA. While the isomers **2.22, 2.23** and **2.24** have the lowest quantum yields in the respective series. This difference has been rationalized on the basis of the poor orbital overlap resulting from the localization of the electron density to either the phenyl ring or the pyrimidone core.

2.2.7. *Experimental section:*

6-methyl-4-phenylpyrimidin-2(1H)-one (2.15): ^{1}H NMR (300 MHz, MeOD): δ (ppm) 2.67(s, 3H), 7.22 (s, 1H), 7.7-7.72 (br t, 2H), 7.79-7.81 (br t, 1H), 7.99 (d, 2H, J = 7.2 Hz); ^{13}C NMR (75 MHz, MeOD): δ (ppm) 104.0, 129.1, 129.5, 130.0, 134.9, 148.4, 162.7, 166.4, 171.7; IR ν_{max} (cm^{-1}): 675, 760, 858, 1096, 1181, 1312, 1511, 1620, 1730, 2506, 3306, 3406; HRMS (ESI) $C_{11}H_{10}N_2O$ [M+H$^+$] calcd 187.0871, found 187.0881; 30% yield

4-(4-methoxyphenyl)-6-methylpyrimidin-2(1H)-one (2.16): ^{1}H NMR (300 MHz, MeOD): δ (ppm) 2.68 (s, 3H), 3.96 (s, 3H), 7.16 (s, 1H), 7.20 (d. 2H, J = 3 Hz), 8.02 (d, 2H, J = 4.8 Hz); ^{13}C NMR (75 MHz, MeOD): δ (ppm) 102.5, 115.5, 120.9, 131.5, 148.6, 165.5, 166.0, 169.6; IR ν_{max} (cm^{-1}): 832, 850, 1005, 1014, 1172, 1278, 1303, 1554, 1594, 1736, 2825, 3033, 3128, 3388; HRMS (ESI) $C_{12}H_{12}N_2O_2$ [M+H]$^+$ calcd 217.0977, found 217.0981; 25% yield.

4-(4-(dimethylamino)phenyl)-6-methylpyrimidin-2(1H)-one (2.17): ^{1}H NMR (300 MHz, DMSO): δ (ppm) 2.42 (s, 3H), 3.11(s, 6H), 6.85 (d, 2H, J = 12Hz), 7.23 (s, 1H), 8.07 (d, 2H, J = 9.6Hz); ^{13}C NMR (100MHz, DMSO): δ (ppm) 20.4, 113.5, 132.3, 149.7, 155.4, 162.6, 165.3; IR ν_{max} (cm^{-1}): 743, 838, 1209, 1313, 1324, 1500, 1534, 1582, 1702, 2630, 2941, 3077, 3265 cm^{-1}; HRMS (ESI) $C_{13}H_{15}N_3O$ [M+H]$^+$ calcd 230.1293, found 230.1299; 20% yield.

1-ethyl-4-phenyl-2(1H)-pyrimidone (2.19):

^{1}H NMR (400 MHz, DMSO): δ (ppm) 1.36 (s, 3H, J = 7.2 Hz), 2.58 (s, 3H), 4.16 (q, 2H, J = 7.0 Hz), 7.01 (s, 1H), 7.48-7.55 (m, 3H), 8.06 (d, 2H, J = 7.0 Hz); ^{13}C NMR (125 MHz, MeOD) δ (ppm) 13.3, 20.2, 30.8, 104.7, 128.8, 129.9, 132.9, 137.3, 159.5, 160.9,

171.1; IR ν_{max} (cm^{-1}): 705, 779, 1345, 1365, 1530, 1576, 1600, 1630, 2926, 3055, 3097; HRMS (ESI) $C_{13}H_{15}N_2O$ $[M+H]^+$ calcd 215.1184, found 215.1187; 11% yield.

1-ethyl-6-phenyl-2(1H)-pyrimidone (2.22):

^{1}H NMR (400 MHz, MeOD): δ (ppm) 1.14 (t, 3H, J = 7.0 Hz), 2.52 (s, 3H), 3.85 (q, 2H, J = 6.8 Hz), 6.86 (s, 1H), 7.56 (d, 2H, J = 7.1 Hz), 7.62-7.64 (m, 3H); ^{13}C NMR (75 MHz, DMSO): δ (ppm) 21.5, 105.4, 130.5, 130.9, 131.4, 136.3, 149.8, 164.1, 167.8., 173.2; IR ν_{max} (cm^{-1}): 712, 771, 781, 829, 1028, 1116, 1338, 1446, 1489, 1564, 1608, 1722, 2612, 3446, 3509 cm^{-1}; HRMS (ESI) $C_{13}H_{15}N_2O$ $[M+H]^+$ calcd 215.1184, found 215.1179; 11% yield**.**

1-ethyl-4,6-diphenyl-2(1H)-pyrimidone (2.18):

^{1}H NMR (500 MHz, CDCl3): δ (ppm) 1.29 (3H, t, J = 6.5 Hz), 4.04 (2H, m), 6.79 (1H, s), 7.40-7.65 (m, 8H), 8.09 (d, 2H, J = 7.5 Hz); ^{13}C NMR (125.74 MHz, $CDCl_3$): δ (ppm) 13.79, 43.06, 104.22, 116.68, 127.58, 128.14, 128.94, 129.19, 130.75, 132.57, 132.99, 134.64, 156.39, 159.53, 159.85, 161.63, 169.28; IR ν_{max} (cm^{-1}): 693, 706, 764, 852, 942, 999, 1023, 1023, 1125, 1181, 1368, 1403, 1444, 1523, 1592, 1604, 1642, 1698; HRMS (ESI) calcd for $C_{18}H_{17}N_2O$ $[M+H]^+$ 277.1341; found 277.1334; 32% yield.

1-ethyl-4-(4-methoxyphenyl)-2(1H)-pyrimidone (2.20):

^{1}H NMR (500 MHz, MeOD): δ (ppm) 1.41 (t, 3H, J = 6.5 Hz), 2.81 (s, 1H), 3.96 (s, 3H), 4.25 (q, 2H, J = 7.0 Hz), 7.21 (d, 2H, J = 8.5 Hz), 7.28 (s, 1H), 8.04 (d, 2H, J = 8.0 Hz); ^{13}C NMR (125 MHz, MeOD) δ (ppm) 12.6, 21.6, 43.9, 56.6, 104.8, 116.5, 121.7, 132.3, 149.8, 163.9, 167.0, 170.9; IR ν_{max} (cm^{-1}): 762, 1076, 1011, 1146, 1198, 1246, 1278, 1531, 1572, 1727, 2791, 3330; HRMS (ESI) $C_{14}H_{17}N_2O_2$ $[M+H]^+$ calcd 245.1290, found 245.1285; 19% yield.

1-ethyl-6-(4-methoxyphenyl)-2(1H)-pyrimidone (2.23):

^{1}H NMR (300 MHz, MeOD): δ (ppm) 1.35 (t, 3H, J = 7.02 Hz), 2.61 (s, 3H), 3.93 (s, 3H), 4.09-4.16 (m, 2H), 6.78 (s, 1H), 7.21 (d, 2H, J = 8.6 Hz), 7.59 (d, 2H, J = 8.6 Hz); ^{13}C NMR (125.75 MHz, DMSO): δ (ppm) 13.3, 24.4, 41.2, 55.2, 106.2, 114.0, 125.3, 129.4, 155.5, 158.7, 160.2, 165.2, 173.6; IR ν_{max} (cm^{-1}): 755, 773, 839, 1016, 1071, 1125, 1183, 1262, 1346, 1444, 1554, 1600, 1723, 3013, 3240 cm^{-1}; HRMS (ESI) $C_{14}H_{17}N_2O_2$ $[M+H]^+$ calcd 245.1290, found 245.1290; 11% yield.

1-ethyl-4,6-bis(4-methoxyphenyl)-2(1H)-pyrimidone (2.25):

^{1}H NMR (500 MHz, $CDCl_3$): δ 1.26 (3H, t, J = 7.0 Hz), 3.88 (3H, s), 3.91 (3H, s), 4.0 (2H, m), 6.62 (1H, s), 6.69 (2H, d, J = 9.0 Hz), 7.03 (2H, d, J = 9.0 Hz), 7.35 (2H, d, J = 9.0 Hz), 8.11 (2H, d, J = 9.0 Hz); ^{13}C NMR (125.74 MHz, $CDCl_3$): δ 14.03, 42.09, 55.43, 55.48, 102.67, 114.01, 114.31, 126.22, 128.51, 129.24, 129.71, 157.29, 159.58, 160.87, 162.75, 168.62; IR ν_{max} (cm^{-1}): 676, 768, 795, 835, 1024, 1156, 1174, 1242, 1346, 1369, 1396, 1495, 1524, 1592, 1609, 1631; MS (HRMS) calcd for $C_{20}H_{21}N_2O$ $[M+H]^+$ 337.1552; found 337.1540; 19% yield.

1-ethyl-4-(4-(dimethylamino)phenyl)-2(1H)-pyrimidone (2.21):

^{1}H NMR (400 MHz, DMSO): δ (ppm) 1.26 (t, 3H, J = 7.1 Hz) 2.32 (s, 3H), 4.00 (q, 2H, J = 7.4 Hz), 6.8 (d, 2H, J = 9.2 Hz), 7.38 (s, 1H), 8.09 (d, 2H, J = 9.0 Hz); ^{13}C NMR (100 MHz, DMSO): δ (ppm) 21.3, 113.6, 132.2, 150.0, 155.4, 160.6, 165.3; IR ν_{max} (cm^{-1}): 748, 833, 1062, 1156, 1313, 1333, 1357, 1394, 1515, 1577, 1717, 2917, 3351, 3438; HRMS (ESI) $C_{15}H_{20}N_3O$ $[M+H]^+$ calcd 258.1606, found 258.1621; 24% yield.

1-ethyl-6-(4-(dimethylamino)phenyl)-2(1H)-pyrimidone (2.24):

^{1}H NMR (500 MHz, MeOD): δ (ppm) 1.22 (s, 3H, J = 6.5 Hz), 4.05 (q, 2H, J = 6.5 Hz), 6.32 (s, 1H), 6.84 (d, 2H, J = 8.5 Hz), 7.31 (d, 2H, J = 8.5 Hz); ^{13}C NMR (125 MHz, MeOD) δ (ppm) 14.0, 24.3, 40.3, 43.5, 99.1, 108.7, 112.8, 121.0, 1302, 153.2, 158.8, 162.8, 175.8; IR ν_{max} (cm^{-1}):798, 808, 1201, 1350, 1440, 1509, 1601, 1644, 2905; HRMS (ESI) $C_{15}H_{20}N_3O$ [M+H^+] calcd 258.1606, found 258.1623; 4% yield.

1-ethyl-4,6-bis(4-(dimethylamino)phenyl)-2(1H)-pyrimidone (2.26):

^{1}H NMR (500 MHz, $CDCl_3$): δ (ppm) 1.25 (3H, t, J = 6.5 Hz), 3.05 (12H, s), 4.04 (2H, m), 6.61 (1H, s), 6.70 (2H, d, J = 9.0 Hz), 6.78 (2H, d, J = 8.5 Hz), 7.28 (2H, d, J = 9.0 Hz), 8.075 (2H, d, J = 9.0 Hz); ^{13}C NMR (125 MHz, $CDCl_3$): δ14.18, 40.09, 40.20, 41.85, 102.27, 111.31, 111.61, 121.49, 123.23, 128.95, 129.46, 151.13, 152.76, 157.81, 159.59, 168.33; IR ν_{max} (cm^{-1}): 672, 702, 729, 793, 808, 944, 1061, 1125, 1158, 1184, 1347, 1361, 1500, 1524, 1579, 1641; HRMS (DP) calcd for $C_{22}H_{26}N_4O$ 362.2107; found 362.2091; 25% yield.

2.3. *Conclusions*: We synthesized a series of phenyl and diphenyl pyrimidone derivatives and their fluorescence spectral properties were evaluated under normal and acidic conditions. These compounds were found to be highly proton-sensitive and exhibit severe hyperchromic and bathochromic shifts in the presence and absence of TFA, showing a good illustration of “turn-on” and “turn-off” fluorescence and this behavior was explained from the molecular orbital topology based on the FMO (frontier molecular orbital) overlap. The presence of pharmacologically active pyrimidone core coupled with these “turn-on” and “turn-off” fluorescence show highly potential for biological applications such as biosensors and in the making of opto-electronic devices, etc.

Chapter 3

Design and Synthesis of DMAQ as a "Turn-on" Fluorescent Probe Targeting ERBB Receptor

3.1. ***Background:***

Fluorescent probes have emerged as one of the most powerful tools in recent years for the visualization and the investigation of biological processes in the complex milieu of living cells and organisms.[5b, 19, 61, 71] Compared to other detection methods, fluorescent probes are more advantageous, as they provide information with high sensitivity and great versatility with minimal perturbation of the cell under investigation.[4,72] They are attractive in particular, as they report the specific binding events without the need for rinsing steps to remove the unbound probe.

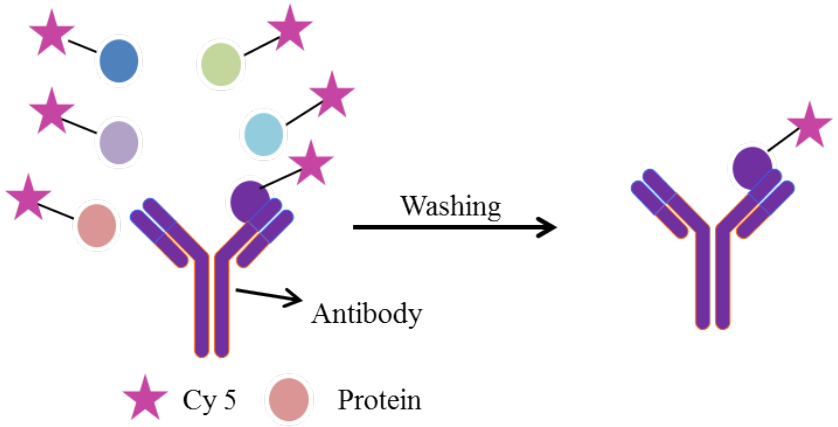

Figure 3.1. **Proteins labeled with Cy5 (fluorescent tag). Only proteins of interest iare recognized by the antibody and washing step removes the unbound protein**

The traditional assays employing fluorescent probes consist of a recognition unit and a fluorophore. The recognition site helps in the binding of the fluorophore to the specific target or analyte.[8,73] The labeling techniques employing these fluorophore and tether recognition units can also have some unbound probes that interfere with the signal-to-

noise ratio thereby reducing it. These techniques greatly hamper the detection in several ways. One major concern is that this technique involves additional steps of washing or rinsing to remove the unbound probe as demonstrated in the Figure 3.1. This rinsing step is not only time consuming but also delays the data acquisition thereby making the detection of cellular dynamics inaccessible. Also it prevents the study of the receptor and protein changes immediately after labeling. Also, depending upon the structure of the receptor/protein of interest, unbound probe may not be washed away. In addition to the above mentioned issues arising from fluorophore tether recognition units, there are other potential concerns if the fluorophore is continuously on such as phototoxicity, production of free radicals, photobleaching, etc. In order to overcome all the above issues arising from the use of fluorogenic/tether recognition units, "turn-on" fluorescent probes are very beneficial as the probes remain silent/inactive in the absence of the target and turn emissive only after a specific biological event/process.[8-9] In the present study, we designed and developed a novel fluorescent turn-on probe "DMAQ" that is a ATP competent inhibitor as illustrated in the Figure 3.2.[30]

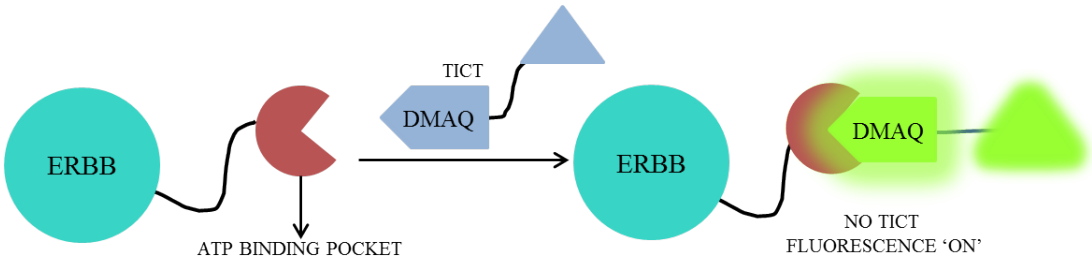

Figure 3.2. **Turn-on fluorescence of DMAQ on binding to ERBB receptor**

3.1.1. ***ERBB receptor***:

Several decades of extensive research on the kinases has revealed the crucial role played by the kinases in the cell metabolism, cell division, proliferation and other biological processes. Abberations in the normal cell regulation can result in cancer onset, progression and metastasis.[41,74,75] These protein enzymes are involved in the transfer of terminal phosphate groups from an ATP molecule to the tyrosine residue of the target protein thus leading to signal transduction. Studies revealed that dysregulation of this family of receptors can lead to several malignant disorders including head, neck, breast, lung and oesophageal cancers. This dysregulation can result from either overexpression of the receptor, mutations, activation by overproduction of ligand and or ligand independent activation. This makes them an attractive area of research and a very important target for cancer treatment.[75] In the recent years, researchers have developed different strategies to target this receptor which can arrest the growth of the tumor cells. Most important of them being the development of monoclonal antibodies that target the extracellular domain of the receptor, inhibition of the receptor tyrosine kinase domain, inhibition of the receptor trafficking to the cell membrane and inhibition of EGFR synthesis through antisense oligonucleotides. Among all the above approaches, the development of monoclonal antibodies (panitumumab, transtuzumab, cetuximab) and the development of small molecule inhibitors targeting the receptor tyrosine kinase have been successfully employed in regulating the tumor growth although both the methods suffer from the shortcomings of drug resistance and cytotoxicity issues.[42, 47]

3.1.2. *Small molecule inhibitors:*

Small molecule inhibitors are the ATP competitive inhibitors that target the catalytic site of the receptor kinases or bind to the catalytic site of the receptor. This approach has already proven to be successful with about 10 small kinase inhibitors approved as anti-cancer agents.[76] There are different types of ATP competitive inhibitors based on their binding mode to the receptor: Type-1, Type-2 inhibitors, Type-3 inhibitors, allosteric and covalent inihibitors.[43,49,77] Type-1 inhibitors constitute the majority of ATP competitive inhibitors that bind to the active conformation of the kinase (e.g., gefitinib, erlotinib,etc.). Type-2 inhibitors on the other hand recognize the inactive conformation of the receptor (e.g., lapatinib). Allosteric inhibitors that bind outside the ATP-binding site and covalent inhibitors are the compounds that form an irreversible covalent bond to the active site of kinase.[51] Some representative examples of small molecule inhibitors are presented in the Figure 3.3.

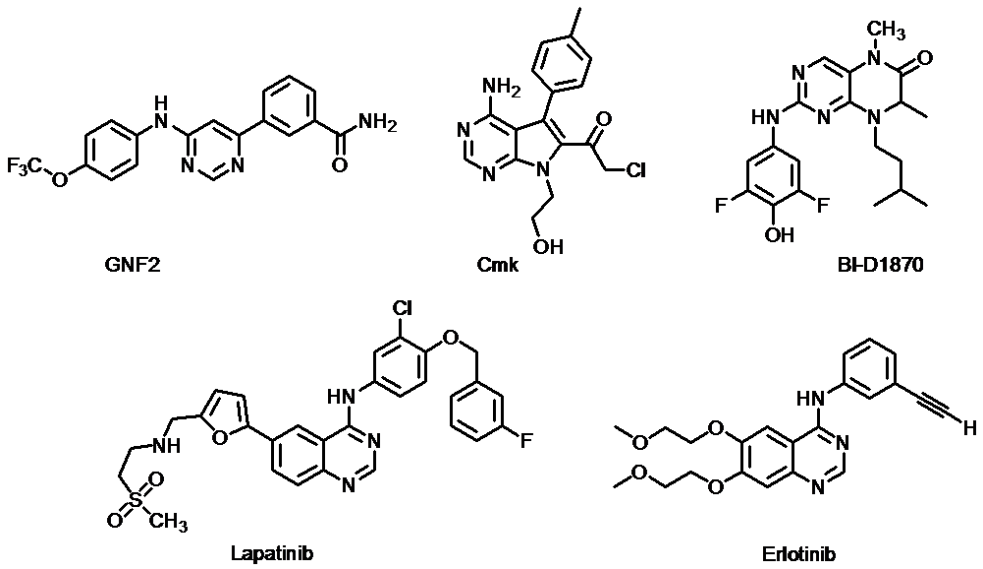

Figure 3.3. **Representative examples of small molecule kinase inhibitors**

3.1.3. Limitations: Although dramatic progress has been achieved in the treatment of cancer using the kinase inhibitor therapy, many challenges still need to be overcome for the successful treatment of these malignant tumors.[78] The intricate array of kinase signaling pathways/cascades in conjunction with mutations and resistance to the inhibitors offer major therapeutic challenges. The crucial factor limiting the efficacy of the small molecule inhibitors is the development of drug resistance which is mainly of two types: acquired and de novo resistances. This highlights the need to study the mechanism underlying drug resistance and the crucial signaling pathways leading to resistance. For this, a deeper understanding of the mechanism of receptor activation and the subsequent signaling pathways is required for the development of effective targeted therapy.[79] Measurement of tyrosine phosphorylated substrates including the tyrosine phosphorylation of the receptor itself provides a most commonly employed technique to study the activated populations of the ERBB receptor. The major shortcoming of this technique is that it cannot differentiate between the high levels of marginally activated populations and small populations of hyperactive receptors with significant mechanistic and clinical relevance. In addition, "pseudoactivation" can occur that can perturb the balance of tyrosine phosphorylation and dephosphorylation. Pseudoactivation can result from the ligand independent activation through other receptor systems such as urokinase plasminogen receptor and the presence of reactive oxygen species (ROS) that inhibit the cellular tyrosine phosphatases. Consequently, elevated ROS can trigger a rapid pseudoactivation of the receptors that competed the ligand stimulation based on phosphotyrosine levels leading to the activation of fundamentally different signaling pathways. This intricate array of interconnected circuits cannot be readily assessed with

the existing methods and therefore more sophisticated methods are required to illuminate the receptor state and activation for a deeper understanding.

3.2. Results and Discussion:

3.2.1. ***Design of DMAQ:***

Our goal was to design and synthesize a highly fluorescent "turn-on" probe to target the ATP binding pocket of ERBB2 receptor with high selectivity and desirable micromolar affinity while retaining the pharmacologically relevant 6-aminoquinazoline core. The striking discovery that 4-anilinoquinazolines and closely related compounds were potent and selective inhibitors of ERBB receptor was done simultaneously by three groups namely Parke-Davis, Zeneca and Ciba-Geigy.[80] Today, there are several kinds of small molecule inhibitors that can bind to the receptor with high potency and selectivity such as pyrrolopyrimidines, pyrimidopyrimidines, quinazolines, and several other fused pyrimidine and quinazoline derivatives. Interestingly, in all these compounds there is one common structural homology which is 4-anilino-pyrimidine fragment which is responsible for the pharmacological activity of the drug/inhibitor.

There are some well known ERBB inhibitors that are potent anticancer drugs such as gefitinib, laptinib, erlotinib and so on. Studies reveal that that both N-phenyl derivatives such as gefitinib or erlotinib and N-benzyl derivatives are potent inhibitors of EGFR with micromolar to nanomolar affinities.[48, 81] Our first step towards the structure based design ERBB inhibitor was selecting the right pharmacophore. As the pharmacological affinity of the quinazoline based inhibitors is already well established with the success of the

quinazoline based drugs, we selected quinazoline as our pharmacophore model for designing kinase inhibitors.

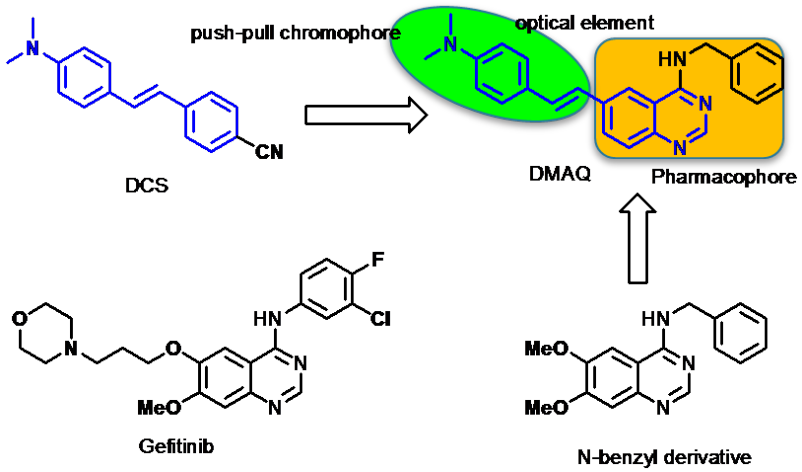

Figure 3.4. **Design strategy for DMAQ:structural resemblance to push-pull chromophore and quinazoline based anti-cancer drug: gefitinib**

We designed a novel "turn-on" probe incorporating a most potent and well established quinazoline pharmacophore conjugated to an optical reporting element. DMAQ (6-(4-dimethylaminostyryl)-*N*-benzylquinazolin-4-amine resembles other fluorescent adenosine mimics but lacks the ribose units found in other adenonise mimics.[82,83] Our probe resembles gefitinib in its structural topology in conjugation with a dimethylamino-substituted styryl arm as demonstrated in the Figure 3.4. The dimethylamino substituent serves as the fluorophore part of the molecule. This unique combination of a pharmacophore and an optical element has successfully led to the development of a novel fluorescent turn-on inihibitor. Our fluorescent probe with electron-rich dimethylamino substituent and an electron-deficient quinazoline core forms a rigid donor-π-acceptor system which is similar to 4-*N,N*-dimethylamino-4'-cyanostilbene (DCS).[84] This unique design renders the molecule with inherent fluorescence which eliminates the need to add an external fluorophore and thereby reduces the steric bulk of the overall probe. This

structural homology makes it highly environment sensitive which is characteristic of a turn-on fluorescent probe. Crystal studies of several inhibitors bound to the ERBB receptor indicate that this chemical modification at the 6-postion does not affect the binding affinity of the pharmacophore to the receptor.[85]

3.2.2. ***Synthesis of DMAQ:***

Synthesis of DMAQ (**3.10**) was accomplished in two steps as shown in the Scheme 3.1. The first step involves the condensation of benzyl amine with 4-chloro-6-iodoquinazoline which was synthesized in two steps from 4-Iodo-anthranilic acid followed by palladium catalyzed Heck-coupling of the resulting intermediate with 4-dimethylamino-styrene.

Scheme 3.1. Synthetic scheme of DMAQ

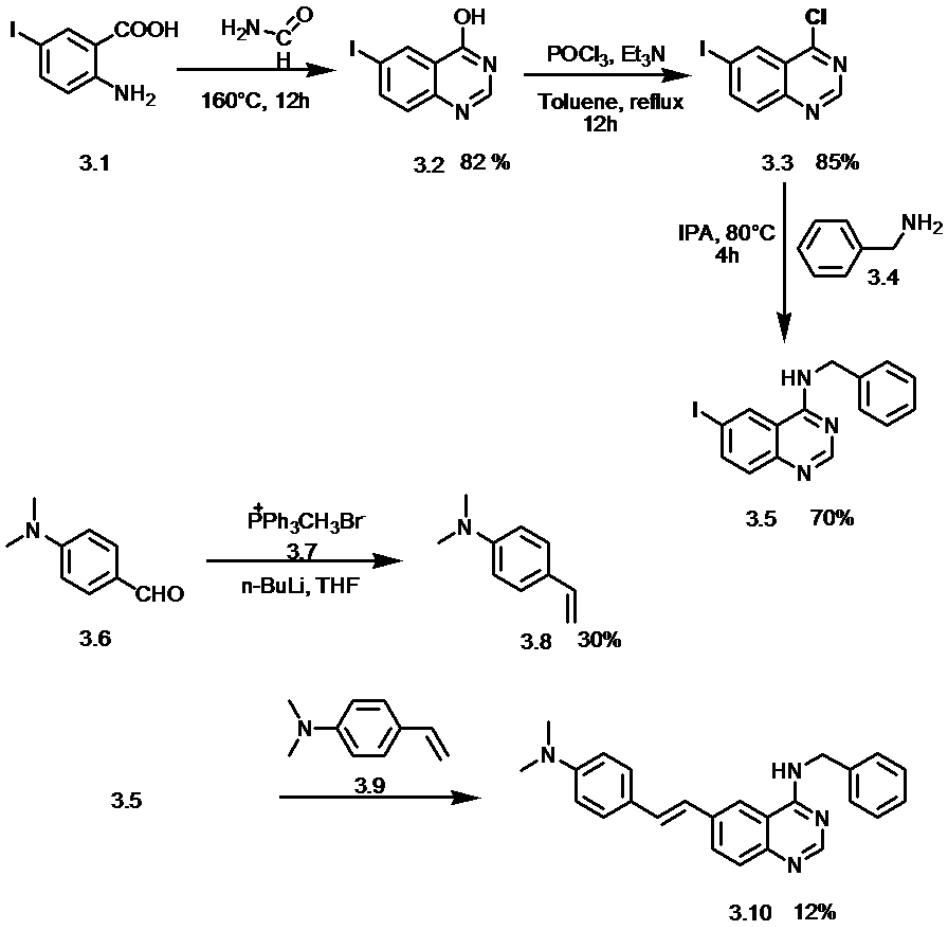

3.2.3. *Absorption spectroscopy*:

When the inhibitor binds to the ATP binding pocket of the receptor, it experiences a considerably rigid and less polar environment.[86] In order to study the fluorescence behavior of the probe in the bound and free states, we took the absorption and emission spectra in PBS, PEG and octanol. Absorption spectroscopy was conducted in PBS, PEG and octanol. PEG and octanol were selectively chosen over a range of solvents as the solution spectroscopy in PEG and octanol mimic a rigid and relatively less polar environment experienced by the bound ligands. The absorption spectrum of DMAQ

reveals a lowest energy optical transition centered in PEG at 380 nm with ε of 22,300 $M^{-1}cm^{-1}$ while in octanol, a slight hypsochromic shift with λ_{max} centered at 374 nm and a hyperchromic shift with ε of 24,300 $M^{-1}cm^{-1}$ was observed (Figure 3.5). Significant/pronounced hypsochromic shift is observed in PBS with λ_{max} centered at 324 nm. This marked difference in the λ_{max} can be attributed to the formation of H-aggregates.[87]

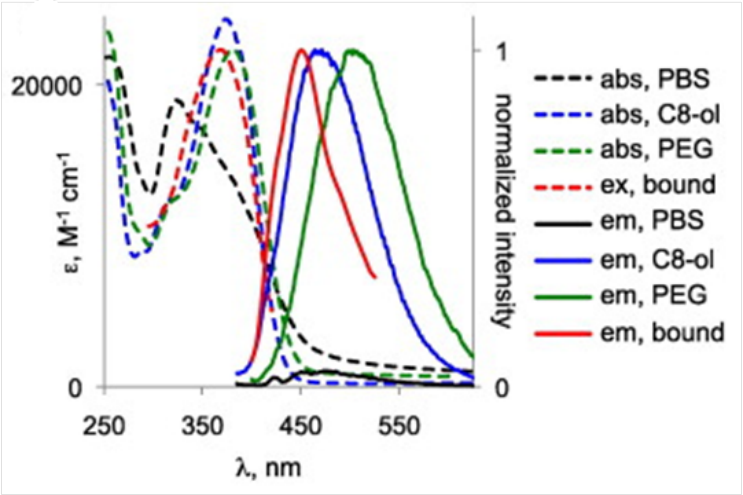

***Figure 3.5*. UV-Vis and fluorescence spectra of DMAQ in PBS, PEG, octanol**

These results clearly demonstrate the potential of DMAQ for imaging purposes as the absorbance data from the above results are comparable to common fluorescent probes such as DAPI and other coumarin derivatives.

3.2.4. ***Emission spectroscopy:***

As the Figure 3.6 demonstrates, very weak fluorescence was observed for DMAQ in PBS with a quantum yield of 0.017, however a dramatic enhancement in the emission intensity was observed for DMAQ in PEG at with a quantum yield of 0.39. Similar emission

enhancement was also observed for the probe in octanol with λ_{max} centered at 471 nm and a quantum yield of 0.38 (Figure 3.5).

Similar emission enhancement was also observed for the probe in octanol with λ_{max} centered at 471 nm and a quantum yield of 0.38. Overall a 23-fold increase in the emission intensity was observed upon going from aqueous solution to a more viscous environment like PEG. We rationalized this emission enhancement as a consequence of two simultaneous phenomena. Firstly, DMAQ tends to form ground state H-aggregates in PBS which results in the intermolecular quenching and therefore fluorescence is very weak or quenched in PBS. On the other hand, switching the solvent from PBS to PEG or octanol, reduces the likelihood of these aggregates, thereby preventing the intermolecular quenching which apparently increases the emission intensity in these solvents.

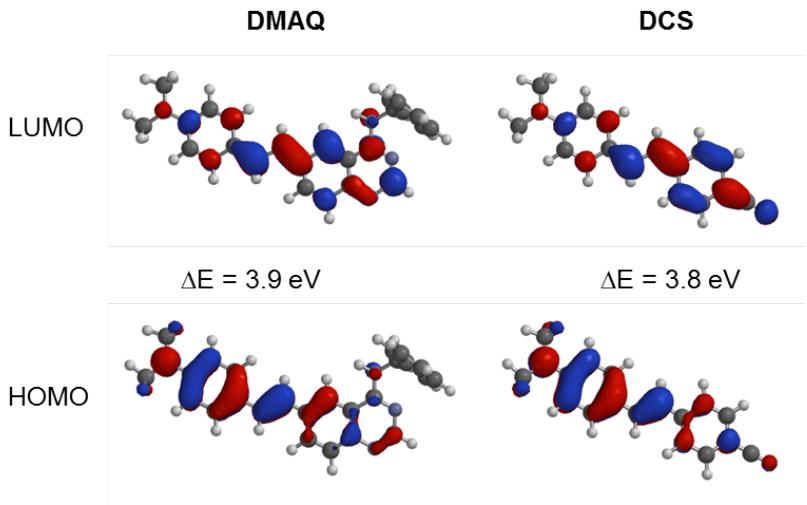

Figure 3.6. **Frontier molecular orbital distribution and energies of DMAQ and DCS: similar energy differences explain the photophysical similarities between DMAQ and DCS**

Moreover the structural resemblance of DMAQ to stilbene like dyes such as DCS possessing both electron-donating and electron withdrawing substituents in the same

molecule renders the molecule highly sensitive to the surrounding environment due to the formation of intramolecular charge transfer (ICT) excited states.[88]

As mentioned before, the presence of dimethylamino group serves as an electron donor and quinazoline ring with two sp^2 hybridized nitrogen atoms acts as a good electron acceptor. Second reason for the increase in the emission enhancement is attributed to the structural confinement of DMAQ when it is docked into the ATP binding pocket of ERBB2. This structural confinement inside the binding pocket prevents the formation of Twisted intramolecular charge transfer (TICT) excited state which consequently leads to the emission enhancement. It was found that stilbene-like dyes such as DCS also show similar emission enhancements when docked/confined in the binding site of antibodies.[84] This close resemblance in the optical properties of DMAQ and DCS prompted us to explore the reasons for the similarities in their photophysical behavior. The frontier molecular orbital (FMO) picture of these compounds provides evidence for this similarity in the photophysical properties. DMAQ and DCS have a very similar FMO topology with almost identical energy differences between HOMO and LUMO illustrating the reason for the photophysical similarities (Figure 3.6).

In order to study the fluorescence behavior of DMAQ on binding with ERBB receptor, we incubated DMAQ with full length, His-tagged ERBB2 receptors which were extracted under mild lysis conditions and subsequently enriched on and eluted from Ni-NTA beads in PBS/EDTA. Upon the addition of DMAQ, the fluorescence 3d scans of the resulting solutions, reveal a excitation centered at 375 nm and emission peak centered at 450 nm. We correlated these spectral results with the solution spectra of DMAQ in PEG and octanol. Strikingly, the absorption and emission spectra of DMAQ when it is bound to the

receptor closely resemble with those in PEG with a λ_{max} of 375 nm and emission maximum at 450 nm as shown in the Figure 3.5.

3.2.5. *Binding of DMAQ to the receptor tyrosine kinases:*

The autophosphorylation of ERBB2 receptor was taken as a measure in order to evaluate the potency of DMAQ to inhibit the receptor. For this purpose, we incubated various concentrations of DMAQ with ERBB2 over-expressing BT474 breast cancer cells for 12 h. We used Western blotting technique to evaluate the autophosphorylation of ERBB2 at Tyr-1139 (normalized for ERBB2 levels). The saturation behavior of fluorescence on enriched ERBB2 preparations (K_d = 2.9 μM) coincides well with the K_i for the inhibition of autophosphorylation (3.1 μM) as depicted in the Figure 3.7. As DMAQ was originally designed to target the ATP binding pocket of ERBB2, the efficiency of DMAQ was measured in terms of the extent to which it targets the ATP binding pocket.

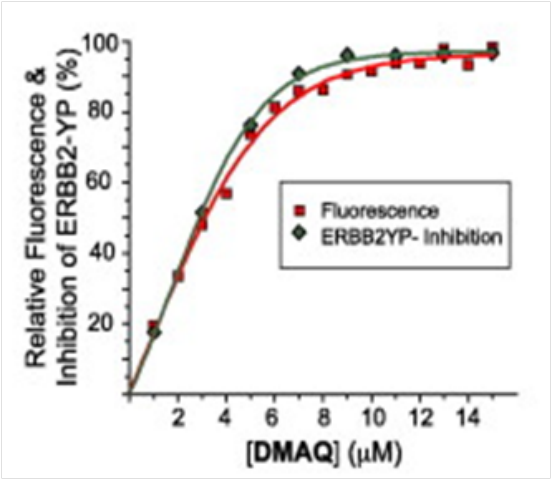

Figure 3.7. **Relative inhibition of ERBB2 autophosphorylation in BT474 cells correlated with saturating titration of DMAQ binding to ERBB receptor**

Among the various receptor tyrosine kinases known in the literature, we selected serine/threonine receptor kinases to evaluate the binding specificity of the current ERBB2 receptor (which as mentioned before belongs to the large family of receptor tyrosine kinases) owing to the common structural characteristics shared between the two receptors such as essential regulatory and catalytic elements.[89] We demonstrated the effect of DMAQ on the PIK3/AKT/mTOR signaling pathway in a MCF7 cell with constitutively active and ERBB independent AKT signaling pathway. The phosphorylation of AKT resulting from the AKT pathway activation was observed during the experiment. Commercially available bifunctional (mTOR/PIK3) inhibitor BEZ23 was used to inhibit the AKT pathway. The Figure 3.8 clearly demonstrates the binding selectivity of DMAQ, where the increasing concentrations of DMAQ appear to have no effect on the AKT pathway. We further validated the specificity of our probe, by demonstrating the ability of DMAQ to inhibit SRC tyrosine kinase which has close structural features with ERBB receptor.

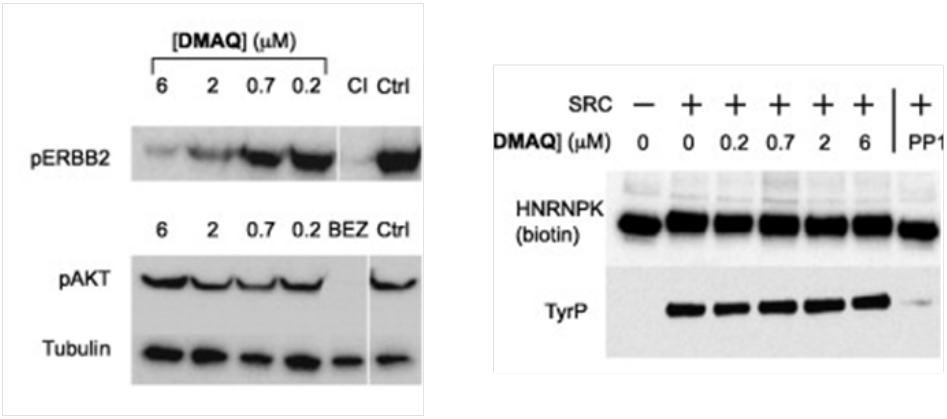

Figure 3.8. **Western blotting evaluation of ERBB2 inhibition by DMAQ and the impact of DMAQ on AKT and SRC phosphorylations**

SRC activity in vitro was validated using recombinant purified SRC and a recombinant biotinylated substrate, the heterogenous ribonucleoprotein K (HNRNPK) and as depicted in the Figure 3.8. SRC dependent phosphorylation was evaluated at different concentrations of SRC after incubation and removal of HNRNPK-biotin. Tyrosine phosphorylation is inhibited in the absence of SRC and the presence of PP1, a known SRC inhibitor (Figure 3.8). We found that the increasing effects of DMAQ have no impact on the phosphorylation of SRC which clearly demonstrates the binding affinity of our probe. We further evaluated the binding affinity of DMAQ by incubating it with the truncated kinase domain of ERBB2 when expressed as a soluble mCherry fusion and presented in the context of whole cell lysate. Canertinib is a commercially available and a known inhibitor of ERBB and it is found that it reversibly modifies a catalytic site proximal cysteine in ERBB1, ERBB2 and ERRB4.[90] Using Canertinib as an ERBB inihibitor, we evaluated the contribution of ERBB2 kinase domain towards fluorescence as delineated in the Figure 3.9.

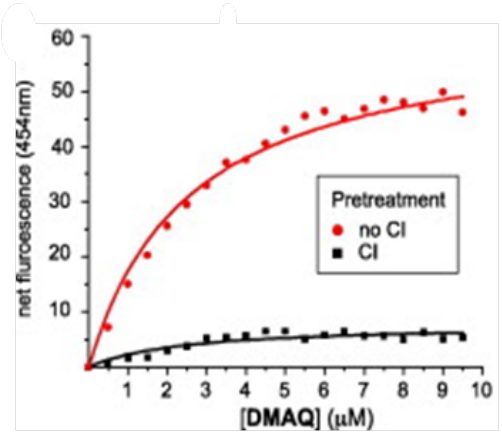

Figure 3.9. **Fluorescence of DMAQ in whole cell lysate with fusion protein of ERBB2 soluble kinase domain and mcherry before and after treatment with Canertinib**

The fluorescence of m-cherry reveals the equivalent recovery of ERBB2 kinase domains from Canertinib treated and non-treated cells. We observed a significant fluorescence from DMAQ despite the low abundance of ERBB2 in cell lysates from less than 10^6 cells (Figure 3.9).

We found that the emission was suppressed by almost 80% in Canertinib pretreated cells which suggests that this signal was contributed by ERBB kinase domain. We presume that the remaining 20% may be derived from alternative targets or from the incomplete covalent modifications of the ERBB2 kinase domain by Canertinib or other sources can be from the unfavorable binding from the covalently coupled and tethered Canertinib with DMAQ still bound to the ATP binding pocket. Also the presence of a large number of low affinity targets contribute to the fluorescence observed in Canertinib treated cells.

3.2.6. ***Experimental section:***

To a clean, dry round bottom flask purged with argon was added 400 mg of 6-iodo-*N*-(phenylmethyl)-4-quinazolinamine[3](1.1 mmol), tris(dibenzylideneacetone)dipalladium 70 mg (0.076 mmol), tri-terbutylphosphine 90 mg (0.44 mm, 0.4 equiv), cesium carbonate 500 mg (1.5 m mmol) followed by the addition of anhydrous dimethylformamide (10 mL). The resulting mixture was degassed with argon and dimethylaminostyrene 160 mg (1.1 mmol) was added and the resulting reaction mixture was heated at 100°C for 24 h to furnish 51 mg of the desired product as a yellow solid after column purification (CH_2Cl_2 → 1:1 CH_2Cl_2:EtOAc) (yield 12%).

6-(4-(dimethylamino)styryl)-N-benzylquinazolin-4-amine (3.10): ^{1}H NMR (400 MHz, DMSO): δ ppm 2.93 (s, 6H), 4.93 (d, 2H, J = 4.1 Hz), 6.72 (d, 2H, J = 7.6 Hz), 7.06 (br d, 1H), 7.24-7.44 (m, 8H), 7.71 (d, 1H, J = 8.1 Hz), 8.1 (d, 1H, J = 8.6 Hz), 8.67 (s, 1H), 8.72 (s, 1H), 10.14 (s, 1H); ^{13}C NMR (125 MHz, DMSO): δ (ppm): 29.0, 44.0, 112.7, 115.6, 119.2, 123.1, 125.1, 127.2, 127.7, 128.0, 128.2, 128.7, 130.3, 131.2, 136.0, 139.9, 148.7, 150.6, 154.9, 159.6; IR ν_{max}cm^{-1}: 700, 754, 777, 817, 878, 967, 1160, 1186, 1225, 1344, 1382, 1445, 1521, 1561, 1598, 2155, 2382, 2790, 3052; HRMS (ESI) *m/z* $C_{25}H_{24}N_4$ $[M+H]^+$ calcd 381.2079, found 381.2075.

3.3. *Conclusions:*

In conclusion, we have successfully designed a fluorescent "Turn-on" ERBB inhibitor targeting the ATP binding pocket of the receptor. DMAQ has been successfully designed and synthesized by the incorporation of a well-known quinazoline pharmacophore and an optical reporting element based on the structure of many stilbene-based dyes. The resulting probe (DMAQ) has attractive physical and optical properties with potential to serve as a good optical tool to investigate the cellular dynamics of ERBB receptor thereby illuminating on the active and inactive populations, receptor activation and signaling pathways. Another fascinating feature of our probes is its cell permeability which can serve as a good foundation for the design of other fluorescent probes for imaging. Moreover, DMAQ allows for the structural modification at the 4-amino position of the pharmacologically relevant quinazoline core to design both Type-1 and Type-2 probes with variable binding to the receptor with tunable optical properties. Additionally, fluorescence can be modulated by modifying the styryl arm fused to the pharmacophore.

In this way, it can serve as a good platform for the design and development of more selective and better inhibitors for the tyrosine kinase inhibitors and the ability to tune the optical properties also shows the potential for imaging purposes. Although DMAQ was designed based on the structure of well-known ERBB inhibitors, there are still some questionable features about its binding. One of them being, the probe may bind to the additional targets at high concentrations due to the close structural resemblances between the receptor tyrosine kinases and secondly large number of distantly related low-affinity ATP-binding scaffolds may cumulatively result in a significant amount of fluorescence. Nevertheless, DMAQ features as one of the first and uniquely designed fluorescent probe which can evolve as a powerful optical tool for the development of efficient inhibitors for receptor tyrosine kinase for the investigation of complex biological processes.

Chapter 4

Evaluation of the Effect of Conjugation Length and Substituents on the Emission and Binding Properties of Fluorescent Kinase Inhibitors

4.1. ***Background:***

Among the vast majority of therapeutic targets against cancer, protein kinases have gained tremendous attention in the recent years.[91] Of the 518 kinases found in the human genome, almost every signaling/signal transduction process is intimately linked through a phosphotransfer cascade which demonstrates the significance of kinases in cellular events. Therefore, the development of small molecule kinase inhibitors against these therapeutic targets has proven to be an effective therapeutic approach/targeted therapy against these malignancies.[43,46,79,91] Despite the high degree of predominance of ATP binding pockets in these kinases, highly selective molecules can be designed and developed with high therapeutic efficiency. Although these small molecule inhibitors have been so far successful in the treatment of several malignant tumors, yet there are some major challenges in this area such as development of drug resistance resulting from mutations, lack of selectivity and efficacy among these inhibitors due to the structural and functional homology of kinases that need to be overcome for achieving high efficacy in these drugs.[78,79]

In this context, monitoring the changes on the receptor kinase states on a qualitative and quantitative basis such as level of expression, oligomerization, conformational changes, phosphorylation and other cellular events is crucial for the deeper/better understanding of kinases.

In this direction, we introduced the concept of "turn-on" fluorescent probes that are ATP competent ERBB/kinase inhibitors to target the ATP binding fold of the receptor tyrosine kinases.[30] We designed our probes incorporating a 4-aminoquinazoline scaffold with aniline substituent at the 4-position and a variable styryl arm at the 6-position. The kinase inhibitors that target the receptor in the active conformation are listed as Type-1 inhibitors (e.g., gefitinib, erlotinib) while those that bind to the inactive conformation belong to Type-2 kinase inhibitors (e.g., imatinib, sorafenib, lapatinib). One can specifically design these inhibitors with variable substitution at the 4-amino position of quinazoline ring which confers specificity and binding affinity to the inhibitor. Additionally, one can design the inhibitors to bind to the specific conformation of the inhibitor by variable substitution at the 4-amino position and we exploited this technique to design state-specific probes. Our pharmacophore arm is composed of quinazoline core with an N-aryl arm at the 4th position. Co-crystal structures of the EGFR kinase domain with inhibitors such as erlotinib (1M17)[92] or lapatinib (1XKK)[85] suggest that the pharmacophore arm is deeply embedded in the ATP binding pocket while the structural variation at the 6-position does not perturb the binding affinity of the inhibitor (Figure 4.1). Based on the above structural information, we designed our probes such that it retains the pharmacological significance without compromising the binding affinity and modified the substituents at the 6-position to tune their optical properties. This implies that one can design the target specific probes with tunable excitation and emission energies by varying the substituents at the 6-position.

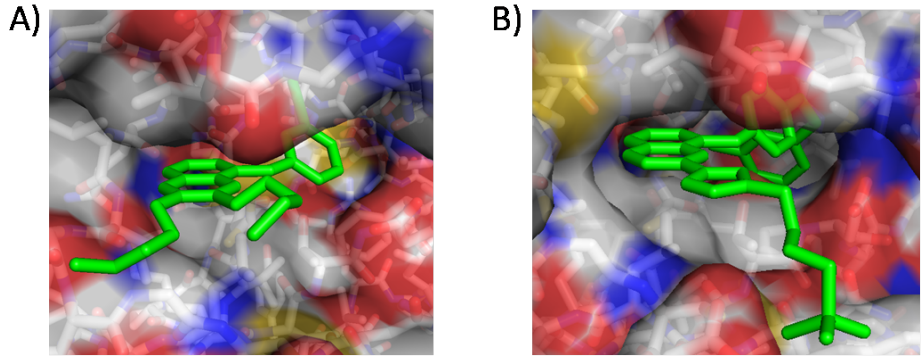

***Figure 4.1*. Crystal structures of the EGFR ATP binding pocket with A) erlotinib (PDB ID: 1M17)[15] and B) lapatinib (PDB ID: 1XKK)[9] reveal the inhibitor binding modes.**

In the current study, we demonstrated the effect of conjugation length and auxochrome substitution on the photophysical properties of a series of *N*-phenyl-4-aminoquinazoline probes. Our studies revealed that extension of the π framework effectively lowers the excitation and emission energies of our probes that compare favorably with other ATP fluorescent analogs.[93,94,95,96] We introduced strong electron donors or strong electron withdrawing groups to generate a strong push-pull system similar to DCS (4-*N,N*-dimethylamino-4'-cyanostilbene) styryl derivatives that are highly sensitive to the external environments. This push-pull system generated several probes with high fluorescence "Turn ON/OFF" ratios, which is crucial for any self-reporting fluorescent kinase inhibitors. Our studies also revealed that the resulting probes have high binding affinity to the ATP binding pocket and the cell permeability is not perturbed with these structural modifications.

4.2. Results and Discussion:

4.2.1. *Design and synthesis of kinase inhibitors:*

We investigated the effect of the electron donating/electron withdrawing ability of substituents and the extension of conjugation between the phenyl ring and the quinazoline core on the optical properties of the ERBB2 binding fluorescent probes.

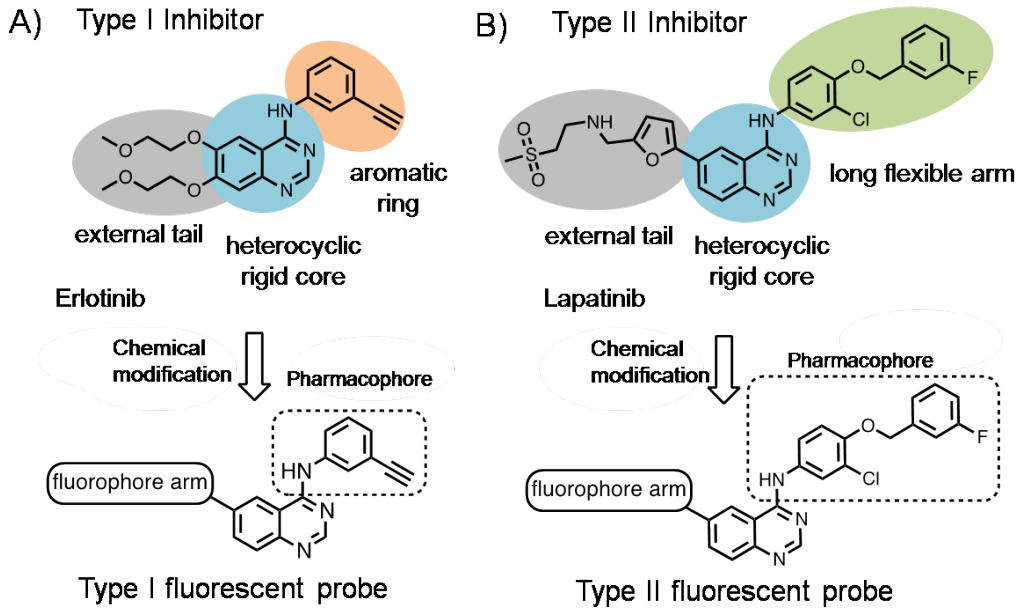

Figure 4.2. The arms at the 6-position of the quinazoline core (blue) of A) and B) may be replaced by fluorophore arms without disturbing the key binding contacts

The substituents on the phenyl ring varied from the strong electron donating dimethylamino group (**4.11**, **4.16** and **4.21**) to strong electron withdrawing nitro substituent (**4.15**, **4.20**, **4.25**) and in the absence of any substituents (**4.13**, **4.18**, **4.23**), phenyl ring served as the electron-donor and quinazoline ring with the imine/sp^2 hybridized nitrogen atoms served as the electron acceptor (Figures 4.2 and 4.3).

Scheme 4.1. Synthetic scheme for the synthesis of 4.5 and the styryl and phenyl butadiene derivatives:

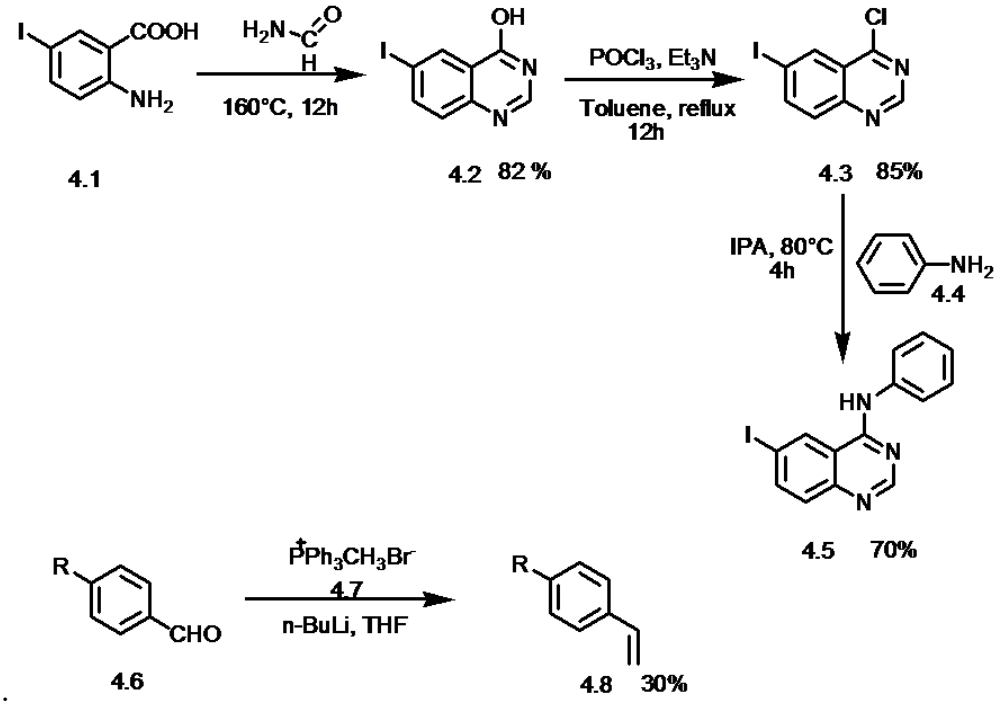

We synthesized a total of 15 kinase inhibitors from one common intermediate 6-iodo-*N*-phenyl-4-quinazolin-amine (**4.5**) which was synthesized from 4-Iodo-anthranilic acid (Scheme 4.1). We synthesized the styryl and the butadiene derivatives by Wittig reaction of the corresponding aldehydes with triphenylphosphonium bromide (Scheme 4.1).

Scheme 4.2. Synthetic routes to fluorescent kinase inhibitors (4.11-4.25)

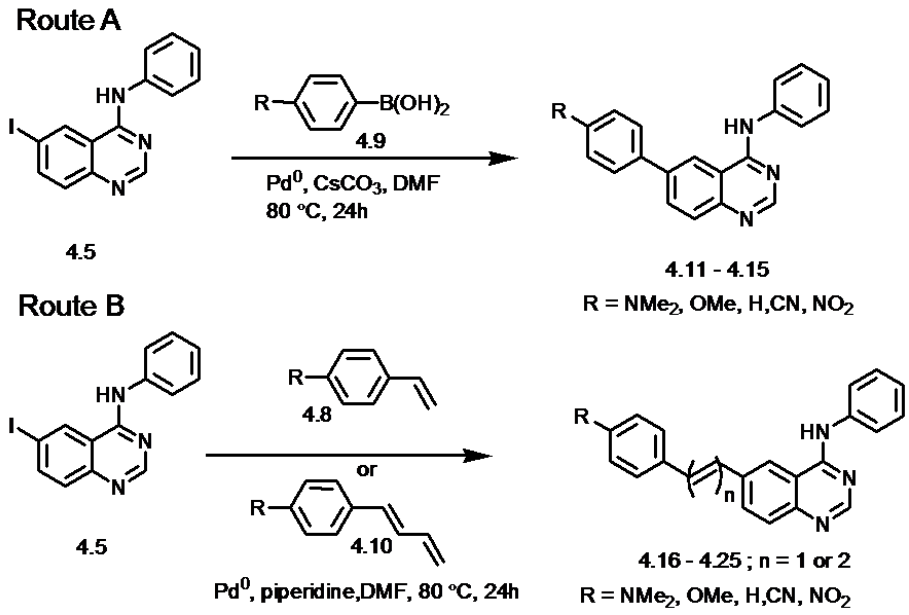

Compounds (**4.11-4.15**) were synthesized by Suzuki coupling of the appropriate aryl boronic acid and compounds (**4.16-4.25**) were synthesized by Heck coupling of styryl and phenyl butadiene arms (Scheme 4.2) followed by subsequent reaction work up and purification by flash chromatography and recrystallization furnished the products in moderate yields.[31] Our probes were obtained as crystals that varied from colorless to bright red or orange-yellow.

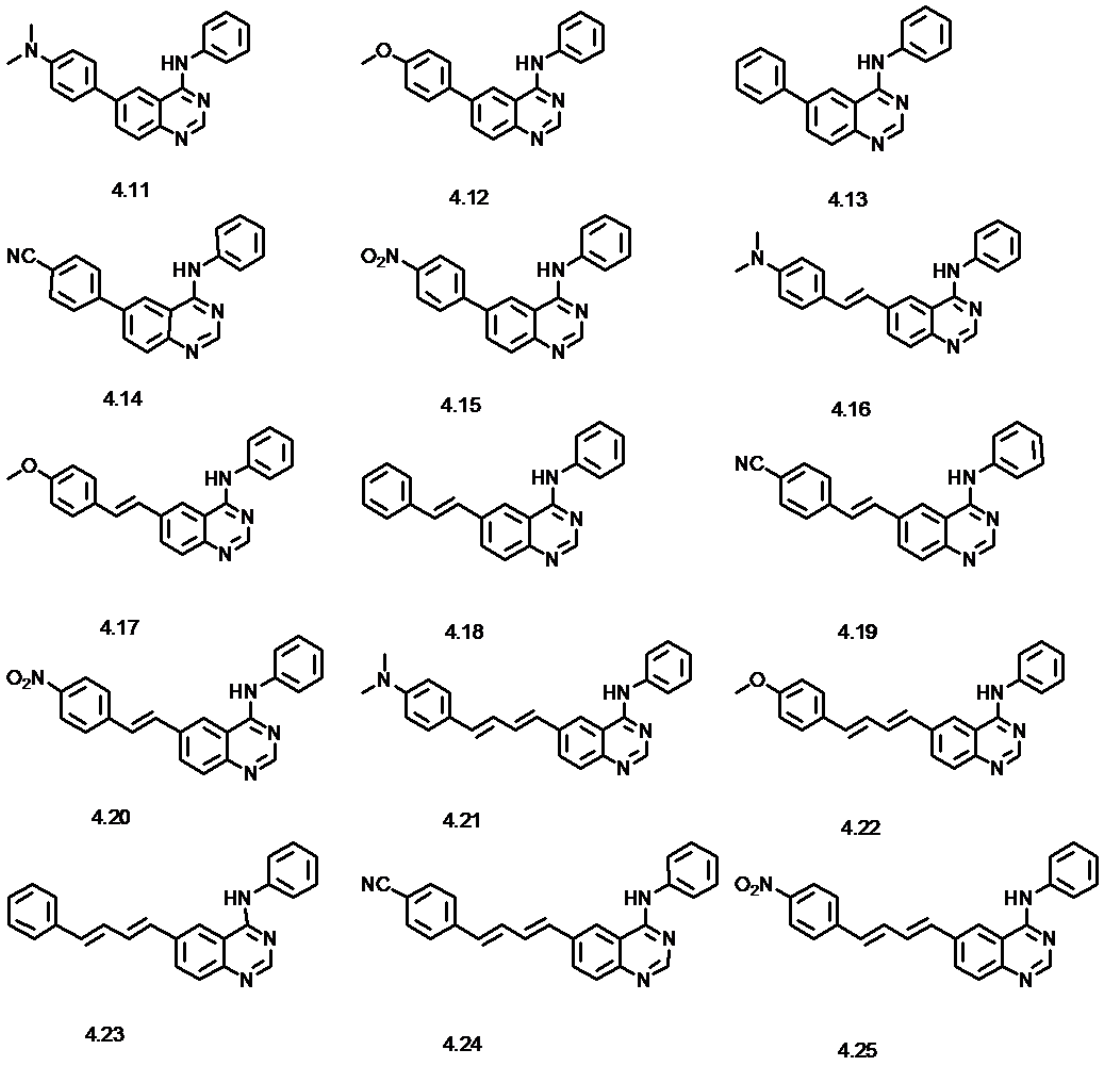

***Figure 4.3*. Structures of fluorescent kinase inhibitors**

Representative synthesis via Route A:

Representative synthesis of ***6-(4-(dimethylamino)phenyl)-N-phenylquinazolin-4-amine (4.11)***: 347 mg (1.0 mmol) of 6-iodo-*N*-phenyl-4-quinazolin-amine (4.5), 248 mg (1.5 mmol) of boronic acid, 425 mg of $CsCO_3$ (1.3 mmol) and 3 mL of DMF were placed in a 25 mL schlenk flask with a stirbar under argon purge. The reaction mixture was degassed for a further 20 minutes under a slow stream of argon at which point 25 mg of a

1:2 mixture of $PdCl_2(PPh_3)_2$ and PPh3 was added. The reaction was heated at 80°C for 24h, cooled and extracted with EtOAc after addition of H_2O. The organic layer was concentrated and purified over silica (100% CH_2Cl_2 to 100% EtOAc), followed by crystallization from 2-propanol/EtOAc to afford **4.11** (47 mg, 14%); mp 257-259 °C (decomp).

Representative synthesis via Route B:

Representative synthesis of ***(E)-6-(4-methoxystyryl)-N-phenylquinazolin-4-amine (4.17)***: 500 mg (1.44 mmol) of 6-iodo-*N*-phenyl-4-quinazolin-amine (**4.5**), 289 mg (2.2 mmol) of 4-vinylanisole, 0.38 mL of Et_3N (2.87 mmol) and 5 mL of DMF were added to a 50 mL schlenk flask under argon. The reaction mixture was degassed for a further 20 minutes under a slow stream of argon at which point 48 mg of $Pd(OAc)_2$ and 56 mg of PPh_3 and the subsequent mixture was further degassed and heated at 80-85°C for 24 h, cooled, poured into 100 mL H_2O and extracted with EtOAc. The organic layer was concentrated and purified over silica (100% CH_2Cl_2 to 100% EtOAc), followed by crystallization from 2-propanol to afford **4.17**.

4.2.2. *Quantum chemical calculations:*

We envisaged that the optical properties of any fluorescent probe can be tuned by varying the electron-donating or withdrawing ability of the substituents and by modifying the conjugation length. In general, fluorescent probes are non-emissive in solution due to the fluorescence quenching by the intra-molecular charge transfer state (ICT) resulting from the electron transfer from the electron-donor to the acceptor in the molecule. While upon binding to the ATP binding pocket, due to the spatial constraints inside the pocket, the

formation of ICT is prevented and the molecule turns-on or becomes fluorescent. Under these conditions, the probe most likely possesses an excited state with a high degree of charge transfer (CT) character and forms a twisted intramolecular charge transfer state (TICT) state which prevents the fluorescence quenching and lights up the probe.

Molecular orbital study from the TD-DFT calculations (6-31G*, CHCl3, SMD solvent model)[97] indicate that both strong electron donors and strong electron acceptors will lead to a S_1 state with charge transfer(CT) character. We found that for all the 15 compounds in the series, S_1 state is accessible via the allowed one electron transition from the HOMO to LUMO with energy differences varying from 2.5eV for **4.25** to 3.6 eV for **4.13**.

The HOMO-LUMO band gap is most effectively lowered by 0.5-0.3 eV with the introduction of a strong electron-donating dimethylamino group while an energy difference of 0.8-0.5 eV is observed for the strong electron-withdrawing nitro group. However, the HOMO-LUMO bandgap/energy differences were found to be low ranging from 0.1 to 0.2 eV for the probes with moderately electron-donating or withdrawing groups(i.e. –OMe or CN) in comparision to other unsubstituted analogs (**4.13**, **4.18** and **4.23**). Also results indicated that the addition of each vinylene bridge lowers the S_1 transition energy by nearly 0.25 eV.

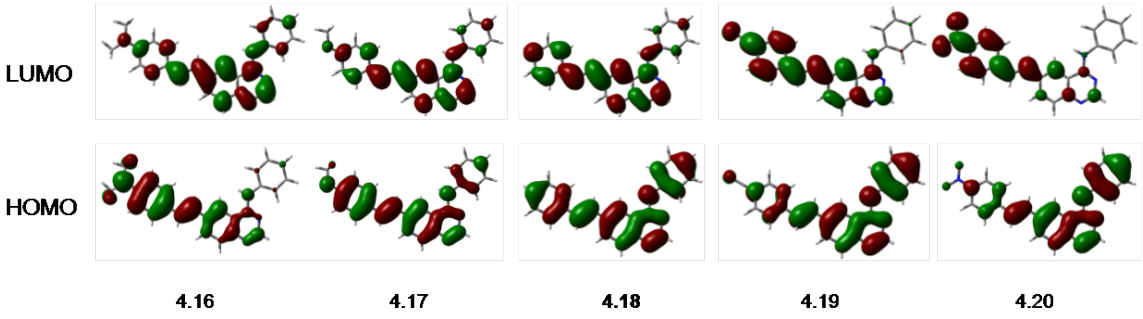

***Figure 4.4*. Frontier molecular orbitals of 4.16-4.20 (calculated at the CAM-B3LYP/6-31G* level and the polarization shifts across the series (4.16 and 4.20)**

Table 4.1: Calculated (TDDFT/CAM-B3LYP/6-31G*)[a] S_1 energies and S_0 to S_1 Oscillator strengths

Compounds	4.11	4.12	4.13	4.14	4.15	4.16	4.17	4.18	4.19	4.20	4.21	4.22	4.23	4.24	4.25
$\Delta E\ S_0 \rightarrow S_1$/eV	3.9	4.0	4.1	4.0	3.9	3.6	3.8	3.8	3.7	3.5	3.3	3.5	3.6	3.4	3.3
f	0.7	0.7	0.7	0.8	0.8	1.7	1.5	1.4	1.6	1.5	2.3	2.1	2.0	2.2	2.0

aCHCl3, SMD solvent model.

Based on these quantum mechanical studies, we found that the electron-donating or electron-withdrawing substituents on the pendant phenyl arm can be used to tune the HOMO-LUMO band gap of the probes and in addition the charge transfer (CT) character of the excited state is also affected by the presence of these groups on the ring. As the figure 4.4 illustrates, the presence of strong electron donating groups such as in the series of dimethylamino substituted compounds (e.g., **4.16**) the HOMO is largely localized to the fluorophore arm while the LUMO is concentrated on the quinazoline core. In contrast, the introduction of an electron-withdrawing group i.e. $-NO_2$ or CN, on the fluorophore arm switches the frontier molecular orbital distribution where the HOMO is localized on the quinazoline core while the LUMO is polarized to the styryl arm which is a strong electron-acceptor and this high CT character in the excited state results in the promotion of electron from the HOMO to the LUMO. Compounds with moderate electron-donating or withdrawing groups from **4.17-4.19** show a gradual redistribution of frontier orbital energies between the two extremes. Compounds **4.11-4.15** and **4.21-4.25** also show a similar distribution of frontier molecular orbitals.

4.2.3. ***Absorption spectroscopy:***

Ideally, "turn-on" fluorescent probes should be non-emissive in the polar solvents and become highly fluorescent in the less-polar solvents. The photophysical properties of our compounds were similar to those of "turn-on" probes as they were emissive in less-polar solvents such as toluene and cyclohexane while they were highly fluorescent in polar solvents such as water and methanol. This optical output can be visually observed in chloroform solutions where most of our probes are highly fluorescent with emissions ranging from bright blue (**4.17** and **4.23)** to green (**4.11** and **4.16**) to yellow or orange (**4.21** and **4.25**) as shown in Figure 4.5. We obtained the UV-Vis and emission spectra for our probes in $CHCl_3$, toluene and methanol.

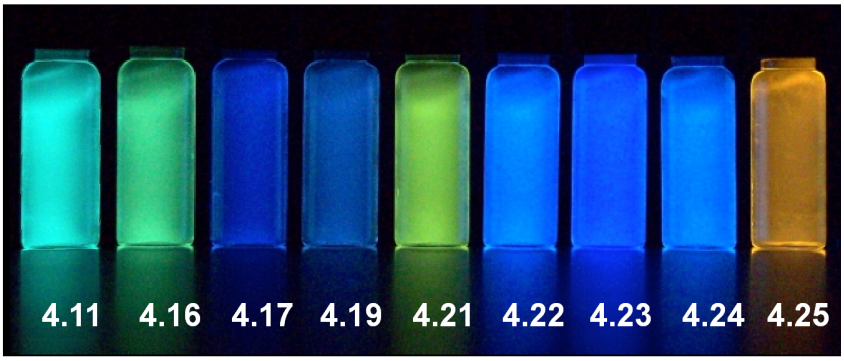

***Figure 4.5*. Chloroform solutions of selected probes (5 µM) under UV light (354 nm)**

We found a good correlation between the absorption maxima (λ_{max}) and the transition energies where with increasing conjugation length as the λ_{max} increases, the transition energies also show a gradual increase (Table 4.1). Our studies revealed that auxochromes have a direct effect on the absorption wavelengths and the transition energies where changes in the auxochromes enhances the CT character resulting in longer wavelength absorption lacking vibronic structure. Compounds with moderate electron-donating or

withdrawing groups show some vibronic structure in the absorption spectra, however their excited states reveal some degree of CT although emission spectra lack any such vibronic progressions. The good to moderate molar aborptivities indicate that the probability of S_0-S_1 transition is relatively high for most of our probes. We found that the extinction coefficients increase with the increase in the conjugation length for our probes and this trend can be rationalized on the basis of spatial overlap of frontier molecular orbitals; Molar absorptivities for compounds **4.16-4.20** were roughly twice the values observed for **4.11-4.15** while molar absorptivities for compounds **4.21-4.25** are roughly three times greater than **4.11-4.15**.

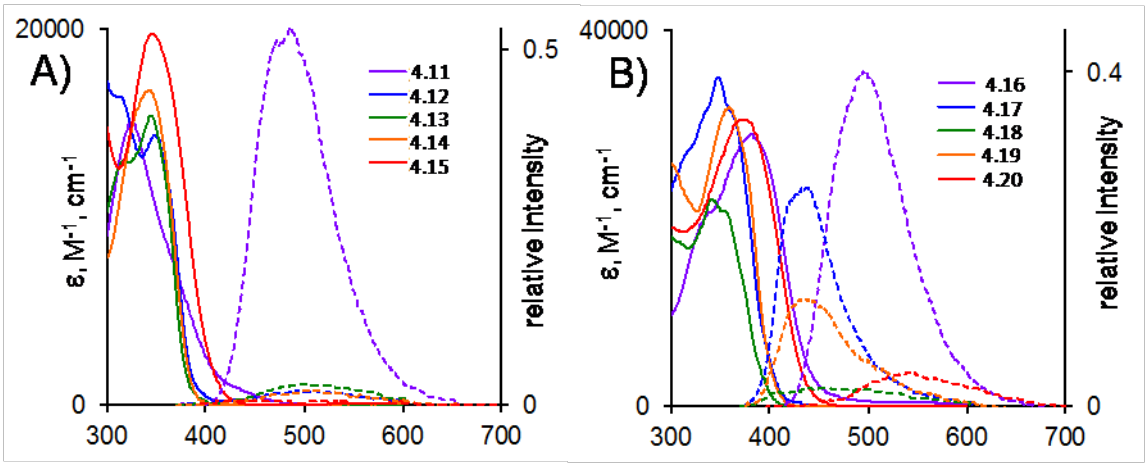

Figure 4.6. **Absorption (solid lines) and emission (dashed lines) spectra of A) 4.11-4.15 B) 4.16-4.20.**

4.2.4. ***Emission spectroscopy:***

Our probes were highly fluorescent with moderate to good quantum yields. We found that the presence of strong electron donating or withdrawing groups and the increase in conjugation length results in longer wavelength emission. As shown in the Figure 4.7,

4.23 exhibits bluest emission while the compound with strong electron withdrawing-NO_2 group (**4.25)** exhibits reddest emission with an emission peak centered at 561 nm.

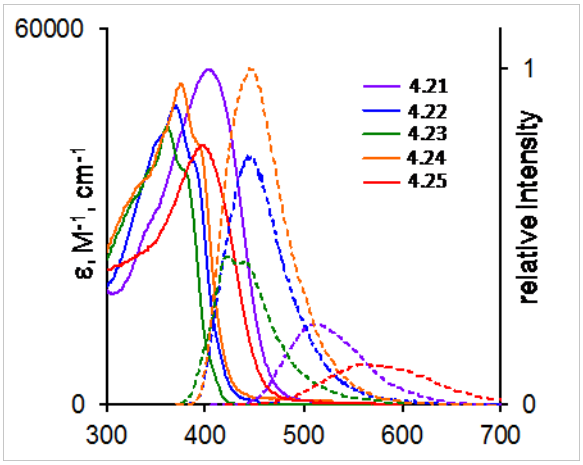

Figure 4.7. **Absorption (solid lines) and emission (dashed lines) spectra of 4.21 – 4.25 in $CHCl_3$.**

Strikingly, we did not see the correlation between the poor quantum yields and strong CT character as the compounds with strong electron donating dimethylaminogroup (**4.11**, **4.16** and **4.21**) have moderate quantum yields although their excited states have high CT character which is indicated by the quantum yield of **4.11** (Φ_{em} = 0.37) and in the styryl quinazoline series, compounds with strong electron-donating dimethylamino group have high quantum yields. However this increase in quantum yield under the auxochrome influence is not consistent throughout the series) as inferred from the Table 4.2 that the quantum yield increases with increasing conjugation length irrespective of the type of auxochrome.

Table 4.2: Photophysical characteristics of 4.11–4.25

Cpd	$\lambda_{max,abs}$ (nm)	ε ($M^{-1}cm^{-1}$)	$\lambda_{max,em}$ (nm)	Φ_{em}[a]	Δn (cm^{-1})	T_1 (ns)	f_1	T_2 (ns)	f_2	χ^2
4.11	325	15000	485	0.37	10,200	1.22	0.03	6.54	0.97	2.46
4.12	348	14300	510	0.02	9130	1.39	0.70	6.76	0.30	5.89
4.13	344	15400	502	0.03	9150	0.56	0.06	1.60	0.94	2.88
4.14	343	16700	508	0.02	9470	0.17	0.18	1.29	0.82	1.47
4.15	346	19700	446	0.006	6480	0.11	0.74	1.56	0.26	10.2
4.16	381	28800	495	0.28	6050	0.69	0.08	2.49	0.92	3.65
4.17	347	34900	440	0.15	6090	0.89	0.57	1.50	0.43	2.17
4.18	341	21900	455	0.02	7350	0.05	0.11	1.75	0.89	4.86
4.19	358	31700	436	0.09	5000	0.12	0.30	1.46	0.70	0.57
4.20	372	30400	539	0.04	8330	0.38	0.83	1.60	0.17	1.77
4.21	403	53300	510	0.17	5210	0.80	0.77	2.48	0.23	1.47
4.22	369	47500	443	0.42	4530	0.77	0.43	1.90	0.57	1.24
4.23	361	44300	422	0.25	4000	0.54	0.32	1.78	0.68	1.33
4.24	375	51000	445	0.57	4200	0.23	0.21	1.57	0.26	0.86
4.25	391	41200	561	0.11	7750	0.40	0.37	1.04	0.63	1.16

a±10%

4.2.5. ***Determination of turn-on ratio:***

Two important factors need to be considered for designing a fluorescent reporter. One is the overall brightness and the second is the turn-on ratio factor which is crucial in choosing the compound as an optical reporter.[98] We chose water and octanol to calculate the turn-on ratios for our compounds as they represent two distinct environments and most widely used solvent systems for biological applications.[99,100] Of all the compounds in the series, **4.11**, **4.16** and **4.25** showed highest ON/OFF ratios with emission enhancements over 50 fold and compounds **4.19**, **4.21**, **4.22** and **4.24** represent the ones with moderate turn-on ratios while compounds in the series 1 practically showed no enhancements (Figure 4.8).

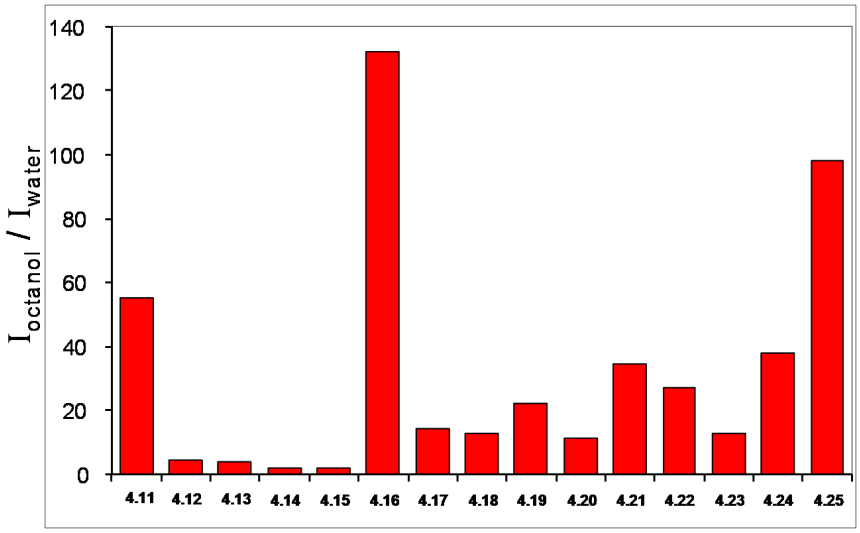

***Figure 4.8*. Emission intensities of 4.11–4.25 obtained in octanol and water reveal high ON/OFF ratios.**

4.2.6. *Inhibition studies of the probes:*

Co-crystal studies of the receptor with inhibitors such as lapatinib[85] and geftinib[101] indicate that the quinazoline core along with the 4-amino position are responsible for binding while the substitution at the 6-position in some cases lowers K_{aff} of inhibitors.[102] In order to evaluate the binding affinity of our probes in a cellular environment, we selected the compounds with high and reasonably high turn-on ratios such as **4.11**, **4.16**, **4.19**, **4.24** and **4.25** and determined their affinity/inhibition on MCF-7 cells using 10 μM and 100 nM probe concentrations (Figure 4.9). We found that all five probes showed inhibition of NRGβ1 (neuregulin family) induced phosphorylation of ERBB2 receptor at 10 μM concentrations. In contrast, probes showed little to no inhibition at 100 nM concentrations. These observations demonstrate two important features of our probes: One is that the permeability of the probes remains unaffected on chemical modification at 6-position which is indicated by their binding to the intracellular domain of the receptor

and the other feature is that their binding affinity is not altered despite the extension of conjugation or the presence of bulky substituents on the 6-position.

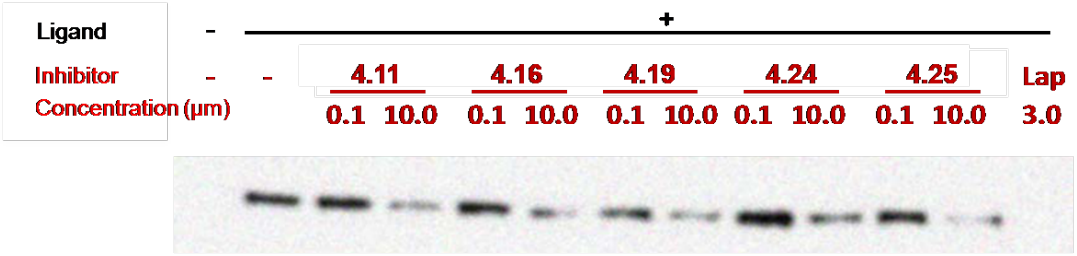

Figure 4.9. **Inhibition of NRG*β*1-induced ERBB2 tyrosine phosphorylation in MCF7 cells at 0.1 and 10 µM concentrations of the selected compounds.**

Inhibition curve:

We further evaluated the inhibition potency of our probes towards ERBB2 receptor by obtaining the inhibition curves (Figure 4.10). We selected the probe with the shortest arm at 6-position (**4.11**) and longest arm (**4.24**) and obtained their inhibition curves. As shown in the Figure 4.9, the binding constants (K_i) for these compounds were similar with values of 10 µM for **4.11** and 9 µM for **4.24**. K_d for the recombinant EGFR kinase domains was found to be 1 nM. [103] K_d for live cells treated with gefitinib was found to be 2-3 nM after the competition with cellular ATP was taken into account.[104] We compared these values with those obtained for our probes and intriguingly our probes showed comparable potency. During our studies, we found that **4.11** showed complete inhibition of ERBB2 phosphorylation at ~20 µM while on the other hand **4.24** with the longest arm did not provide the similar results as is evident from the Figure 4.9. We could not rationalize the above finding based on $\mathbf{P}_{\text{octanol/water}}$ were found to be 1.50 and 1.55 respectively.

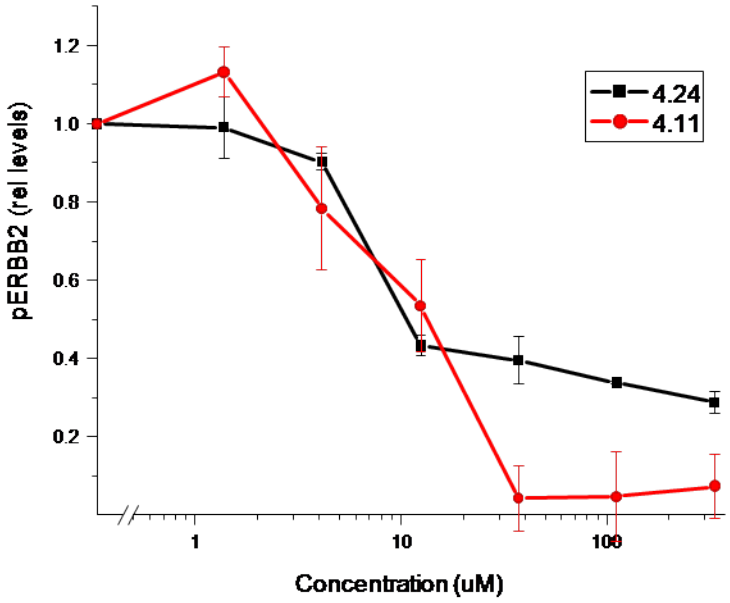

Figure 4.10. **Differences in the inhibition of ERBB2 phosphorylation by compounds 4.11 and 4.24**

These differences in inhibition curves were explained based on the previous studies where gefitinib (Type I inhibitor) and lapatinib (Type II inhibitor) exhibit different binding modes. For instance, gefitinib shows partial inhibition whereas lapatinib shows complete inhibition. Further studies on the binding modes of these compounds are currently in progress.

4.2.7. ***Binding-induced turn-on emission:***

After evaluating the turn-on efficiency and the inhibition potency of our compounds, we investigated if our probes exhibited turn-on emission upon binding to ERBB2 receptor. For this purpose, we selected **4.11**, **4.16** and **4.25** that showed highest "turn-on" ratios and obtained the emission spectra of these compounds in the presence and absence of the soluble ERBB2 kinase domain in PBS (Figure 4.11). The probes behaved in accordance

with our assumption and we found that the fluorescence of the probe was completely quenched in PBS alone, however with the addition of ERBB2 kinase domain, the probes **4.11** and **4.16** with the dimethylamino substituent showed significant emission enhancement while **4.25** did not show any such enhancements. For **4.11**, the increase was 4-fold with an enhancement of 10 nm and emission wavelength centered at 435 nm while for **4.16**, the emission enhancement was 8-fold with an emission increment of 12 nm centered at 560 nm. For this experiment, we used 1 μM of **1a** and **2a** and 100 nM of ERBB2 and wavelength of excitation (λ_{max}) is 370 nm.

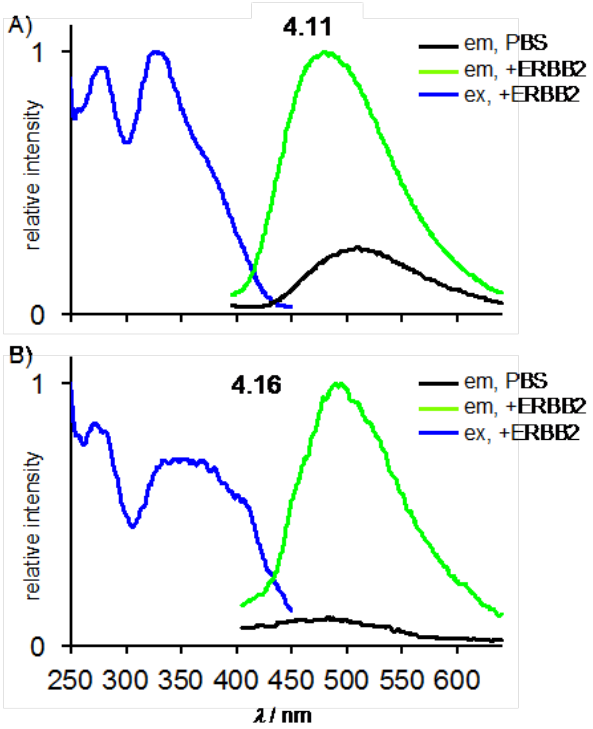

Figure 4.11. **Turn-on emission of compounds 4.11 and 4.16 upon binding to the soluble ERBB2 kinase domain:Emission quenching was observed in PBS alone and the turn-on response on binding to ERBB2 kinase domain.**

Surprisingly, no emission enhancement was observed for **4.25**, although it exhibits solvent sensitivity and inhibition of ERBB2 autophosphorylation. We assumed that this may be resulting from the extension of the longer conjugated arm beyond the binding pocket and the subsequent exposure of the probe to the polar solvent environment or PBS.

4.2.8. ***Experimental section:***

General Methods. Reagents and solvents were obtained from commercial suppliers and used without further purification. ^{1}H NMR and ^{13}C NMR spectra were recorded on a 500 MHz spectrometer. Absorbance spectra were obtained using probe concentrations of 10 μM. Fluorescence studies were performed using probe concentrations of 1 μM. For determination of ϕ_{em} solutions were prepared to an optical density of 0.05 or less in order to minimize inner filter effects. Perylene in cyclohexane was used as a reference for quantum yields.[25]

Computational Methods. Quantum chemical calculations were carried out utilizing the Gaussian '09 suite of electronic structure modeling software.[26] Ground state geometries of the dyes were optimized by DFT with the B3LYP/6-31G* method using Truhlar's SMD solvation model.[16] Vertical transition energies were obtained by TD-DFT calculations with the B3LYP/6-31G* with the SMD model. Molecular orbitals were visualized using the GaussView 5 program. The coordinates of optimized geometries are provided in the Supporting Information.

Inhibition of ligand induced receptor activation. MCF cells were seeded with equal quantity (200 thousand/well) in six-well plates. After 48 hours, cells were pre-treated

with small molecule inhibitors of various concentrations for 1 hour before induction by neuregulin (NRGβ1, 20 *nM*, 15 minutes). Cell lysates were generated immediately by SDS lysis. Equal aliquots were subjected to SDS-PAGE and Western blot analysis. ERBB2 phosphorylation was evaluated for Tyr1239 located close to the extreme cytoplasmic C-terminus of the receptor (validated by pan-TyrP detection (4G10). The signal obtained for pTyr1239 relative to the ERBB2 receptor levels was determined as the relative receptor phosphorylation.

6-(4-(dimethylamino)phenyl)-N-phenylquinazolin-4-amine (4.11):; ^{1}H NMR (500 MHz, DMSO-D_6): δ (ppm) 2.98 (s, 6H), 6.87 (d, 2H, J = 8.9 Hz), 7.15 (t, 1H, J = 7.4 Hz), 7.41 (t, 2H, J = 8.3 Hz), 7.78 (t, 3H 8.4 Hz), 7.86 (d, 2H, J = 8.4 Hz), 8.14 (dd, 1H, J = 8.7, 1.8 Hz), 8.53 (s, 1H), 8.73 (s, 1H), 9.88 (s, 1H); ^{13}C NMR (125 MHz, DMSO-D_6): δ (ppm) 40.4, 112.9, 116, 118.6, 123, 124.1, 126.8, 128, 128.6, 128.9, 131.4, 138.7, 139.6, 148.7, 150.5,.154.2, 158.1; IR ν_{max} (cm^{-1}): 2957.1, 1934.3, 1600.9, 1568.8, 1523.8, 1499.1, 1446.5, 1403.8, 1357.4, 1327.4, 1290.7, 1228.1, 810.1, 744.4, 692.5 HR-ESI (Q-TOF) *m/z*: calcd for $C_{22}H_{21}N_4$ $[M+H]^+$ calcd 341.1766, found 341.1770.

(E)-6-(4-methoxystyryl)-N-phenylquinazolin-4-amine (4.17). Yield: 111 mg, 22%; mp: 238-241 °C (decomp.); IR ν_{max} (cm^{-1}): 3034.4, 1600.9, 1568.2, 1524.6, 1512.3, 1495.0, 1445.8, 1409.0, 1358.4, 1272.8, 1250.3, 1174.0, 837.0, 751.3, 688.5; ^{1}H NMR (500 MHz, DMSO-D_6): δ (ppm) 3.80 (s, 3H), 7.00 (d, 2H, J = 8.7 Hz), 7.15 (t, 1H, J = 7.3 Hz), 7.24 (d, 1H, J = 16.4 Hz), 7.40– 7.45 (m, 3H), 7.60 (d, 2H, J = 8.6 Hz), 7.76 (d, 1H, J = 8.6 Hz), 7.86 (d, 2H, J = 7.6 Hz), 8.10 (d, 1H, J = 8.0 Hz), 8.55 (s, 1H), 8.67 (s, 1H), 9.79 (s, 1H); ^{13}C NMR (125 MHz, DMSO-D_6): δ (ppm) 55.6, 114.8, 115.9, 120.2, 122.8, 124.2,

125.7, 128.3, 128.5, 128.9, 129.9, 130.1, 131.6, 136.0, 139.6, 149.6, 154.5, 158.0, 159.7; HR-ESI (Q-TOF) *m/z*: calcd for $C_{23}H_{21}N_3O$ $[M+H]^+$ calcd 354.1606, found: 354.1621.

6-(4-methoxyphenyl)-N-phenylquinazolin-4-amine (4.12). Yield: 52 mg, 16%; mp 245-247 °C. IR ν_{max} (cm^{-1}): 2999.8, 2835.4, 1937.5, 1600.6, 1570.2, 1522.6, 1496.5, 1445.4, 1400.9, 1358.3, 1270.5, 1247.2, 828.7, 818.3 753.3; ^1H NMR (500 MHz, DMSO-D_6): δ (ppm) 3.83 (s, 3H), 7.11 (d, 1H, J = 8.7 Hz), 7.15 (t, 2H, J = 7.4 Hz), 7.42 (t, 2H, J = 8.1 Hz), 7.81-7.86 (m, 5H), 8.15 (dd, 1H, J = 8.7, 1.5 Hz), 8.57 (s, 1H), 8.79 (s, 1H), 9.93 (s, 1H); ^{13}C NMR (125 MHz, DMSO-D_6, TFA) δ (ppm) 55.7, 114.6, 115.0, 120.8, 122.1, 124.9, 126.8, 128.8, 129.2, 130.7, 134.3, 137.4, 139.7, 140.1, 151.7, 159.8, 160.2; HRMS HR-ESI (Q-TOF) *m/z*: calcd for $C_{21}H_{18}N_3O$ $[M+H]^+$ calcd 328.1449, found: 328.1453.

N, 6-diphenylquinazolin-4-amine (4.13). Yield: 41 mg, 14%; mp 258-262 °C; IR ν_{max} (cm^{-1}): 3067.3, 1939.0, 1600.5 1567.8, 1528.9, 1488.6, 1445.3, 1405.6, 1359.8, 1325.9, 1295.0, 840.7, 748.5, 689.2; ^1H NMR (500 MHz, DMSO-D_6): δ (ppm) 7.16 (t, 1H, J = 7.3 Hz), 7.40 - 7.46 (m, 3H), 7.56 (t, 2H, J = 7.6 Hz), 7.85 – 7.91 (m, 5H), 8.20 (d, 1H, J = 8.7 Hz), 8.59 (s, 1H), 8.86 (s, 1H), 9.96 (s, 1H); ^{13}C NMR (125 MHz, DMSO-D_6) δ (ppm) 115.8, 120.9, 123.1, 124.3, 127.6, 128.4, 128.8, 128.9, 129.5, 132.2, 138.4, 139.5, 139.6, 149.5, 155.0, 158.3; HR-ESI (Q-TOF) *m/z*: calcd for C $C_{20}H_{16}N_3^+$ $[M+H]^+$ calcd 298.1344, found 298.1352.

4-(4-phenylamino)quinazolin-6-yl)benzonitrile (4.14). Yield: 48 mg, 15%; mp 242-245 °C; IR ν_{max} (cm^{-1}): 3107.2, 2228.4, 1624.1, 1596.7, 1571.4, 1527.8, 1496.9, 1443.8, 1403.4, 1326.6, 1255.8, 1106.2, 829.1, 747.3, 690.4; ^1H NMR (500 MHz, DMSO-D_6): δ (ppm) 7.31 (t, 1H, J = 7.4 Hz), 7.57 (t, 2H, J = 8.3 Hz), 7.98 (d, 2H, J = 7.8 Hz), 8.02 (d, 1H, J = 8.7 Hz), 8.19 (d, 2H, J = 8.5 Hz), 8.26 (d, 2H, J = 8.4 Hz), 8.41 (dd, 1H, J = 8.7,

1.9 Hz), 8.75 (s, 1H), 9.09 (s, 1H), 10.15 (s, 1H); ^{13}C NMR (125 MHz, DMSO-D_6): δ (ppm) 110.8, 115.8, 118.4, 119.2, 121.9, 123.2, 124.5, 128.3, 129.0, 132.0, 133.3, 136.3, 139.3, 144.0, 150.2, 155.5, 158.4; HR-ESI (Q-TOF) *m/z*: calcd for $C_{21}H_{15}N_4^+$ $[M+H]^+$ calcd 323.1296, found 323.1305.

6-(4-nitrophenyl)-N-phenylquinazolin-4-amine (4.15). Yield: 55 mg, 16%; mp 262–264 °C; IR ν_{max} (cm^{-1}): 3089.6, 1934.3, 1597.5, 1569.0, 1531.1, 1514.6, 1488.0, 1449.5, 1401.4, 1417.5, 1341.8, 1271.0, 834.7, 752.1, 693.2; ^{1}H NMR (500 MHz, DMSO-D_6): δ (ppm) 7.32 (t, 1H, J = 7.4 Hz), 7.57 (t, 2H, J = 8.1 Hz), 7.98 (d, 2H, J = 7.6 Hz), 8.05 (d, 1H, J = 8.6 Hz), 8.33 (d, 2H, J = 8.8 Hz), 8.44 (dd, 1H, J = 8.7, 1.7 Hz), 8.55 (d, 2H, J = 8.8 Hz), 8.76 (s, 1H), 9.14 (d, 1H, J = 1.3 Hz), 10.20 (s, 1H); ^{13}C NMR (125 MHz, DMSO-D_6): δ (ppm) 115.8, 122.3, 123.2, 124.5, 128.6, 128.9, 129.1, 132.1, 135.8, 139.3, 145.9, 147.3, 150.3, 155.7, 158.5; HR-ESI (Q-TOF) *m/z*: calcd for $C_{20}H_{15}N_4O_2^+$ $[M+H]^+$ calcd 343.1195, found: 343.1194.

(E)-6-(4-dimethylaminostyryl)-N-phenylquinazolin-4-amine (4.16). Yield: 130 mg, 25%; mp 220 °C (decomp.); IR ν_{max}(cm^{-1}): 3206.0, 2940.8, 1646.0, 1599.4, 1564.6, 1521.6, 1493.6, 1443.9, 1403.9, 1382.3, 1363.2, 1254.4, 957.2, 752.1, 691.3; ^{1}H NMR (400 MHz, DMSO): δ (ppm) 2.94 (s, 6H), 6.76 (d, 2H, J = 8.7 Hz), 7.10-7.14 (m, 2H), 7.34 - 7.42 (m, 3H), 7.48 (d, 2H, J = 8.7 Hz), 7.73 (d, 1H, J = 8.7 Hz), 7.87 (d, 2H, J = 7.8 Hz), 8.07 (d, 1H, J = 8.7 Hz), 8.52 (s, 1H), 8.60 (s, 1H), 9.78 (s, 1H); ^{13}C NMR (125 MHz, DMSO): δ (ppm) 112.3, 115.5, 119.1, 122.4, 123.8, 124.6, 127.7, 128.0, 128.5, 130.5, 131.1, 136.2, 139.3, 148.7, 150.3, 153.8, 157.6; HR-ESI (Q-TOF) *m/z*: calcd for $C_{24}H_{23}N_4^+$ $[M+H]^+$ 367.1923, found: 367.1929.

(E)-N-phenyl-6-styrylquinazolin-4-amine (4.18). Yield: 74 mg, 16%; mp 248-252 °C (decomp.); IR ν_{max} (cm^{-1}): 3048.8, 1949.9, 1622.7, 1600.8, 1570.5, 1523.4, 1494.9, 1446.5, 1409.5, 1385.9, 1360.5, 1332.6, 1254.5, 827.7, 747.8, 687.8; ^{1}H NMR (500 MHz, DMSO-D_6): δ (ppm) 7.16 (t, 1H, J = 7.2 Hz), 7.32 (t, 1H, J = 7.2 Hz), 7.38-7.51 (m, 6H), 7.66 (d, 2H, J = 7.4 Hz), 7.78 (d, 1H, J = 8.6 Hz), 7.87 (d, 2H, J = 7.6 Hz), 8.14 (d, 1H, J = 8.3 Hz), 8.56 (s, 1H), 8.72 (s, 1H), 9.81 (s, 1H); ^{13}C NMR (125 MHz, DMSO-D_6): δ (ppm) 115.8, 120.8, 122.9, 124.2, 127.0, 128.0, 128.4, 128.6, 128.9, 129.3, 130.3, 131.7, 135.6, 137.2, 139.6, 149.8, 154.8, 158.1; HR-ESI (Q-TOF) *m/z*: calcd for $C_{22}H_{18}N_3^+$ $[M+H]^+$ calcd 324.1500, found: 324.1516.

4-((E-2-(4-(phenylamino)quinazoline-6-yl)vinyl)benzonitrile (4.19). Yield: 98 mg, 20%; mp 250–254 °C; IR ν_{max} (cm^{-1}): 3071.4, 2221.6, 1599.8, 1571.8, 1498.4, 1441.7, 1403.6, 1362.3, 964.8, 838.4, 752.4, 693.8; ^{1}H NMR (500 MHz, DMSO-D_6): δ (ppm) 7.15 (t, 1H, J = 7.4 Hz), 7.42 (t, 2 H, J = 8.3 Hz), 7.56 (d, 1H, J = 16.4 Hz), 7.59 (d, 1H, J = 16.4 Hz), 7.79 – 7. 89 (br m, 7H), 8.17 (dd, 1H, J = 8.7, 1.7 Hz), 8.57 (s, 1H), 8.76 (s, 1H), 9.88 (s, 1H); ^{13}C NMR (125 MHz, DMSO-D_6): δ (ppm) 110.2, 115.8, 119.3, 121.8, 122.9, 124.2, 127.5, 128.5, 129.1, 129.2, 131.9 133.1, 134.7, 139.5, 141.9, 150.2, 155.1, 158.2; HR-ESI (Q-TOF) *m/z*: calcd for $C_{23}H_{17}N_4^+$ $[M+H]^+$ 349.1453, found 349.1453

(E)-6-(4-nitrostyryl)-N-phenylquinazolin-4-amine (4.20). Yield: 128 mg, 24%; mp 240 °C (decomp.); IR ν_{max}(cm^{-1}): 3085.1, 1932.2, 1602.1, 1591.5, 1571.4, 1527.7, 1501.7, 1328.8, 1404.1, 1443.2, 1365.5, 1255.4, 1105.2, 968.0, 749.5, 684.1, 694.9; ^{1}H NMR (500 MHz, DMSO-D_6): δ (ppm) 7.30 (t, 1H, J = 7.3 Hz), 7.56 (t, 2H, J = 7.8 Hz), 7.72 (d, 1H, J = 16.5 Hz), 7.76 (d, 1H, J = 16.5 Hz), 7.93 (d, 1H, J = 8.6 Hz), 8.01(t, 4H, J = 7.8 Hz), 8.30, (d, 1H, J = 8.6 Hz), 8.40 (d, 2H, J = 8.4 Hz), 8.71 (s, 1H), 8.91(s, 1H),

9.98 (s, 1H); ^{13}C NMR (125 MHz, DMSO-D_6): δ (ppm) 115.8, 122.1, 122.9, 124.3, 124.6, 127.8, 128.1, 128.7, 128.9, 131.9, 132.7, 134.7, 139.4, 144.1, 146.8, 150.3, 155.2, 158.2; HR-ESI (Q-TOF) *m/z*: calcd for $C_{22}H_{17}N_4O_2^+$ $[M+H]^+$ calcd 369.1351, found 369.1346.

6-(1E,3E)-(4-(4-dimethylaminophenyl)buta-1,3-dienyl)-N-phenylquinazolin-4-amine (4.21). Yield: 90 mg, 16%; mp 255-258°C (decomp.); IR ν_{max} (cm^{-1}): 2980.6, 1596.3, 1570.0, 1521.7, 1496.4, 1445.6, 1409.3, 1385.4, 1354.0, 1186.4, 987.4, 801.0, 746.0, 689.8; ^{1}H NMR (500 MHz, DMSO-D_6): δ (ppm) 2.94 (s, 6H), 6.71 (d, 2H, J = 8.7 Hz), 6.77 (d, 2H, J = 15.6 Hz), 6.95 (dd, 1H, J = 15.2, 11.7 Hz), 7.15 (t, 1H, J = 7.0 Hz), 7.27 (dd, 1H, J = 15.0, 11.1 Hz), 7.38-7.43 (m, 4H), 7.72 (d, 1H, J = 8.4 Hz), 7.87 (d, 2H, J = 7.3 Hz), 8.00 (d, 1H, J = 8.3 Hz), 8.54 (d, 2H, J = 15.6 Hz), 9.8 (s, 1H); ^{13}C NMR (125 MHz, DMSO-D_6): δ (ppm) 112.6, 115.9, 119.9, 122.9, 124.2, 125.0, 125.2, 128.1, 128.5, 128.9, 129.2, 131.2, 132.2, 134.7, 136.2, 139.6, 149.5, 150.5, 154.4, 158.0; HR-ESI (Q-TOF) *m/z*: calcd for $C_{26}H_{25}N_4^+$ $[M+H]^+$ 393.2079, found 393.2088.

6-(1E,3E)-4-(4-(methoxyphenyl)buta-1,3-dienyl)-N-phenylquinazolin-4-amine (4.22). Yield: 70 mg, 13%); mp 245-248°C (decomp.); IR ν_{max} (cm^{-1}): 3029.9, 1939.7, 1599.1, 1568.7 1525.3, 1498.5, 1446.4, 1410.1, 1385.1, 1357.7, 1300.1, 1248.8, 988.5, 806.7, 740.2, 690.7; ^{1}H NMR (500 MHz, DMSO-D_6): δ (ppm) 3.84 (s, 3H), 6.77 (d, 1H, J = 15.5 Hz), 6.85 (d, 1H, J = 15.5 Hz), 6.95 (d, 2H, J = 8.6 Hz), 7.07 (dd, 1H, J = 15.4, 10.7 Hz), 7.15 (t, 1H, J = 7.3 Hz), 7.29 (dd, 1H, J = 15.5, 10.7 Hz), 7.42 (t, 2H, J = 7.9 Hz), 7.51 (d, 2H, J = 8.5 Hz), 7.73 (d, 1H, J = 8.6 Hz), 7.86 (d, 2H, J = 7.7 Hz), 8.04 (d, 1H, J = 8.6 Hz), 8.54 (s, 1H), 8.59 (s, 1H), 9.84 (s, 1H); ^{13}C NMR (125 MHz, DMSO-D_6): δ (ppm) 55.6, 114.7, 115.9, 120.4, 122.9, 124.2, 127.5, 128.3, 128.6, 128.9, 130.0, 130.8,

131.3, 131.7, 133.7, 135.9, 139.6, 149.6, 154.6, 158.0, 159.6; HR-ESI (Q-TOF) *m/z*: calcd for $C_{25}H_{22}N_3O^+$ $[M+H]^+$ 380.1763, found 380.1766.

N-phenyl-6-((1E,3E)-4-phenylbuta-1,3-dienyl)quinazolin-4-amine (4.23). Yield: 70 mg, 14%; mp 258-260°C (decomp.); IR ν_{max} (cm^{-1}): 3259.1, 3055.1, 1924.2, 1604.2, 1569.2, 1528.3, 1496.2, 1440.3, 1406.5, 1388.2, 1363.4, 1329.5, 1310.3, 1253.8, 978.0, 901.4, 750.3, 686.5; ^1H NMR (500 MHz, DMSO-D_6): δ (ppm) 6.81 (d, 1H, J = 15.2 Hz), 6.91 (d, 1H, J = 15.2 Hz), 7.11 (t, 1H, J = 7.2 Hz), 7.19-7.32 (m, 3H), 7.38 (d, 2H, J = 7.4 Hz), 7.39 (d, 2H, J = 7.4 Hz), 7.56 (d, 2H, J = 7.6 Hz), 7.68 (d, 1H, J = 8.5 Hz), 7.80 (d, 2H, J = 7.6 Hz), 8.01 (d, 1H, J = 8.5 Hz), 8.47 (s, 1H), 8.58 (s, 1H), 9.84 (s, 1H); ^{13}C NMR (125 MHz, DMSO-D_6): δ (ppm) 116.1, 121.1, 123.0, 123.8, 126.9, 128.2, 128.4, 128.8, 129.2, 129.8, 131.0, 132.3, 133.7, 135.3, 137.4, 140.7, 149.9, 154.9, 158.1; HR-ESI (Q-TOF) *m/z*: calcd for $C_{24}H_{20}N_3^+$ $[M+H]^+$ 350.1657, found 350.1673.

4-((1E,3E-4-(4-(phenylamino)quinazolin-6-yl)buta-1,3-dienyl)benzonitrile (4.24). Yield: 134 mg, 25%; mp 242-245°C (decomp.); IR ν_{max} (cm^{-1}): 3365.8, 3028.7, 2224.5, 1598.1, 1568.6, 1525.6, 1496.8, 1443.5, 1402.4, 1387.6, 1361.7, 1252.8, 983.0, 746.2, 848.0, 687.4; ^1H NMR (500 MHz, DMSO-D_6): δ (ppm) 7.02 (d, 1H, J = 15.2 Hz), 7.16 (d, 1H, J = 15.1 Hz), 7.30 (t, 1H, J = 7.4 Hz), 7.46 – 7.60 (m, 4H), 7.90 (d, 3H, J = 8.5 Hz), 7.96 (d, 2H, J = 8.35 Hz), 8.00 (d, 2H, J = 7.65 Hz), 8.22 (dd, 1H, J = 8.7, 1.0 Hz), 8.69 (s, 1H), 8.79 (s, 1H), 9.98 (s, 1H); ^{13}C NMR (125 MHz, DMSO-D_6): δ (ppm) 109.9, 115.8, 119.4, 121.4, 122.9, 124.2, 127.5, 128.7, 128.9, 130.6, 131.3, 131.8, 133.0, 133.5, 134.4, 135.2, 139.5, 142.1, 150.1, 154.9, 158.1;HR-ESI (Q-TOF) *m/z*: calcd for $C_{25}H_{19}N_4^+$ $[M+H]^+$ 375.1609, found 375.1610.

6-((1E,3E)-4-(4-nitrophenyl)buta-1,3-dienyl)-N-phenylquinazolin-4-amine (4.25).

Yield: 113 mg, 20%; mp 273-275°C (decomp.); IR ν_{max} (cm^{-1}): 3421.3, 3020.7, 1927.9, 1603.3, 1585.6, 1571.5, 1557.7, 1535.3, 1494.4, 1444.3, 1331.5, 1253.8, 1109.3, 987.1, 743.6, 804.3; ^{1}H NMR (500 MHz, DMSO-D_6): δ (ppm) 6.92 (d, 1H, J = 15.4 Hz), 7.03 (d, 1H, J = 15.3 Hz), 7.13 (t, 1H, J = 7.2 Hz), 7.32 – 7.41 (m, 3H), 7.48 (dd, 1H, J = 15.4, 10.7 Hz), 7.73 (d, 1H, J = 8.6 Hz), 7.81 (d, 2H, J = 8.8 Hz), 7.83 (d, 2H, J = 8.8 Hz), 8.08 (d, 1H, J = 8.6 Hz), 8.20 (d, 2H, J = 8.6 Hz), 8.53 (s, 1H), 8.64 (s, 1H), 9.86 (s, 1H); ^{13}C NMR (125 MHz, DMSO-D_6): δ (ppm) 115.8, 121.5, 123.0, 124.3, 124.4, 127.6, 128.7, 128.9, 130.6, 131.4, 132.0, 134.5, 135.1, 135.2, 139.5, 144.2, 146.6, 150.1, 155.0, 158.1; HR-ESI (Q-TOF) *m/z*: calcd for $C_{24}H_{19}N_4O_2^+$ $[M+H]^+$ 395.1508, found 395.1503.

4.3. ***Conclusions:***

We have successfully synthesized a series of ATP-competent fluorescent probes targeting ERBB2 receptor. We investigated the influence of various electron-donating and electron withdrawing substituents on the 6-position of quinazoline and the effect of increasing conjugation on the fluorescence of our probes. We evaluated the inhibition and "turn-on" efficiency of our probes and found that the inhibition efficiency of kinase inhibitors remains unperturbed through the substitution or chemical modification on the 6-position of quinazoline core. Extension of conjugation generates probes with longer wavelength emission that appear yellow to orange in color. Introduction of strong electron-donating or withdrawing substituents on the 6-position generates probes with high turn-on ratios.

We also found that not all probes with high turn-on ratios result in complete inhibition of ERBB2 phosphorylation suggesting the existence of alternate modes of binding for

different probes which requires further investigation into the binding kinetics of the probes. Of all the compounds in the series, **4.11** and **4.16** with high turn-on ratios result in turn-on emission upon binding to ERBB2 kinase domain in solution. In conclusion, we have designed and synthesized a series of highly fluorescent kinase inhibitors targeting the ATP binding pocket of ERBB2 receptor although some minor issues like hydrophobicity need to be overcome for their successful application for the study of receptor dynamics, signaling pathways, etc.

Chapter 5

Synthesis and Photophysical Properties of Novel Highly Fluorescent Quinazoline Based Derivatives

5.1. ***Background:***

The photophysics and spectroscopy of stilbene based dyes (push-pull stilbenes) with donor acceptor groups has been the intensive area of research in the recent years due to their ability to produce photo-induced intramolecular charge transfer (ICT) and the twisting of the double bond that produces *E* and *Z* isomers with attractive physical, chemical and optical properties.[105,106,107] The *cis-trans* isomerization is a hallmark of several naturally occurring molecules that include carotenoids such as *β*-carotene, violaxanthin, lycopene, visual pigments such as rhodopsin, bilirubin, photoactive yellow proteins, auto-fluorescent proteins such as green, red and yellow fluorescent proteins, etc.[108] Among the donor-acceptor stilbenes, DCS (4-(dimethylamino)-4′-cyanostilbene) is the most extensively investigated molecule (Figure 5.1).[25] We recently reported the fluorescent "turn-on" kinase inhibitors targeting the ATP binding pocket of ERBB2 receptor. DMAQ was the first "turn-on" fluorescent kinase inhibitor which was followed by a series of 15 kinase inhibitors.[30, 31]

In addition, there are many well-known anticancer drugs with quinazoline core (e.g., lapatinib, gefitinib, sorafinib, imatinib) which underlines the significance of quinazoline containing compounds as potent ERBB2 inhibitors.[40] Due to the pharmacological significance of the quinazoline core, we became interested to synthesize and study the optical properties of a novel series of highly fluorescent styryl quinazoline derivatives.

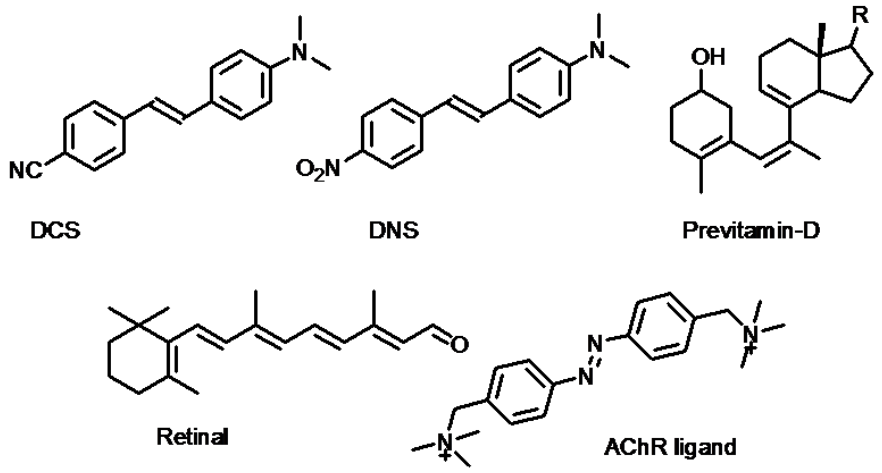

Figure 5.1. E**xamples of compounds showing *cis-trans* photoisomerization-[DCS - *trans*-4-(*N,N*-dimethylamino)-4'-cyanostilbene;DNS - *trans*-4-(*N, N*-dimethylamino)-4'-nitrostilbene;AChR – acetylcholine receptor]**

During the synthesis of our compounds, we noticed that our compounds undergo photo *cis-trans* isomerization on exposure to visible light. This prompted us to investigate the photochemical and photophysical changes of our compounds upon irradiation by UV light/laser. Experimental evidence of photoisomerization from *trans* to *cis* isomer was obtained from UV-Vis and fluorescence spectroscopies including ^{1}HNMR studies. The isomerization from ***E*** to **Z** was found to be irreversible as there was no change in the ^{1}HNMR even after leaving the compound in dark for more than 24 h. The structural assignment of ***E*** and ***Z*** isomers was done using ^{1}H NMR and changes in the UV-Vis and fluorescence spectra.

5.1.1. ***Photoisomerization:***

Absorption of a photon by compounds with an olefinic linkage or a double bond induces the torsion of a double bond resulting in isomerization and the process is known as

photoisomerization. It is one of the most common photo-induced reactions resulting in switching of the double bond shown by ethylenes and compounds with olefinic linkages such as C=C, N=N, etc. and forms the basis for the tunable fluorescence of several fluorescent probes under the influence of light. Studies reveal that depending on the nature of the substituents, isomerization can occur via a singlet or triplet state. The photoisomerization of stilbenes[109] though appears to be simple involving the torsion of the double bond is actually more complicated at the deeper level due to the presence of multiple electronic states and multiple degrees of freedom (Figure 5.2). *Trans-cis* photoisomerization of trans-stilbene was extensively investigated by Saltiel and co-workers.

Figure 5.2. **Stilbene undergoing photo induced *cis-trans* isomerization**

5.2. Results and Discussion:

5.2.1. ***Synthesis of styryl quinazolines:***

Compounds **5.7** to **5.12** were synthesized using the synthetic scheme 5.1. The first step involves the condensation of 4-hydroxy-6-iodoquinazoline with formamide followed by palladium catalyzed Heck-coupling of the resulting intermediate with the corresponding styryl or phenyl-butadiene arms.

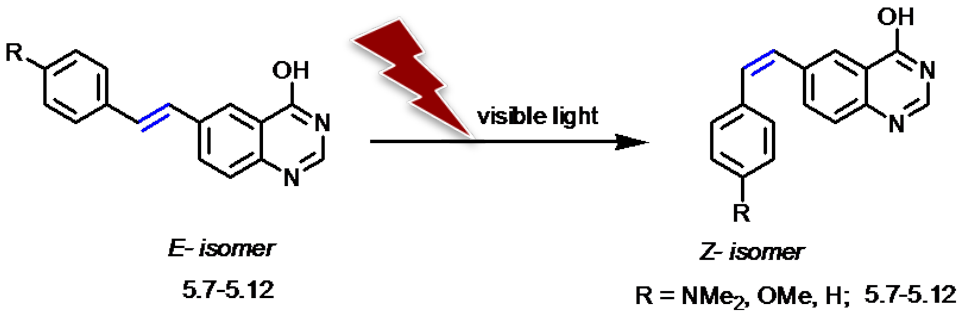

***Figure 5.3. E-Z* photoisomerization of styryl quinazoline derivatives**

The crude compound was subjected to subsequent reaction work up and purification by flash chromatography and recrystallizations in dark furnished the *E*-isomers of **5.7-5.12** in moderate to poor yields. Our probes were obtained as crystals that varied from off-white to bright yellow.

Owing to the pharmacological significance of the quinazoline containing compounds/derivatives and the attractive photophysical and photochemical properties of push-pull stilbene based dyes has prompted us to synthesize and investigate the optical properties of these novel quinazoline derivatives (Figure 5.3). Besides the effect of substitution with strong electron-donating groups such as NMe_2 and -OMe, we also evaluated the effect of extension conjugation on the optical properties by varying the conjugation length between quinazoline core and the phenyl arm.

Scheme 5.1. Synthetic scheme for the synthesis of styryl quinazoline derivatives

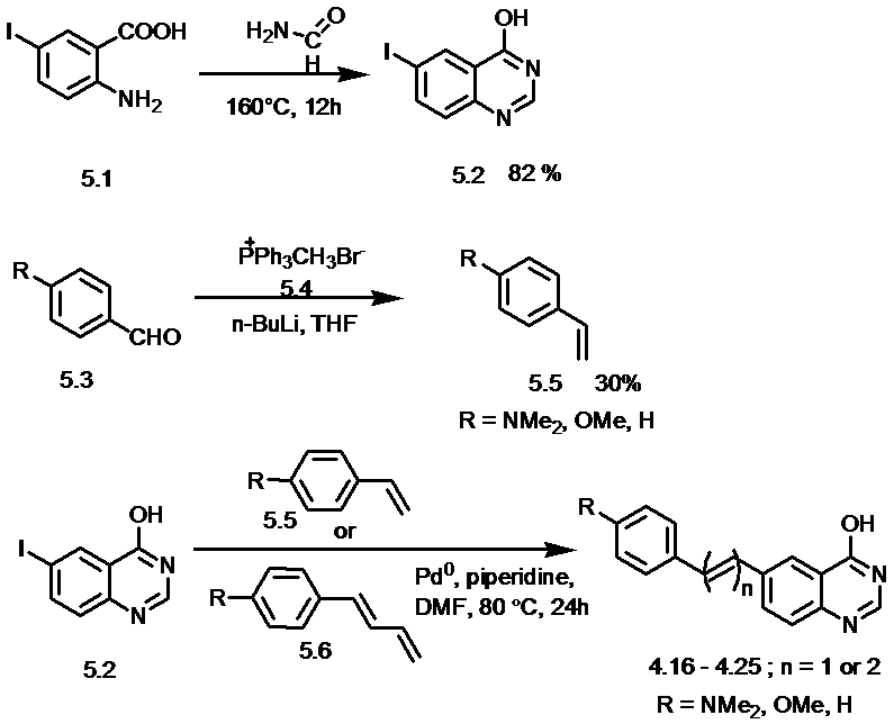

In the presence of strong electron donating groups such as NMe_2 and OMe, quinazoline core with the two sp^2 hybridized Nitrogen atoms serves as an electron acceptor while in the absence of strong electron withdrawing groups (**5.7** and **5.8**), the quinazoline core functions as an electron donor.

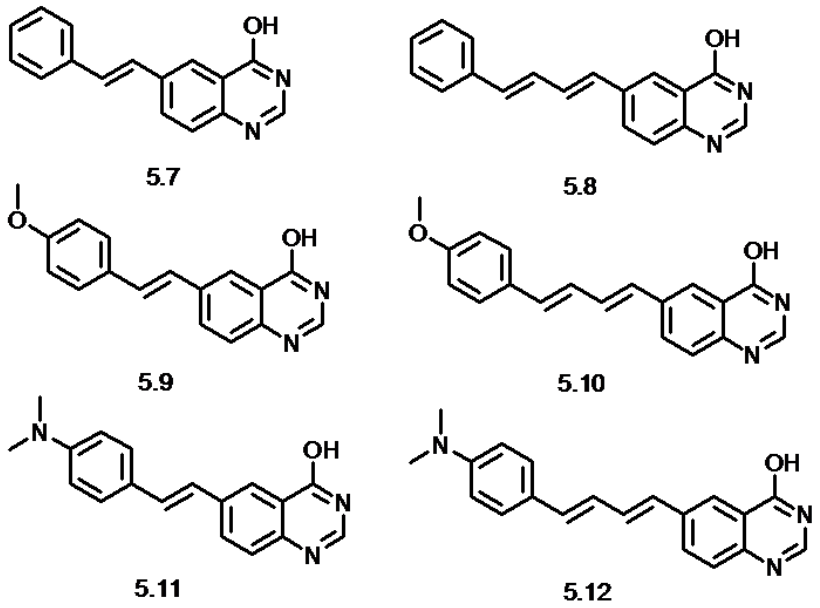

Figure 5.4. **Styryl quinazolines (5.7 - 5.9)**

5.2.2. ***Photophysical studies:***

The most striking feature of these chromophores is the solvent dependent fluorescence behavior which can be attributed to the rapid relaxation of the initially formed Frank-Condon excited state to the Charge-transfer (CT) state.

Table 5.1. Photophysical characteristics of compounds (5.7-5.12) in toluene

Cpd	$\lambda_{max, abs}$	ε	$\lambda_{max, em}$	ϕ	Stoke's shift
5.7	327	48809.24645	388	0.326846489	4807.843879
5.8	356	70165.88767	407	0.63632911	3519.86307
5.9	336	42268.42298	398	0.256629685	4636.276621
5.10	365	53793.79294	425	0.421111634	3867.848509
5.11	376	13553.58951	446	0.258963679	4174.220017
5.12	396	60337.44137	461	0.214015321	3560.551283

Of all the compounds in the series, **5.8** exhibits maximum quantum yield and molar absorptivity. The compounds **5.7** and **5.9** with a single double bond are found to have the high quantum yields compared to their extended conjugation counter parts or diene counterparts **5.8** and **5.10** except **5.12** which has low quantum yield compared to **5.11** with a single double bond. This bathochromic shift can be rationalized based on the increased conjugation which further reduces the HOMO-LUMO gap thereby shifting the emission to the longer wavelengths.

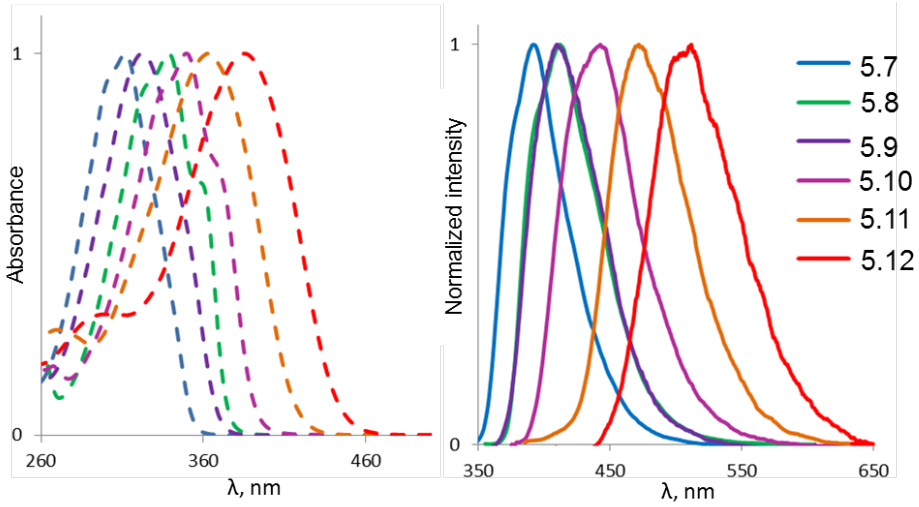

Figure 5.5. **UV-Vis and emission spectra of 5.7 – 5.12 in chloroform**

The UV-Vis and emission spectra for **5.7** - **5.12** are shown in Figure 5.5. Compound **5.7** with no strong electron donating groups exhibits bluest emission, while the compound with strong electron donating -NMe_2 group emits in the longer wavelength region. Compound with moderate electron donating -OMe group has the λ_{max} of emission intermediate between the two extremes. As the compounds were found to undergo photoisomerization under visible light, we investigated their UV-Vis and emission responses under UV (365 nm) and laser (405 nm) irradiation. We found no difference in the spectra between the two irradiations.

5.2.3. ***Absorption spectroscopy:***

All the compounds were highly fluorescent and compound **5.8** exhibits higher molar absorptivity of all the analogues in the series followed by **5.12** and **5.10**. We also observed that these compounds with extended conjugation have higher molar absorptivities compared to their single bond counterparts such as **5.7**, **5.9** and **5.11**.

Irradiation studies were conducted using a UV-Vis lamp at λ of 365 nm. Irradiation of **5.9** led to significant changes in the absorption spectra of compound as shown in the figure **5.6**. The absorbance of the first absorption band (1 in the Figure 5.6) corresponding to the pure (*E*) isomer of **5.9** gradually decreases on irradiation and shifts to the shorter wavelengths.

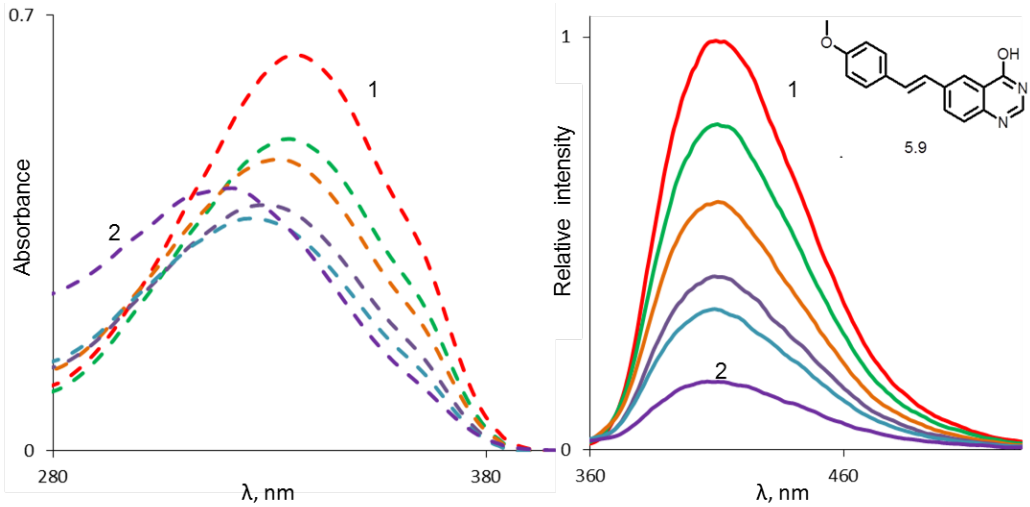

Figure 5.6. **UV-Vis and emission spectral changes of 5.9 in toluene**

This implies that the *cis* (***Z***) isomer of the compound has low molar absorptivity than the corresponding *trans* (***E***) isomer. We did not observe any changes in the absorption spectra or ^{1}HNMR of irradiated solution of **5.9** even after leaving it in the dark for more than 24 h. This can be rationalized on the fact that there is a high energetic barrier between the two isomers which could not be overcome at room temperature and therefore we found that the *cis-trans* isomerization was not reversible. For further insights, frontier molecular orbital studies are needed to calculate the energy differences between the two states.

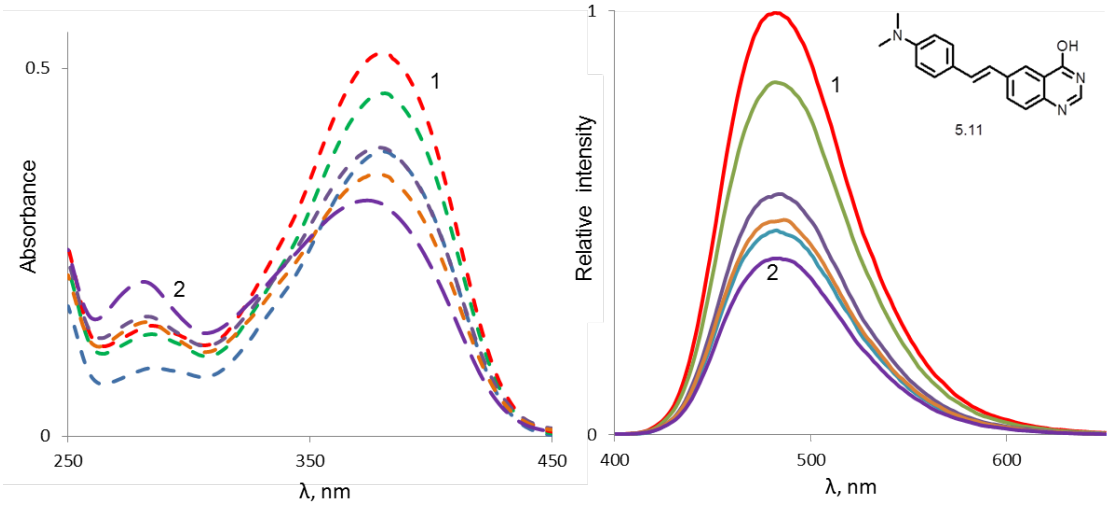

Figure 5.7. **UV-Vis and emission spectral changes of 5.11 in toluene**

Irradiation of **5.11** also leads to the decrease in the absorbance of the absorption band of peak 1 which corresponds to the pure ***(E)*** isomer of **5.11** and it gradually shifts to the shorter wavelengths shown by peak 2 in the Figure 5.7.Similar changes were observed for compound **5.12** which shows bathochromic shift on irradiation (Figure 5.7).

5.2.4. ***Emission spectroscopy:***

Compound **5.8** exhibits the highest quantum yield (0.63) in the series followed by **5.10** and **5.7**. We found that the quantum yield of the **5.8** (0.63) with extended conjugation is double that of its single bond counterpart (0.32). Similarly, compound **5.10** has higher quantum yield (0.42) over **5.9** with one double bond (0.25). Overall all the compounds in the series show a gradual decrease in the absorbance in the absorption band of pure ***E*** isomer.

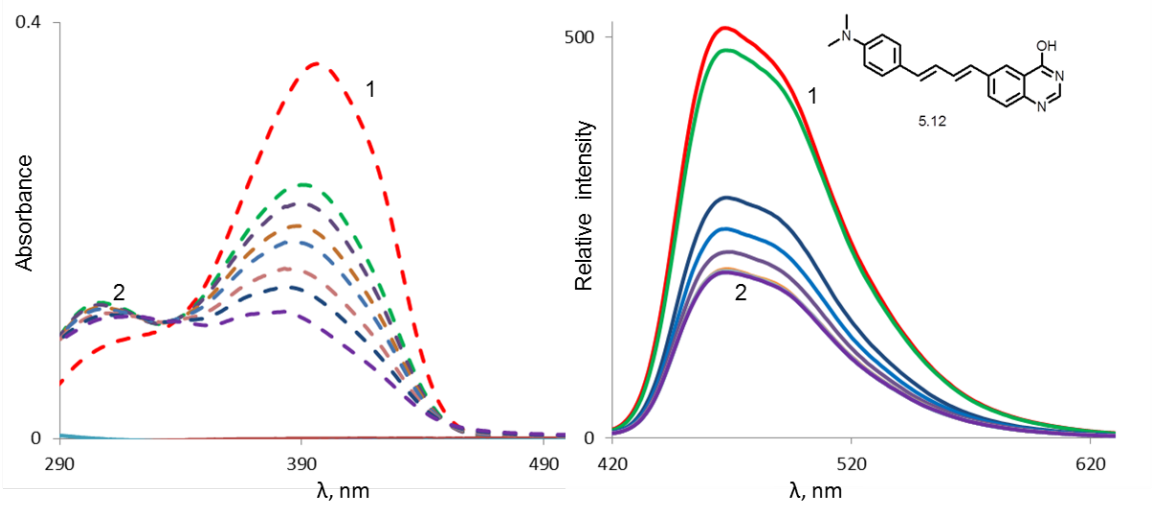

Figure 5.8. **UV-Vis and emission spectral changes of 5.12 in toluene**

Strikingly, compound with strong electron donating group -NMe_2 does not show the similar trend and therefore **5.12** shows lower quantum yield over **5.11** (Figure 5.5). Irradiation of the toluene solutions of **5.7** to **5.12** at the wavelengths corresponding to the λ_{max} of absorbance led to a gradual decrease in the emission intensities (Figure 5.6, 5.7 and 5.8). In all the fluorescence spectra, emission peak 1 corresponds to the pure (***E***) isomer and peak 2 corresponds to the (***Z***) isomer after 24 h irradation. The decreased emission intesnsity for all the compounds after irradition indicate that the resulting (***Z***) compounds after photoisomerization are weak/non-fluorescent.

5.2.5. *^{1}H NMR studies:*

Another supporting evidence demonstrating that our compounds undergo photo-isomerization was obtained from ^{1}HNMR (Figures 5.9 and 5.10). Spectra were recorded at 500 MHz in DMSO. In Figures 5.9 and 5.10, the spectra at the bottom correspond to ***E***-isomer while on the top, it corresponds to ***Z***-isomer. Although all the compounds were

found to undergo photoisomerization, the time taken and the extent of isomerization was different for different compounds. For instance, photoisomerization begun imediately for **5.11** with strong electron donating $-NMe_2$ group and the isomerization is not complete even after 24 h of irradiation (Figure 5.10).

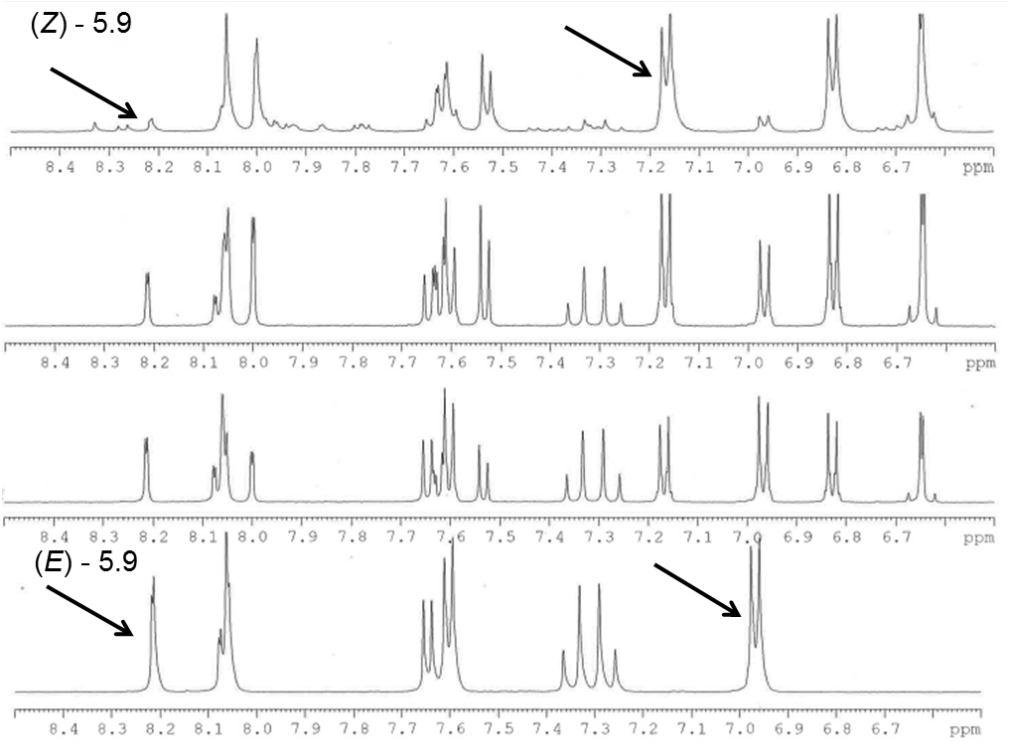

Figure 5.9. **^{1}H NMR spectral changes of 5.9 in DMSO (500 MHz at 25°C)**

Disappearance of the peaks corresponding to the ***E***-isomer and the appearance of new peaks corresponding to ***Z***-siomer (shown by arrows in the Figures 5.9 and 5.10) confirm that the compounds undergo photoisomerization from *trans* to *cis* at room temperature.

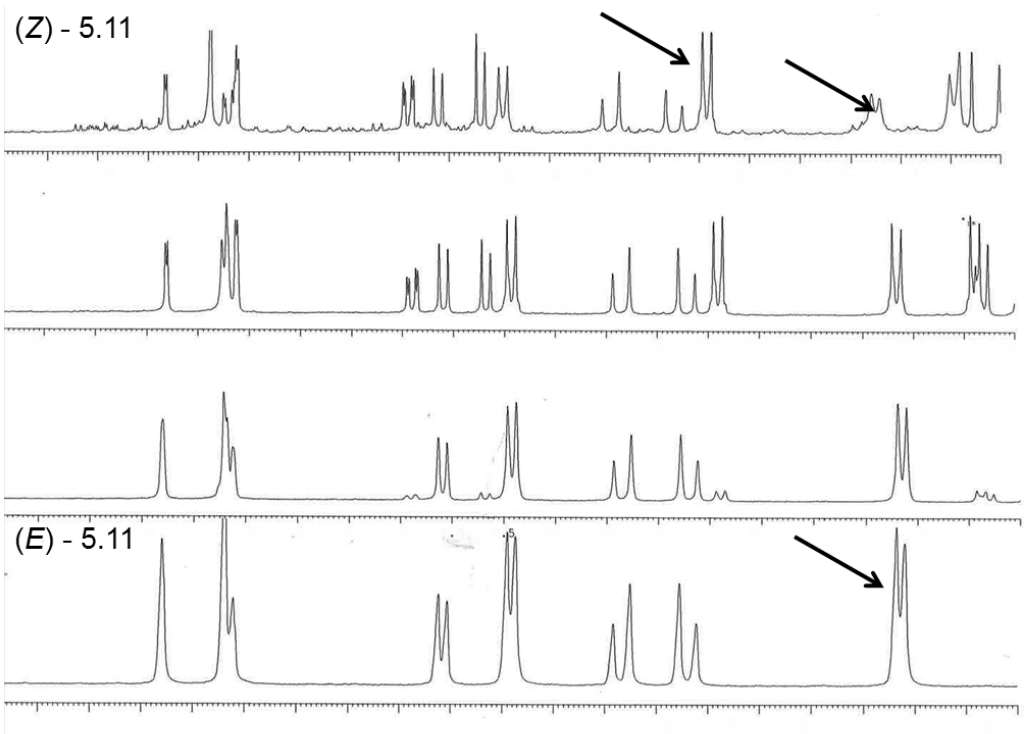

Figure 5.10. **^{1}H NMR spectral changes of 5.11 in DMSO (500 MHz at 25^{o}C)**

5.2.6. ***Experimental section:***

6-styrylquinazolin-4-ol (5.7): ^{1}H NMR (500 MHz, DMSO) δ (ppm): 6.96 (d, 1H, J = 15.5 Hz), 7.03 (d, 1H, J = 15.5 Hz), 7.24-7.29 (m, 1H), 7.35-7.41 (m, 2H), 7.48-7.52 (br t, 2H), 7.66 (d, 2H, J = 7.5 Hz), 7.77 (d, 1H, J = 8.5 Hz), 8.15 (dd, 1H, J = 1.5 Hz), 8.21 (s, 1H), 8.28 (s, 1H), 12.42 (s, 1H); ^{13}C NMR (125 MHz, DMSO) δ (ppm) 123.4, 123.8, 126.8, 128.1, 128.2, 129.2, 129.6, 131.2, 131.8, 132.0, 134.0, 136.1, 137.4, 145.6, 148.6, 161.1; HRMS (ESI) *m/z* $C_{18}H_{15}N_2O$ $[M+H]^+$ calcd 275.1178, found 275.1179; IR ν_{max}(cm^{-1}): 682, 741, 924, 982, 1168, 1253, 1601, 1654, 1695, 2625, 2927, 3020, 3133; M.P.: 266 - 268°C (d).

6-((1E,3E)-4-phenylbuta-1,3-dienyl)quinazolin-4-ol (5.8): ^{1}H NMR (500 MHz, DMSO): δ (ppm) 7.43 (m, 1H), 7.52-7.61 (m, 4H), 7.8 (d, 3H, J = 7.5 Hz), 8.22-8.26 (m, 3H), 8.41

(s, 1H), 12.42 (s, 1H); ^{13}C NMR (125 MHz, DMSO): δ (ppm) 123.4, 124.1, 127.1, 127.7, 128.1, 128.3, 129.1, 130.2, 132.2, 136.1, 137.2, 145.6, 148.7, 161.1; HRMS (ESI) m/z $C_{16}H_{13}N_2O$ $[M+H]^+$ calcd 249.1022, found 249.1030; IR ν_{max} (cm^{-1}): 683, 824, 957, 1216, 1228, 1369, 1654, 1695, 1740, 2840, 2937, 2970, 3020, 3455; M.P.: 272 - 274° C (d).

5.9 -6-(4-methoxystyryl)quinazolin-4-ol (5.9): ^{1}H NMR (500 MHz, DMSO) δ (ppm): 3.78 (s, 3H), 6.97 (d, 2H, *J* = 8.5 Hz), 7.27 (d, 1H, *J* = 16 Hz), 7.35 (d, 1H, *J* = 16.5 Hz), 7.6 (d, 2H, *J* = 8.5 Hz), 7.64 (d, 1H, *J* = 8 Hz), 8.06 – 8.07 (m, 2H), 8.21 (s, 1H), 12.25 (s, 1H); ^{13}C NMR (125 MHz, DMSO) δ (ppm) 55.6, 114.6, 123.3, 123.6, 125.3, 128, 128.5, 129.8, 129.9, 132, 136.5, 145.4, 148.3, 159.6, 161.1; HRMS (ESI) m/z $C_{17}H_{14}N_2O_2$ $[M+H]^+$ calcd 277.0977, found 277.0983; IR ν_{max} (cm^{-1}): 830, 910, 956, 1250, 1294, 1511, 1602, 1655, 1697, 1739, 2831, 3021, 3137; M.P.: 258 - 260° C (d).

6-(1E,3E)-4-(4-methoxyphenyl)buta-1,3-dienyl)quinazolin-4-ol (5.10): ^{1}H NMR (500 MHz, DMSO): δ (ppm) 3.9 (s, 3H), 6.88-7.14 (m, 5H), 7.31-7.36 (br t, 1H), 7.6 (d, 2H, *J* = 7.5 Hz), 7.76 (d, 1H, *J* = 8.5 Hz), 8.13 (d, 1H, *J* = 8 Hz), 8.19 (s, 1H), 8.24 (s, 1H), 12.48 (s, 1H); ^{13}C NMR (125 MHz, DMSO) δ (ppm) 55.6, 114.7, 123.4, 123.5, 127.4, 128.1, 128.2, 130.1, 130.4, 131.5, 131.9, 133.8, 136.3, 145.4, 148.4, 159.6, 161; HRMS (ESI) m/z $C_{19}H_{17}N_2O_2$ $[M+H]^+$ calcd 305.1284, found 305.1292; IR ν_{max} (cm^{-1}): 980, 1217, 1229, 1366, 1507, 1599, 1655, 1738, 2132, 2838, 2946, 2970, 3015, 3458; M.P.:260 - 262° C (d).

6-(4-(dimethylamino)styryl)quinazolin-4-ol (5.11): ^{1}H NMR (500 MHz, DMSO): δ (ppm) 2.94 (s, 6H), 6.73 (d, 2H, *J* = 9 Hz), 7.13 (d, 1H, *J* = 16.5 Hz), 7.26 (d, 1H, *J* = 16.5 Hz), 7.48 (d, 2H, *J* = 8.5 Hz), 7.62 (d, 1H, *J* = 8.5 Hz), 8.01 (d, 1H, *J* = Hz), 8.03 (s,

1H), 8.16 (d, 1H, *J* = 2 Hz), 12.18 (s, 1H); ^{13}C NMR (125 MHz, DMSO) δ (ppm): 40.3, 112.6, 122.7, 122.9, 123.4, 125.1, 127.9, 128.2, 130.65, 131.8, 137.09, 145.1, 147.9, 150.6, 161.1; HRMS (ESI) m/z $C_{18}H_{17}N_3O$ $[M+H]^+$ calcd. 292.1450, found 292.1444; IR ν_{max}(cm^{-1}): 829, 909, 924, 1165, 1192, 1518, 1601, 1652, 1784, 2853, 3026; M.P.: 230-233°C (d).

6-((1E,3E)-4-(4-(dimethylamino)phenyl)buta-1,3-dienyl)quinazolin-4-ol (5.12):

^{1}H NMR (500 MHz, DMSO): δ (ppm) 3.1 (s, 6H), 6.85-7.07 (m, 5H), 7.34 (m, 1H), 7.53 (d, 2H, *J* = 8.5 Hz), 7.77 (d, 1H, *J* = 8.5 Hz), 8.14 (dd, 1H, *J* = 1.5 Hz), 8.23 (s, 1H), 8.32 (s, 1H); ^{13}C NMR (125 MHz, DMSO) δ (ppm): 41.2, 114.1, 119.8, 123.2, 123.4, 125.8, 127.1, 128.1, 129.3, 132, 132.1, 134.6, 136.8, 145.8, 146.7, 149.4, 160.9; HRMS (ESI)m/z $C_{20}H_{20}N_3O$ $[M+H]^+$ calcd 318.1600, found 318.1601; IR ν_{max} (cm^{-1}): 797, 981, 1252, 1334, 1479, 1516, 1598, 1652, 1694, 2785, 2930, 3131; M.P.: 246-248°C (d).

5.3. *Conclusions:*

We have successfully synthesized and investigated the photophysical characteristics of styryl and phenyl-butadiene substituted quinazoline derivatives (**5.7-5.12)**.Our compounds undergo photoisomerization on exposure to UV/visible light. Photoisomerization was found to be irreversible as the ***Z***-isomer was not reverting back to ***E***-isomer even after the compound was left in dark indicating that the energy barrier is too high for the isomerization to occur at room temperature. Our compounds represent a novel class of push-pull stilbene based quinazoline derivatives and all the compounds were highly fluorescent with fair to good quantum yields. Compounds with extended conjugation (**5.8** and **5.10**) showed high molar absorptivity and high quantum yields

over their single double bond counterparts (**5.7** and **5.9**) with the exception of **5.12**. The irradiation of the compounds with UV light (360 nm) or laser (405 nm) resulted in photoisomerization. The observed photoisomerization was studied using UV-Vis and fluoresence spectoscopies including ^{1}HNMR. Further investigation of the optical properties and molecular orbital studies are required for the application of these compounds for biological studies. These quinazoline based compounds with high fluorescence and photo-switching abilities can be exploited in future for the study of the kinase receptor after careful investigation of the photoisomerization in these compounds.

Chapter 6

Additional Synthesized Molecules

6.1. Background:

After the successful synthesis of turn-on kinase inhibitors and the evaluation of their binding properties, we were interested in the design and synthesis of novel fluorescent probes that can overcome the limitations of the existing inhibitors. Hydrophobicity and aggregation were the major concerns for the application of these inhibitors for biological studies. For this reason, we introduced hydrophilic functional groups that can improve the hydrophilicity of our probes. For instance, compound **6.4** (Figure 6.1) was synthesized by conjugating the quinazoline core with N-methyl piperazine derivative. As mentioned in chapter-4, we noticed that compound **4.24** was showing partial inhibition of the receptor, although it has the same turn-on ratio as **4.11**.[31] In order to investigate, if the presence of CN groups on the substituents was contributing to the aggregation issues, we synthesized more derivatives with CN functional groups retaining the same pharmacophore. Strikingly, we observed that most of our compounds with CN substitituents were showing aggregation induced enhanced emission (AIEE). Further studies on AIEE behavior of our compounds are currently in progress.

We also synthesized Type-2 based probes to target the inactive conformation of the receptor kinase. These probes were designed based on lapatinib which is a well-known Type-2 inhibitor. Compounds **6.12** and **6.13** belong to this category.

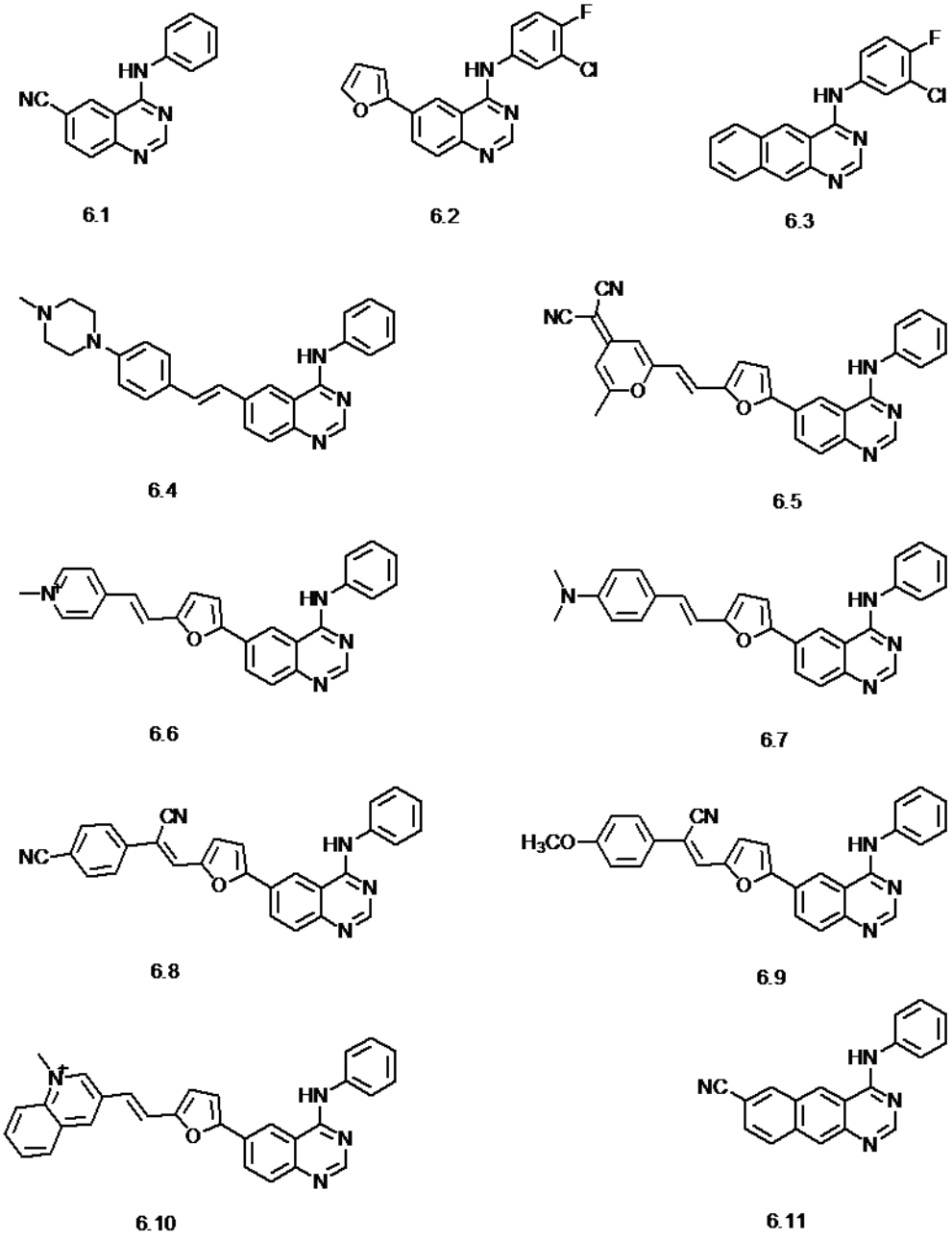

Figure 6.1. Structures of the synthesized fluorescent probes

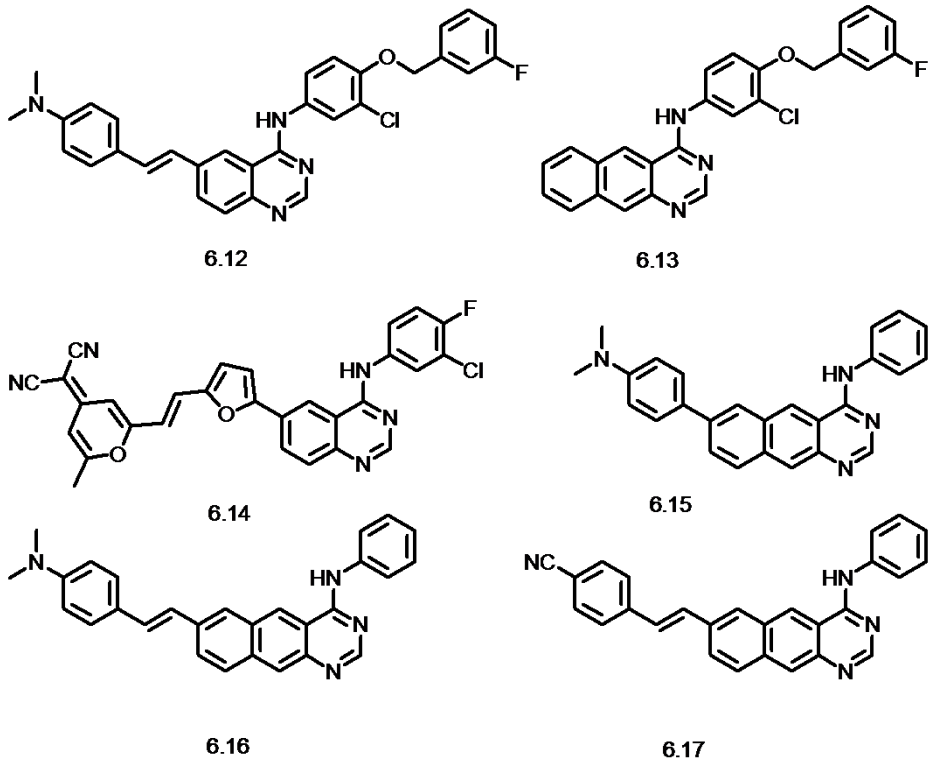

Figure 6.2. Structures of the synthesized fluorescent probes

6.2. ***Synthetic methods:***

Chemicals required for the syntheses were purchased from Aldrich and other commercial suppliers. For Heck and Suzuki coupling reactions, anhydrous solvents from Aldrich were used. All reactions were monitored by thin layer chromatography and purification was done by column chromatography or recrystallization techniques. As most of our compounds are highly polar, we used dichloromethane, ethyl acetate and methanol for column chromatography.

Scheme 6.1. Synthetic scheme for the synthesis of styryl derivatives

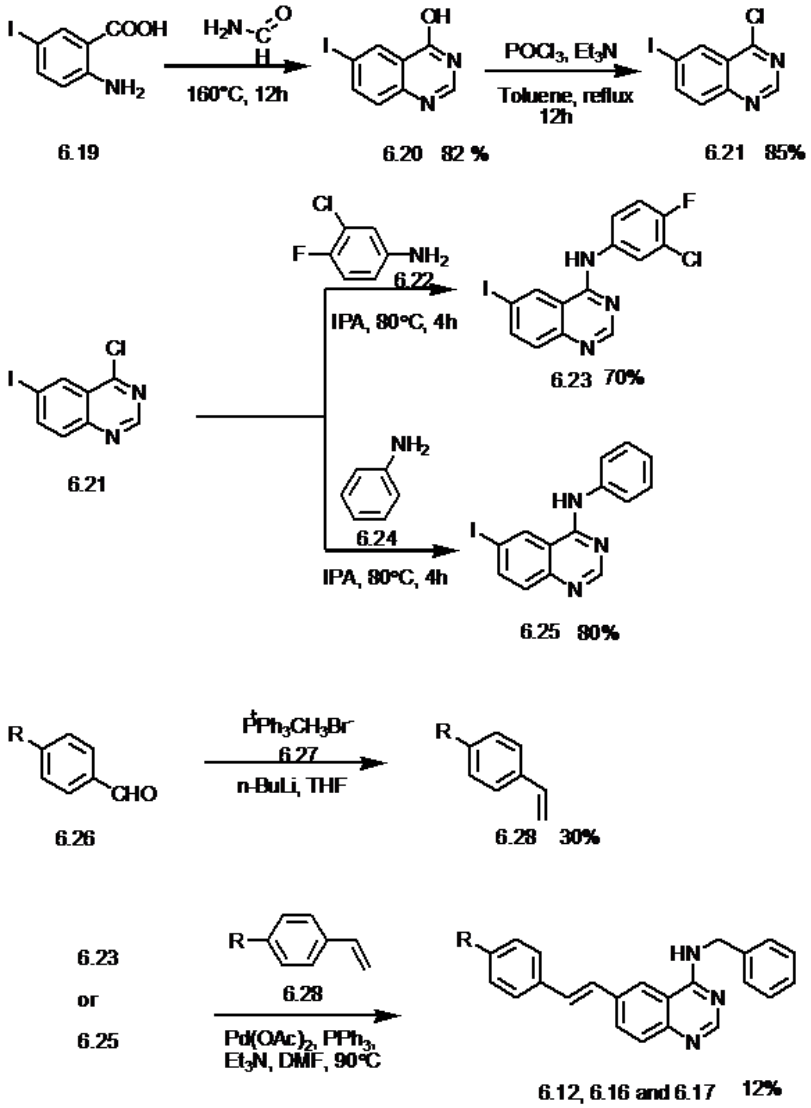

Scheme 6.2. Synthetic scheme for the synthesis of **6.12** and **6.13**

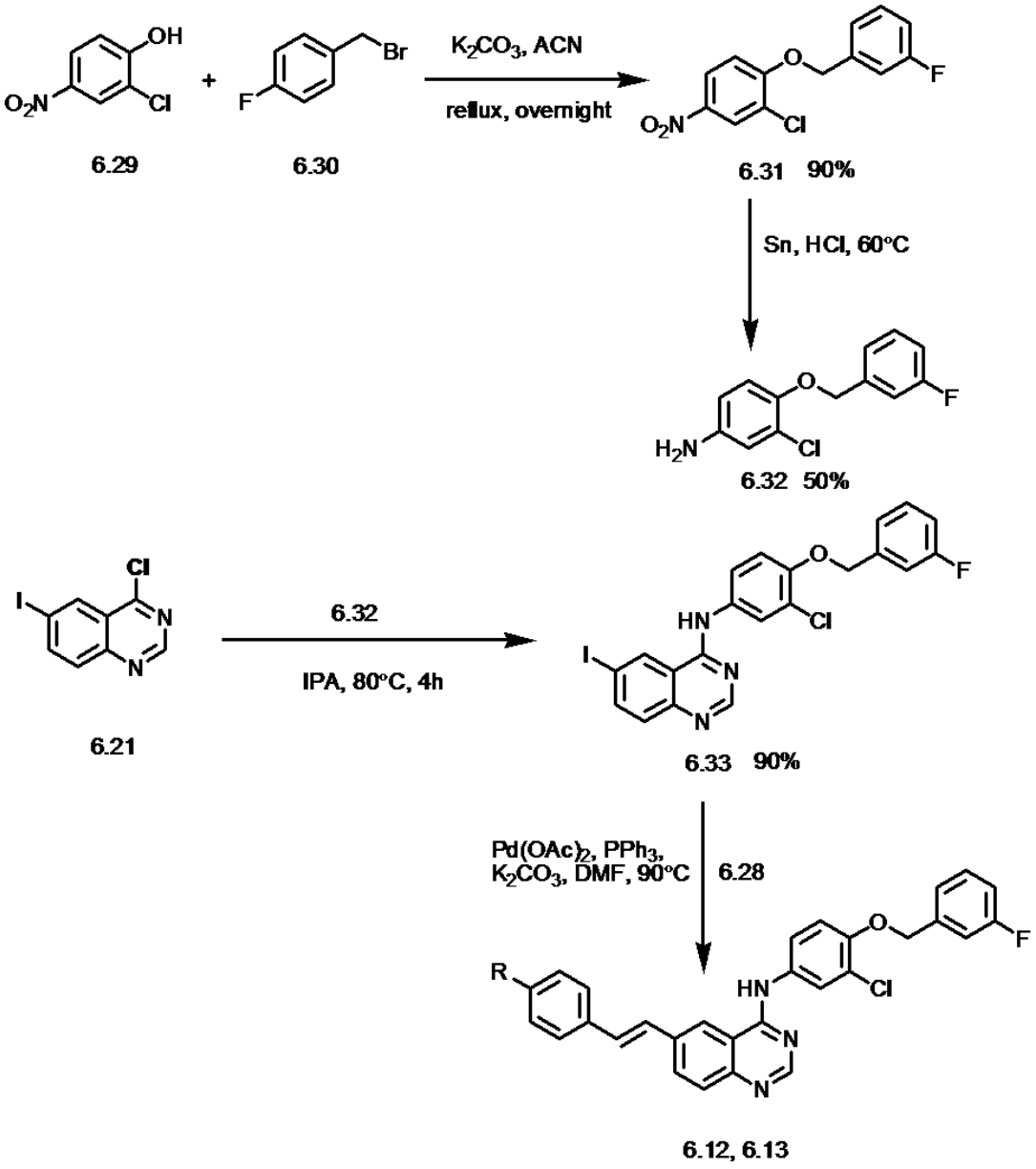

Compounds **6.12** and **6.13** with long arms at 4-position of quinazoline core resemble lapatinib and have been synthesized using synthetic scheme 6.2.

Scheme 6.3. Synthetic scheme for the synthesis of **6.15** - **6.17**

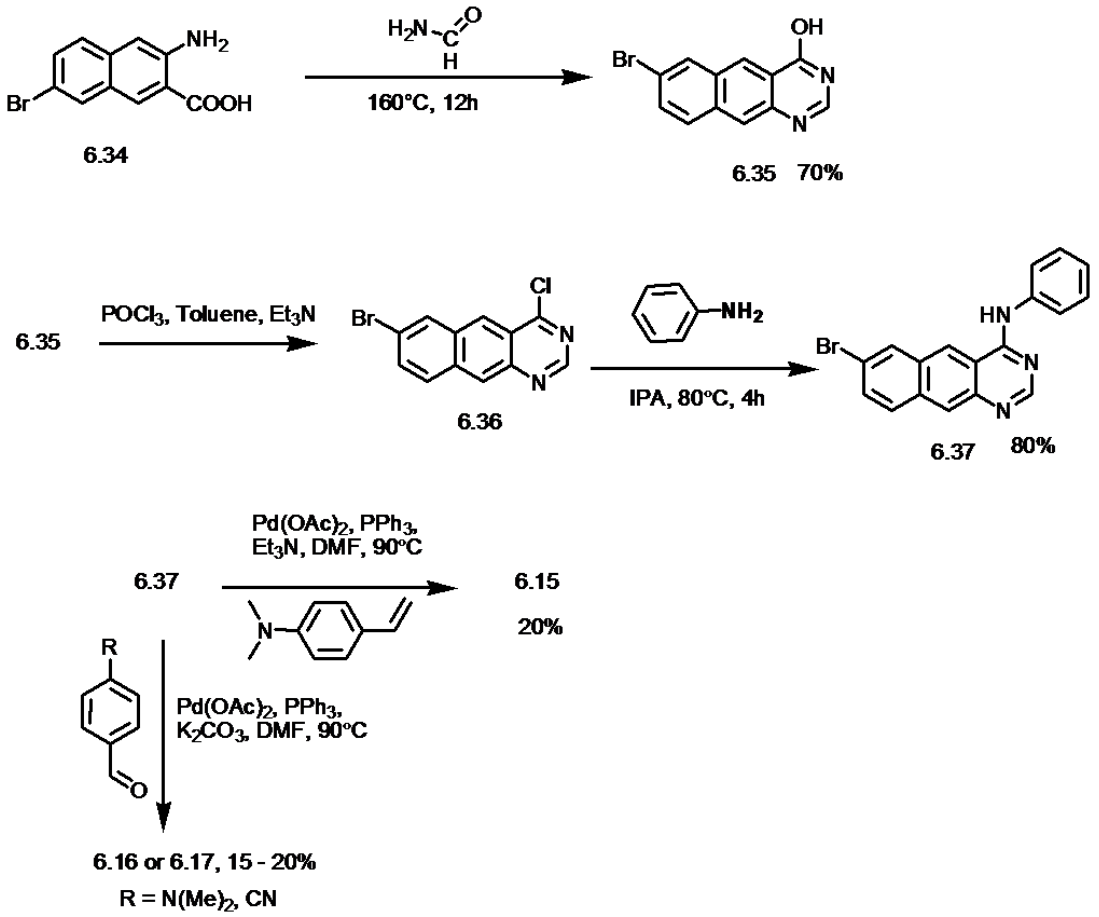

Styryl arms were synthesized by Wittig reaction (Scheme 6.1) and coupled to the corresponding aldehydes to obtain styryl substituted derivatives (**6.4**, **6.16**, **6.17**). Furanoyl aldehyde intermediates (**6.40**) were condensed with the corresponding aldehydes to obtain the furanoyl substituted derivatives (**6.5** - **6.10** and **6.14**) using Knoevenegal conditions (Scheme 6.4). Compound **6.15** was synthesized using Heck coupling from the 4-*N, N*-Dimethylamino-styrene (Scheme 6.3). Synthesis of compounds **6.16** and **6.17** were obtained by Suzuki coupling with the corresponding aldehydes (Scheme 6.3).

Scheme 6.4. General synthetic scheme for the synthesis of furanoyl derivatives

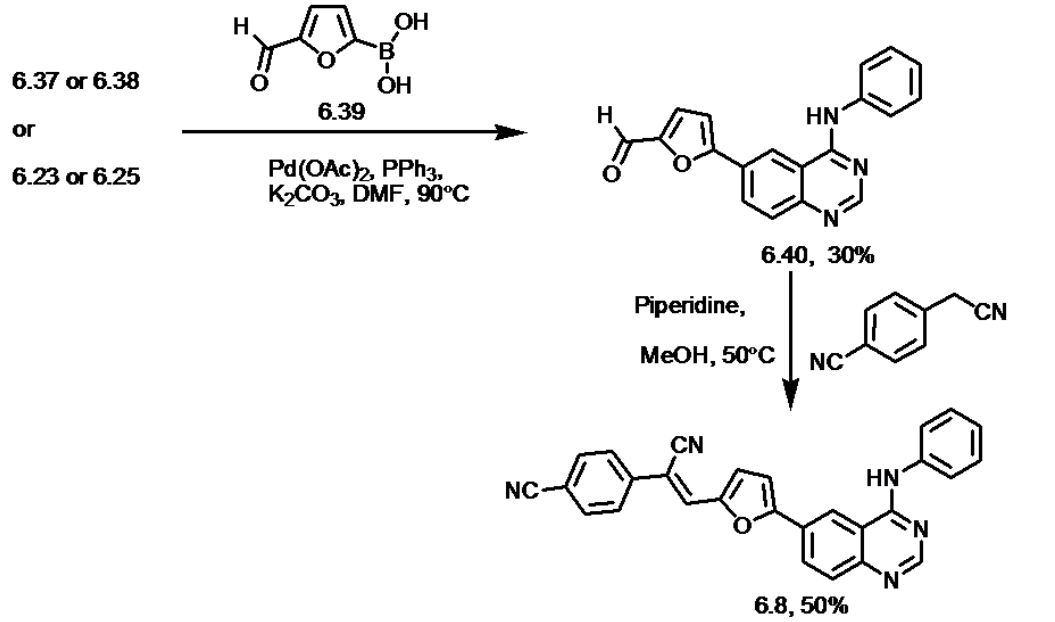

6.3. *Experimental section:*

***4-(phenylamino)quinazoline-6-carbonitrile (6.1)*:** ^{1}H NMR (500 MHz, DMSO): δ (ppm) 7.31-7.34 (m, 1H), 7.55-7.58 (m, 2H), 7.99(d, 2H, J = 7.5 Hz), 8.03 (d, 1H, J = 8.5 Hz), 8.29 (d, 1H, J = 7.0 Hz), 8.83 (s, 1H), 9.3 (s, 1H), 10.19 (s, 1H); ^{13}C NMR (125 MHz, DMSO): δ (ppm) 108.7, 115.4, 118.9, 123, 124.8, 129, 129.5, 130.2, 134.5, 138.9, 152, 157.6, 158; HRMS (ESI) $C_{15}H_{10}N_4$ $[M+H]^+$ calcd 247.0984, found 247.0991.

***N-(3-chloro-4-fluorophenyl)-6-(furan-2-yl)quinazolin-4-amine (6.2)*:** ^{1}H NMR (500 MHz, DMSO): δ (ppm) 6.71 (s, 1H), 7.15 (s, 1H), 7.47(t, 1H, J = 9.1 Hz), 7.82 – 7.90 (m, 2H), 8.19 – 8.22 (m, 2H), 8.61 (s, 1H), 8.82 (s, 1H), 10.07 (s, 1H); ^{13}C NMR (125 MHz, DMSO): δ (ppm) 107.8, 112.9, 115.7, 116.9, 117.0, 119.1, 119.3, 123.0, 123.1, 124.2,

128.8, 129.0, 129.4, 136.8, 144.1, 149.4, 152.8, 154.5, 154.8, 157.9; HRMS (ESI) $C_{18}H_{12}ClFN_3O$ $[M+H]^+$ calcd 340.0652, found 340.0666.

N-(3-chloro-4-fluorophenyl)benzo[g]quinazolin-4-amine (6.3): ^{1}H NMR (500 MHz, DMSO): δ (ppm) 7.53 (t, 1H, J = 9.0 Hz), 7.67 (t, 1H, J = 7.5 Hz), 7.74 (br t, 1H), 7.88 (s, 1H), 8.14 - 8.22 (m, 3H), 8.41 (s, 1H), 8.79 (s, 1H), 9.52 (s, 1H); ^{13}C NMR (125 MHz, DMSO): δ (ppm) 114.3, 117.1, 117.4, 119.5, 121.4, 124.4, 125.5, 127.5, 128.2, 129.5, 131.6, 136.0, 139.7, 153.1, 153.8, 155.8, 159.7; HRMS (ESI) $C_{18}H_{11}ClFN_3$ $[M+H]^+$ calcd 324.0703, found 324.0703.

6-(4-(4-methylpiperazin-1-yl)styryl)-N-phenylquinazolin-4-amine (6.4): ^{1}H NMR (500 MHz, DMSO): δ (ppm) 2.58 (t, 4H, J = 4.5 Hz), 3.34 (t, 4H, J = 4.5 Hz), 3.48 (s, 3H), 7.11 (d, 2H, J = 8.5 Hz), 7.27-7.34 (m, 2H), 7.50-7.57 (m, 3H), 7.64 (d, 2H, J = 9 Hz), 7.88 (d, 1H, J = 8.5 Hz), 8.01 (d, 2H, J = 8.5 Hz), 8.22 (d, 1H, J = 8.5 Hz), 8.67 (s, 1H), 8.78 (s, 1H), 9.95 (s, 1H); ^{13}C NMR (125 MHz, DMSO): δ (ppm) 46.2, 47.9, 54.9, 115.5, 115.9, 119.8, 122.8, 124.1, 124.3, 127.5, 127.9, 128.5, 128.9, 130.4, 131.5, 136.3, 139.6, 149.4, 151.1, 154.4, 158.0; HRMS (ESI) $C_{27}H_{27}N_5$ $[M+H]^+$ calcd 422.2345, found 422.2352.

2-(2-methyl-6-((E)-2-(5-(4-(phenylamino)quinazolin-6-yl)furan-2-yl)vinyl)-4H-pyran-4-ylidene)malononitrile (6.5): ^{1}H NMR (500 MHz, DMSO): δ (ppm) 2.6 (s, 3H), 6.85 (s, 1H), 7.06 (d, 1H, J = 2 Hz), 7.29 (d, 1H, J = 4.0 Hz), 7.38 (s, 1H), 7.41 (s, 1H), 7.48 (t, 2H, J = 15 Hz), 7.51(d, 1H, J = 3.5 Hz), 7.6 (s, 1H), 7.63 - 7.67 (m, 3H), 7.88 (d, 2H, J = 7.5 Hz), 8.03 (d, 1H, J = 9.0 Hz), 8.63 (d, 1H, J = 9.0 Hz), 8.97 (s, 1H), 9.2 (s, 1H); ^{13}C NMR (125 MHz, DMSO): δ (ppm) 19.8, 56.4, 106.1, 107.5, 111.8, 114.7, 115.7,

115.8, 117.4, 118.4, 119.3, 122.8, 124, 125.1, 126.8, 129.2, 131.4, 137.3, 141.1, 152.2, 153.9, 156.7, 159.6, 159.7, 164.3; IR ν_{max} (cm^{-1}): 2957, 1934, 1600, 1568, 1523, 1499, 1446, 1403, 1357, 1327, 1290, 1228, 810, 744, 692; HRMS (ESI) $C_{22}H_{20}N_4$ $[M+H]^+$ calcd 341.1766, found 341.1770; 25% yield. M.P.: 257-259°C (d).

N-phenyl-6-(5-((E)-2-(4-N-methyl-pyridin-4-yl)vinyl)furan-2-yl)quinazolin-4-amine 6.6): ^{1}H NMR (500 MHz, DMSO): δ (ppm) 3.48 (s, 3H), 7.3 (d, 1H, J = 3 Hz), 7.33 (t, 1H, J = 14.5 Hz), 7.51 - 7.6 (br m, 4H), 7.98 – 8.03 (m, 3H), 8.09 (d, 1H, J = 15 Hz), 8.33 (d, 2H, J = 6 Hz), 8.48 (d, 1H, J = 8.5 Hz), 8.73 (s, 1H), 8.96 (J = 6.5 Hz), 9.13 (s, 1H), 10.11 (s, 1H); ^{13}C NMR (125 MHz, DMSO) δ (ppm) 47.3, 110.9, 115.9, 118.9, 119.3, 121.2, 123.3, 123.6, 124.6, 127.4, 129, 129.1, 129.4, 139.2, 145.3, 150.2, 152, 155.4, 155.6, 158.3; IR ν_{max} (cm^{-1}): 2999, 1937, 1600, 1570, 1522, 1496, 1445, 1400, 1358, 1270, 1247, 828, 818, 753; HRMS (ESI) $C_{21}H_{17}N_3O$ $[M+H]^+$ calcd 328.1449, found 328.1453;.M.P.: 245-247°C.

6-(5-(4-(dimethylamino)styryl)furan-2-yl)-N-phenylquinazolin-4-amine (6.7): ^{1}H NMR (500 MHz, DMSO): δ (ppm) 2.97 (s, 6 H), 6.64 (br m, 3H), 7.56 (t, 2H, J = 15.0 Hz), 7.85 – 7.91 (m, 5H), 8.2 (d, 1H, J = 9.0 Hz), 8.59 (s, 1H), 8.86 (s, 1H), 9.96 (s, 1H); ^{13}C NMR (125 MHz, DMSO) δ (ppm) 49.06, 110.11, 110.46, 112.09, 112.77, 116.04, 116.93, 123.35, 124.45, 124.85, 128.02, 128.53, 128.58, 128.93, 128.98, 129.20, 150.56, 151.6, 154.58, 154.72, 158.22; IR ν_{max} (cm^{-1}): 3067, 1939, 600, 1567, 1528, 1488, 1445, 1405, 1359, 1325, 1295, 840, 748, 689; HRMS (ESI) $C_{20}H_{15}N_3$ $[M+H]^+$ calcd 298.1344, found 298.1352; M.P.: 258 - 262° C (d).

4-((Z)-1-cyano-2-(5-(4-(phenylamino)quinazolin-6-yl)furan-2-yl)vinyl)benzonitrile (6.8): ^{1}H NMR (500 MHz, DMSO): δ (ppm) 3.49 (s, 1H), 7.17 (t, 1H, J = 14.7 Hz), 7.37-7.44 (br m, 5H), 7.84 (d, 2H, J = 8.6 Hz), 7.87 - 7.97 (br m, 5H), 8.16 (s, 1H), 8.3 (dd, 1H, J = 8.6 Hz), 8.58 (s, 1H), 8.99 (s, 1H), 9.79 (s, 1H); ^{13}C NMR (125 MHz, DMSO): δ (ppm) 104.7, 111.4, 111.7, 114.3, 117.6, 118.8, 120.3, 121.6, 122.2, 124.9, 126.3, 127.3, 129, 129.3, 129.9, 131.2, 133.3, 136.8, 137.9, 139.2, 150, 151.7, 154.6, 159.7; HRMS (ESI) $C_{28}H_{17}N_5O$ $[M+H]^+$ calcd 440.1511, found 440.1514.

(Z)-2-(4-methoxyphenyl)-3-(5-(4-(phenylamino)quinazolin-6-yl)furan-2-yl)acrylonitrile (6.9): ^{1}H NMR (500 MHz, DMSO): δ (ppm) 3.96 (s, 3H), 7.23 (d, 2H, J = 8.5 Hz), 7.33 (t, 1H, J = 9 Hz), 7.39 (s, 1H, J = 3.5 Hz), 7.52 (s, 1H, J = 3.5 Hz), 7.58 (t, 2H, J = 16 Hz), 7.85 (d, 2H, J = 9 Hz), 7.98- 8.04 (m, 4H), 8.46 (dd, 1H, J = 9.0 Hz), 8.73 (s, 1H), 9.12 (s, 1H), 9.96 (s, 1H); ^{13}C NMR (125 MHz, DMSO): δ (ppm) 55.8, 105.8, 110.2, 115.1, 115.8, 118.7, 119, 119.3 122.9, 124.4, 125.9, 126.1, 127.2, 127.3, 128.8, 129, 129.1, 139.3, 149.9, 150.1, 154.8, 155.2, 158, 160.3; HRMS (ESI) $C_{28}H_{20}N_4O_2$ $[M+H]^+$ calcd 445.1665, found 445.1674.

N-phenyl-6-(5-((E)-2-(3-N-methyl)-quinolin-3-yl)vinyl)furan-2-yl)quinazolin-4-amine (6.10): ^{1}H NMR (500 MHz, DMSO): δ (ppm) 4.67 (s, 3H), 7.34 (t, 1H, J = 14.5 Hz), 7.47 (d, 1H, J = 3 Hz), 7.58 – 7.63 (m, 3H), 8.04 (d, 1H, J = 8.5Hz), 8.09 (d, 2H, J = 8.0 Hz), 8.22 (t, 1H, J = 15.0 Hz), 8.29 – 8.45 (br m, 3H), 8.58 – 8.63 (m, 3H), 8.77 (s, 1H), 9.23 (d, 1H, J = 8.5 Hz), 9.26 (s, 1H), 9.43 (d, 1H, J = 6.5 Hz), 10.1 (s, 1H); ^{13}C NMR (125 MHz, DMSO): δ (ppm) 45.0, 111.2, 115.8, 115.8, 117.3, 119.2, 119.7, 120.4, 122.8,

124.3, 126.4, 126.6, 127.2, 129.0, 129.5, 135.4, 139.1, 139.4, 148.0, 151.9, 152.4, 155.4, 156.0, 158.1; HRMS (ESI) $C_{30}H_{23}N_4O^+$ $[M+H]^+$ calcd 455.1866, found 455.1876.

***4-(phenylamino)benzo[g]quinazoline-7-carbonitrile (6.11)*:** ^{1}H NMR (500 MHz, DMSO): δ (ppm) 7.20 (t, 1H, J = 7.5 Hz), 7.45 (t, 2H, J = 8.0 Hz), 7.86 (d, 1H, J = 8.5 Hz), 7.92 (d, 2H, J = 8.0 Hz), 8.31 (d, 1H, J = 9.0 Hz), 8.50 (s, 1H), 8.63 (s, 1H), 8.69 (s, 1H), 9.39 (s, 1H), 10.38 (s, 1H); ^{13}C NMR (125 MHz, DMSO): δ (ppm) 110.4, 114.2, 177.6, 118.8, 125.2, 127.7, 128.2, 129.3, 129.8, 129.9, 130.1, 136.0, 136.5, 136.8, 153.3, 160.7; HRMS (ESI) $C_{19}H_{12}N_4$ $[M+H]^+$ calcd 297.1140 found 297.1144.

N-(4-(3-fluorobenzyloxy)-3-chlorophenyl)-6-(4-(dimethylamino)styryl)quinazolin-4-amine (6.12): ^{1}H NMR (500 MHz, DMSO): δ (ppm) 3.08 (s, 6H), 5.39 (s, 2H), 6.89 (d, 2H, J = 8.5 Hz), 7.24 (d, 1H, J = 16.0 Hz), 7.33 (t, 1H, J = 16 Hz), 7.41-7.51 (m, 4H), 7.61 - 7.62 (m, 3H), 7.86 (d, 1H, J = 8.5 Hz), 7.91 (dd, 1H, J = 9.0 Hz, 2.5 Hz), 8.18 - 8.20 (m, 2H), 8.68 (d, 2H, J = 12.5 Hz), 9.92 (s, 1H); ^{13}C NMR (125 MHz, DMSO): δ (ppm) 69.9, 112.7, 114.4, 114.5, 114.8, 115.0, 115.2, 115.8, 119.3, 121.5, 122.5, 123.0, 123.7, 124.4, 125.0, 128.1, 128.5, 130.8, 130.9, 131.5, 133.8, 136.6, 140.1, 149.2, 150.0, 150.6, 154.2, 157.7, 161.7, 163.6; IR ν_{max} (cm^{-1}): 3018, 2970, 1739, 1599, 1522, 1489, 1423, 1364, 1218, 831; HRMS (ESI) $C_{31}H_{26}ClFN_4O$ $[M+H]^+$ calcd 525.1857, found 525.1852.

N-(4-(3-fluorobenzyloxy)-3-chlorophenyl)benzo[g]quinazolin-4-amine (6.13): ^{1}H NMR (500 MHz, DMSO): δ (ppm) 5.25 (s, 2H), 7.18 (brt, 1H), 7.30 - 7.35 (m, 3H), 7.30 – 7.35 (q, 1H), 7.60 - 7.68 (m, 2H), 7.85 (d, 1H, J = 7.0 Hz), 8.11 – 8.15 (m, 3H), 8.40 (s, 1H), 8.59 (s, 1H), 9.22 (s, 1H), 10.0 (s, 1H); ^{13}C NMR (125 MHz, DMSO): δ (ppm) 70.0,

114.3, 114.5, 114.8, 115.0, 115.2, 115.4, 121.6, 122.7, 123.5, 123.7, 124.5, 125.3, 126.6, 128.2, 128.3, 129.2, 130.9, 131.0, 131.3, 133.7, 135.8, 140.1, 145.4, 150.2, 154.5, 158.5, 161.7, 163.6; HRMS (ESI) $C_{25}H_{17}ClFN_3O$ $[M+H]^+$ calcd 430.1122, found 432.1127.

2-(2-((E)-2-(5-(4-(3-chloro-4-fluorophenylamino)quinazolin-6-yl)furan-2-yl)vinyl)-6-methyl-4H-pyran-4-ylidene)malononitrile (6.14): ^{1}H NMR (500 MHz, DMSO): δ (ppm) 2.50 (s, 3H), 7.19 (td, 1H), 7.30 - 7.34 (m, 2H), 7.45 – 7.50 (m, 2H), 7.64 (d, 1H, J = 4.0 Hz), 7.17 (dd, 1H, J = 9.0 Hz, 2.5 Hz), 7.90 (d, 1H, J = 8.5 Hz), 8.01 (d, 1H, J = 4.0 Hz), 8.24 (dd, 1H, J = 9.0 Hz, 2.5 Hz), 8.32 (s, 1H), 8.61 (s, 1H), 9.00 (s, 1H), 9.85 (s, 1H); ^{13}C NMR (125 MHz, DMSO): δ (ppm) 69.8, 74.3, 111.9, 114.5, 114.6, 115.2, 121.2, 121.6, 123.1, 123.7, 124.8, 126.3, 128.0, 128.8, 129.2, 131.0, 132.8, 140.0, 143.5, 148.2, 150.7, 155.4, 158.1, 159.3, 161.7, 163.6; HRMS (ESI) $C_{29}H_{17}ClFN_5O_2$ $[M+H]^+$ calcd 522.1133, found 522.1131.

7-(4-(dimethylamino)phenyl)-N-phenylbenzo[g]quinazolin-4-amine (6.15): ^{1}H NMR (500 MHz, DMSO): δ (ppm) 2.99 (s, 6H), 6.89 (d, 2H, J = 9.0 Hz), 7.17 (t, 1H, J = 7.5 Hz), 7.44 (t, 2H, J = 8.0 Hz), 7.75 (d, 2H, J = 8.5 Hz), 7.99 (br t, 3H), 8.19 (d, 1H, J = 9 Hz), 8.22 (s, 1H), 8.38 (s, 1H), 8.57 (s, 1H), 9.26 (s, 1H), 10.11 (s, 1H); ^{13}C NMR (125 MHz, DMSO): δ (ppm) 40.1, 113.2, 115.9, 122.8, 123.2, 123.5, 124.3, 125.0, 127.1, 127.7, 127.8, 128.7, 128.9, 132.0, 134.5, 138.1, 139.7, 145.3, 150.6, 154.2, 158.6; HRMS (ESI) $C_{26}H_{22}N_4$ $[M+H]^+$ calcd 391.1922, found 391.1922.

7-(4-(dimethylamino)styryl)-N-phenylbenzo[g]quinazolin-4-amine (6.16): ^{1}H NMR (500 MHz, DMSO): δ (ppm) 2.96 (s, 6H), 6.76 (d, 2H, J = 8.5 Hz), 7.17(t, 1H, J = 7.5 Hz), 7.28 (dd, 3H, J = 48 Hz, 16.5 Hz), 7.44 (t, 2H, J = 8.5 Hz), 7.54 (d, 2H, J = 9.0 Hz),

7.96 (d, 2H, *J* = 7.5 Hz), 8.03 (d, 2H, *J* = 8.5 Hz), 8.10 (d, 1H, *J* = 9.0 Hz), 8.33 (s, 1H), 8.58 (s, 1H), 9.18 (s, 1H), 10.09 (s, 1H); ^{13}C NMR (125 MHz, DMSO): δ (ppm) 40.8, 104.6, 111.3, 111.6, 114.2, 114.7, 116.9, 119.8, 119.9,120.1, 122.1, 122.3, 125.1, 126.2, 126.5, 129.0, 131.2, 133.3, 134.1, 137.9, 139.6, 150.0, 151.9, 154.6, 159.4; HRMS (ESI) $C_{28}H_{24}N_4$ $[M+H]^+$ calcd 417.2079, found 417.2081.

4-((E)-2-(4-(phenylamino)benzo[g]quinazolin-7-yl)vinyl)benzonitrile (6.17): ^{1}H NMR (500 MHz, DMSO): δ (ppm) 7.18 (t, 1H, *J* = 7.5 Hz), 7.44 (t, 2H, *J* = 8 Hz), 7. 58 (d, 1H, *J* = 16.5 Hz), 7. 58 (d, 1H, *J* = 16.5 Hz), 7.79 (d, 1H, *J* = 16 Hz), 7.87 - 7.96 (m, 5H), 8.11(d, 1H, *J* = 9.0 Hz), 8.17(d, 2H, *J* = 4.5 Hz), 8.38 (s, 1H), 8.59 (s, 1H), 9.27 (s, 1H), 10.20 (s, 1H); ^{13}C NMR (125 MHz, DMSO): δ (ppm) 110.1, 115.9, 119.4, 123.1, 123.9, 124.5, 125.3, 125.5, 127.7, 128.3, 128.9, 129.0, 131.4, 132.4, 133.0, 134.6, 135.6, 139.4, 142.2, 146.0, 154.7, 158.6; HRMS (ESI) $C_{27}H_{18}N_4$ $[M+H]^+$ calcd 399.1609, found 399.1604.

References:

1. Gomes, A.; Fernandes, E.; Lima, J. L. F. C., Fluorescence probes used for detection of reactive oxygen species. *Journal of Biochemical and Biophysical Methods* **2005,** *65*, (2-3), 45-80.

2. Ueno, T.; Nagano, T.,, Fluorescent probes for sensing and imaging. *Nature Methods* **2011,** *8* (8), 642-645.

3. Xu, Q.; Lee, K.-A.; Lee, S.; Lee, K. M.; Lee, W.-J.; Yoon, J., A highly specific fluorescent probe for hypochlorous acid and its application in imaging microbe-induced HOCl production. *Journal of the American Chemical Society* **2013,** *135* (26), 9944-9949.

4. Johnson, I., Review: Fluorescent probes for living cells. *Histochem J* **1998,** *30* (3), 123-140.

5. Zhang, L.; Duan, D.; Liu, Y.; Ge, C.; Cui, X.; Sun, J.; Fang, J., Highly selective off–on fluorescent probe for imaging thioredoxin reductase in living cells. *Journal of the American Chemical Society* **2013,** *136* (1), 226-233.

6. Zheng, G.; Lovell, J. F., Activatable smart probes for molecular optical imaging and therapy. *Journal of Innovative Optical Health Sciences* **2008,** *01* (01), 45-61.

7. Kobayashi, H.; Ogawa, M.; Alford, R.; Choyke, P. L.; Urano, Y., New strategies for fluorescent probe design in medical diagnostic imaging. *Chemical Reviews* **2009,** *110* (5), 2620-2640.

8. Zhuang, Y.-D.; Chiang, P.-Y.; Wang, C.-W.; Tan, K.-T., Environment-sensitive fluorescent turn-on probes targeting hydrophobic ligand-binding domains for selective protein detection. *Angewandte Chemie International Edition* **2013,** *52* (31), 8124-8128.

9. Lacivita, E.; Leopoldo, M.; Berardi, F.; Colabufo, N. A.; Perrone, R., Activatable fluorescent probes: A new concept in optical molecular imaging. *Current Medicinal Chemistry* **2012,** *19* (28), 4731-4741

10. Tung, C.-H.; Bredow, S.; Mahmood, U.; Weissleder, R., Preparation of a cathepsin D sensitive near-infrared fluorescence probe for imaging. *Bioconjugate Chemistry* **1999,** *10* (5), 892-896.

11. Abd-Elgaliel, W. R.; Cruz-Monserrate, Z.; Logsdon, C. D.; Tung, C.-H., Molecular imaging of cathepsin E-positive tumors in mice using a novel protease-activatable fluorescent probe. *Molecular BioSystems* **2011,** *7* (12), 3207-3213.

12. Ogawa, M.; Kosaka, N.; Choyke, P. L.; Kobayashi, H., H-Type dimer formation of fluorophores: A mechanism for activatable, in vivo optical molecular imaging. *ACS Chemical Biology* **2009,** *4* (7), 535-546.

13. Chang, M. C. Y.; Pralle, A.; Isacoff, E. Y.; Chang, C. J., A selective, cell-permeable optical probe for hydrogen peroxide in living cells. *Journal of the American Chemical Society* **2004,** *126* (47), 15392-15393.

14. Setsukinai, K.; Urano, Y.; Kakinuma, K.; Majima, H. J.; Nagano, T., Development of novel fluorescence probes that can reliably detect reactive oxygen species and distinguish specific species. *Journal of Biological Chemistry* **2003,** *278* (5), 3170-3175.

15. Lim, M. H.; Xu, D.; Lippard, S. J., Visualization of nitric oxide in living cells by a copper-based fluorescent probe. *Nature Chemical Biology* **2006,** *2* (7), 375 - 380

16. Yuan, L.; Lin, W.; Zheng, K.; Zhu, S., FRET-based small-molecule fluorescent probes: rational design and bioimaging applications. *Accounts of Chemical Research* **2013,** *46* (7), 1462-1473.

17. Liu, S.; Li, D.; Zhang, Z.; Surya Prakash, G. K.; Conti, P. S.; Li, Z., Efficient synthesis of fluorescent-PET probes based on [18F]BODIPY dye. *Chemical Communication*s **2014**, *50* (55), 7371-7373.

18. Zhang, W.; Ma, Z.; Du, L.; Li, M., Design strategy for photoinduced electron transfer-based small-molecule fluorescent probes of biomacromolecules. *Analyst* **2014,** *139* (11), 2641-2649.

19. Nagano, T., Development of fluorescent probes for bioimaging applications. *Proceedings of the Japan Academy. Series B, Physical and Biological Sciences.* **2010,** *86* (8), 837–847.

20. Sakabe, M.; Asanuma, D.; Kamiya, M.; Iwatate, R. J.; Hanaoka, K.; Terai, T.; Nagano, T.; Urano, Y., Rational design of highly sensitive fluorescence probes for protease and glycosidase based on precisely controlled spirocyclization. *Journal of the American Chemical Society* **2012,** *135* (1), 409-414.

21. Kim, H. N.; Lee, M. H.; Kim, H. J.; Kim, J. S.; Yoon, J., A new trend in rhodamine-based chemosensors: application of spirolactam ring-opening to sensing ions. *Chemical Society Reviews* **2008,** *37* (8), 1465-1472.

22. Kenmoku, S.; Urano, Y.; Kojima, H.; Nagano, T., Development of a highly specific rhodamine-based fluorescence probe for hypochlorous acid and its application to real-time imaging of phagocytosis. *Journal of the American Chemical Society* **2007,** *129* (23), 7313-7318.

23. Chipem, F. A. S.; Mishra, A.; Krishnamoorthy, G., The role of hydrogen bonding in excited state intramolecular charge transfer. *Physical Chemistry Chemical Physics* **2012,** *14* (25), 8775-8790.

24. Yong Lee, J.; Kim, K. S.; Jin Mhin, B., Intramolecular charge transfer of π-conjugated push–pull systems in terms of polarizability and electronegativity. *The Journal of Chemical Physics* **2001,** *115* (20), 9484-9489.

25. Yang, J.-S.; Liau, K.-L.; Hwang, C.-Y.; Wang, C.-M., Photoinduced single- versus double-bond torsion in donor−acceptor−substituted trans-stilbenes. *The Journal of Physical Chemistry A* **2006,** *110* (26), 8003-8010.

26. Soujanya, T.; Fessenden, R. W.; Samanta, A., Role of nonfluorescent twisted intramolecular charge transfer state on the photophysical behavior of aminophthalimide dyes. *The Journal of Physical Chemistry* **1996,** *100* (9), 3507-3512.

27. Bajorek, A.; Pączkowski, J., Influence of the attachment of chromophores to a polymer chain on their twisted intramolecular charge-transfer state in dilute solution. *Macromolecules* **1998,** *31* (1), 86-95.

28. Grabowski, Z. R.; Rotkiewicz, K.; Rettig, W., Structural changes accompanying intramolecular electron transfer: focus on twisted intramolecular charge-transfer states and structures. *Chemical Reviews* **2003,** *103* (10), 3899-4032.

29. Dhuguru, J.; Gheewala, C.; Kumar, N. S. S.; Wilson, J. N., Highly chromic, proton responsive phenyl pyrimidones. *Organic Letters* **2011,** *13* (16), 4188-4191.

30. Sicard, R.; Dhuguru, J.; Liu, W.; Patel, N.; Landgraf, R.; Wilson, J. N., A fluorescent reporter of ATP binding-competent receptor kinases. *Bioorganic & Medicinal Chemistry Letters* **2012,** *22* (17), 5532-5535.

31. Dhuguru, J.; Liu, W.; Gonzalez, W. G.; Babinchak, W. M.; Miksovska, J.; Landgraf, R.; Wilson, J. N., Emission tuning of fluorescent kinase inhibitors: conjugation length and substituent effects. *The Journal of Organic Chemistry* **2014,** *79* (11), 4940-4947.

32. Krause, D. S.; Van Etten, R. A., Tyrosine kinases as targets for cancer therapy. *New England Journal of Medicine* **2005,** *353* (2), 172-187.

33. Manash K. Paul , A. K. M., Tyrosine kinase – role and significance in cancer. *International Journal of Medical Sciences* **2004,** *1* (2), 101-115.

34. Fischer, P. M., The design of drug candidate molecules as selective inhibitors of therapeutically relevant protein kinases. *Current Medicinal Chemistry* **2004,** *11* (12), 1563-83.

35. Bedada, A. T.; Gayesa, R. T., Tyrosine kinase as target for cancer treatment. *International Journal of Pharmaceutical Sciences and Research* **2014,** *5* (1), 1.

36. Hanahan, D.; Weinberg, Robert A., Hallmarks of cancer: The next generation. *Cell 144* (5), 646-674.

37. (a) Bennasroune, A.; Gardin, A.; Aunis, D.; Crémel, G.; Hubert, P., Tyrosine kinase receptors as attractive targets of cancer therapy. *Critical Reviews in Oncology/Hematology* **2004,** *50* (1), 23-38; (b) Vlahovic, G.; Crawford, J., Activation of tyrosine kinases in Cancer. *The Oncologist* **2003,** *8* (6), 531-538.

38. Takeuchi, K.; Ito, F., Receptor tyrosine kinases and targeted cancer therapeutics. *Biological and Pharmaceutical Bulletin* **2011,** *34* (12), 1774-1780.

39. Pao, W.; Miller, V. A., Epidermal growth factor receptor mutations, small-molecule kinase inhibitors, and non–small-cell lung cancer: Current knowledge and future directions. *Journal of Clinical Oncology* **2005,** *23* (11), 2556-2568.

40. Ahmad, N. G. A. T., ErbB receptor tyrosine kinase inhibitors as therapeutic agents. *Frontiers in Bioscience* **2002,** *7* (1-3), 1926-1940.

41. de Bono, J. S.; Rowinsky, E. K., The ErbB receptor family: a therapeutic target for cancer. *Trends in Molecular Medicine* **2002,** *8* (4), S19-S26.

42. Denny, W. A., Irreversible inhibitors of the erbB family of protein tyrosine kinases. *Pharmacology & Therapeutics* **2002,** *93* (2–3), 253-261.

43. Denny, W. A., The 4-anilinoquinazoline class of inhibitors of the ErbB family of receptor tyrosine kinases. *Il Farmaco* **2001,** *56* (1–2), 51-56.

44. Liu, Y.; Gray, N. S., Rational design of inhibitors that bind to inactive kinase conformations. *Nature Chemical Biology* **2006,** *2* (7), 358-64.

45. Niall Tebbutt, M. W. P. T. G. J., Targeting the ERBB family in cancer: couples therapy. *Nature Reviews Cancer* **2013,** *13* (9), 663–673.

46. Ciavarella, S.; Milano, A.; Dammacco, F.; Silvestris, F., Targeted therapies in cancer.*BioDrugs* **2010,** *24* (2), 77-88.

47. Arteaga, C. L.; Moulder, S. L.; Yakes, F. M., HER (erbB) tyrosine kinase inhibitors in the treatment of breast cancer. *Seminars in Oncology* **2002,** *29* (3), 4-10.

48. Blanc, J.; Geney R.; Menet C.; Type II kinase inhibitors: An opportunity in cancer for rational design. *Anti-Cancer Agents in Medicinal Chemistry* **2013,** *13* (5), 731-47.

49. Arora, A.; Scholar, E. M., Role of tyrosine kinase inhibitors in cancer therapy. *Journal of Pharmacology and Experimental Therapeutics* **2005,** *315* (3), 971-979.

50. Fasano, M.; Della Corte, C. M.; Califano, R.; Capuano, A.; Troiani, T.; Martinelli, E.; Ciardiello, F.; Morgillo, F., Type III or allosteric kinase inhibitors for the treatment of non-small cell lung cancer. *Expert Opinion on Investigational Drugs* **2014,** *23* (6), 809-821.

51. Dietrich, J. D.; Sciences, T. U. O. A. P., The design, synthesis, and evaluation of novel DFG-out allosteric kinase inhibitors. The University of Arizona: 2008.

52. Powers, D. L.; Sowell, J. W.; Freeman, J. J.; Kosh, J. W., Anticonvulsant properties of selected pyrrolo[2,3-d]pyrimidine-2,4-diones and intermediates. *Journal of Pharmaceutical Sciences* **1980,** *69* (4), 473-475.

53. El-Agrody, A. M.; Ali, F. M.; Eid, F. A.; El-Nassag, M. A. A.; El-Sherbeny, G.; Bedair, A. H, Synthesis and antimicrobial activity of thioxopyrimidines and related derivatives. *Phosphorus Sulfur and Silicon and The Related Elements* **2006,** *181* (4), 839-864.

54. Mahmoud, M. R.; El-Ziaty, A. K.; Ismail, M. F.; Shiba, S. A., Synthesis of novel pyrimidine and fused pyrimidine derivatives. *European Journal of Chemistry* **2011***, 2* (3), 347-355.

55. Díaz-Gavilán, M.; Gómez-Vidal, J. A.; Rodríguez-Serrano, F.; Marchal, J. A.; Caba, O.; Aránega, A.; Gallo, M. A.; Espinosa, A.; Campos, J. M., Anticancer activity of (1,2,3,5-tetrahydro-4,1-benzoxazepine-3-yl)-pyrimidines and -purines against the MCF-7 cell line: Preliminary cDNA microarray studies. *Bioorganic & Medicinal Chemistry Letters* **2008,** *18* (4), 1457-1460.

56. Dudhe, R.; Sharma, P.K.; Verma, P.; Chaudhary, A., Pyrimidine as anticancer agent: A review *Journal of Advanced Scientific Research* **2011,** *2* (3), 10-17.

57. Battenberg, O. A.; Nodwell, M. B.; Sieber, S. A., Evaluation of α-pyrones and pyrimidones as photoaffinity probes for affinity-based protein profiling. *The Journal of Organic Chemistry* **2011,** *76* (15), 6075-6087.

58. Chakrabarti, R.; Vikramadithyan, R. K.; Kumar, M. P.; Kumar, S. K. B.; Mamidi, N. V. S.; Misra, P.; Suresh, J.; Hiriyan, J.; Rao, C. S.; Rajagopalan, R., PMT13, a pyrimidone analogue of thiazolidinedione improves insulin resistance-associated disorders in animal models of type 2 diabetes. *Diabetes, Obesity and Metabolism* **2002,** *4* (5), 319-328.

59. Schlapbach, A.; Feifel, R.; Hawtin, S.; Heng, R.; Koch, G.; Moebitz, H.; Revesz, L.;Scheufler, C.; Velcicky, J.; Waelchli, R.; Huppertz, C., Pyrrolo-pyrimidones: A novel class of MK2 inhibitors with potent cellular activity. *Bioorganic & Medicinal Chemistry Letters* **2008,** *18* (23), 6142-6146.

60. Zhang, J.; Campbell, R. E.; Ting, A. Y.; Tsien, R. Y., Creating new fluorescent probes for cell biology. *Nature Reviews Molecular Cell Biology* **2002,** *3 (1)*, 906–918.

61. Fernandez-Suarez, M.; Ting, A. Y., Fluorescent probes for super-resolution imaging in living cells. *Nature Reviews Molecular Cell Biology* **2008,** *9 (12)*, 929-943.

62. Carlson, J. C. T.; Meimetis, L. G.; Hilderbrand, S. A.; Weissleder, R., BODIPY–tetrazine derivatives as superbright bioorthogonal turn-on probes. *Angewandte Chemie International Edition* **2013,** *52* (27), 6917-6920.

63. Dodonova, J.; Skardziute, L.; Kazlauskas, K.; Jursenas, S.; Tumkevicius, S., Synthesis of 4-aryl-, 2,4-diaryl- and 2,4,7-triarylpyrrolo[2,3-d]pyrimidines by a combination of the Suzuki cross-coupling and N-arylation reactions. *Tetrahedron* **2012,** *68* (1), 329-339.

64. Liu, B.; Hu, X.-L.; Liu, J.; Zhao, Y.-D.; Huang, Z.-L., Synthesis and photophysical properties of novel pyrimidine-based two-photon absorption chromophores. *Tetrahedron Letters* **2007,** *48* (34), 5958-5962.

65. Shafer, C. M.; Lindvall, M.; Bellamacina, C.; Gesner, T. G.; Yabannavar, A.; Jia, W.; Lin, S.; Walter, A., 4-(1H-Indazol-5-yl)-6-phenylpyrimidin-2(1H)-one analogs as potent CDC7 inhibitors. *Bioorganic & Medicinal Chemistry Letters* **2008,** *18* (16), 4482-4485.

66. Wu, H.; Chen, X.-m.; Wan, Y.; Ye, L.; Xin, H.-q.; Xu, H.-h.; Pang, L.-l.; Ma, R.; Yue, C.-h., Synthesis, fluorescence properties and Zn2+ recognition of 4-Aryl-6-phenylpyrimidin-2(1H)-one. *Journal of Chemical Research* **2008,** *2008* (12), 711-714.

67. Michelson, D. A. M., Hyperchromicity and nucleic acids. *Nature* **1958,** *182* (4648), 1502-1503.

68. Ding, D.; Zhao, C.-G., Primary amine catalyzed Biginelli reaction for the enantioselective synthesis of 3,4-Dihydropyrimidin-2(1H)-ones. *European Journal of Organic Chemistry* **2010**, 2010 (20), 3802-3005.

69. Società chimica, i., Gazzetta chimica Italiana. *Gazzetta chimica Italiana.* **1871**.

70. Kasende, O., Zeegers-Huyskens, T., Hydrogen bonding and the protonation site in 3-methyl-4-pyrimidone. *Journal of Molecular Structure* **1981,** *75* (2), 201-207.

71. (a) Bao, G.; Rhee, W. J.; Tsourkas, A., Fluorescent probes for live-cell RNA detection. *Annual Review of Biomedical Engineering* **2009,** *11* (1), 25-47; (b) Boutorine, A.; Novopashina, D.; Krasheninina, O.; Nozeret, K.; Venyaminova, A., Fluorescent probes for nucleic acid visualization in fixed and live Cells. *Molecules* **2013,** *18* (12), 15357-15397.

72. Zhang, J.; Campbell, R. E.; Ting, A. Y.; Tsien, R. Y., Creating new fluorescent probes for cell biology. *Nature Reviews. Molecular Cell Biology* **2002,** *3* (12), 906-18.

73. Eun Jun, M.; Roy, B.; Han Ahn, K., "Turn-on" fluorescent sensing with "reactive" probes. *Chemical Communications* **2011,** *47* (27), 7583-7601.

74. Hynes, N. E.; MacDonald, G., ErbB receptors and signaling pathways in cancer. *Current Opinion in Cell Biology* **2009,** *21* (2), 177-184.

75. Hynes, N. E.; Lane, H. A., ERBB receptors and cancer: the complexity of targeted inhibitors. *Nature Reviews Cancer* **2005,** *5 (5),* 341-354

76. Gray, N. S.; Yang, P. L.; Zhang, J., Targeting cancer with small molecule kinase inhibitors. *Nature Reviews Cancer* **2009,** *9* (1), 28.

77. Baselga, J.; Swain, S. M., Novel anticancer targets: revisiting ERBB2 and discovering ERBB3. *Nature Reviews Cancer* **2009,** *9* (7), 463-475.

78. Jänne, P. A.; Gray, N.; Settleman, J., Factors underlying sensitivity of cancers to small-molecule kinase inhibitors. *Nature Reviews Drug Discovery* **2009,** *8* (9), 709-723.

79. Daub, H.; Specht, K.; Ullrich, A., Strategies to overcome resistance to targeted protein kinase inhibitors. *Nature Reviews Drug Discovery* **2004,** *3* (12), 1001-1010.

80. Denny, W. A.; Rewcastle, G. W.; Bridges, A. J.; Fry, D. W.; Kraker, A. J.,, Structure-activity relationships for 4-anilinoquinazolines as potent inhibitors at the ATP binding site of the epidermal growth factor receptor in vitro. *Clinical and Experimental Pharmacology and Physiology* **1996,** *23* (5), 424-427.

81. VanBrocklin, H. F.; Lim, J. K.; Coffing, S. L.; Hom, D. L.; Negash, K.; Ono, M. Y.; Gilmore, J. L.; Bryant, I.; Riese, D. J., Anilinodialkoxyquinazolines: Screening epidermal growth factor receptor tyrosine kinase inhibitors for potential tumor imaging probes. *Journal of Medicinal Chemistry* **2005,** *48* (23), 7445-7456.

82. Bridges, A. J.; Zhou, H.; Cody, D. R.; Rewcastle, G. W.; McMichael, A.; Showalter, H. D. H.; Fry, D. W.; Kraker, A. J.; Denny, W. A., Tyrosine kinase inhibitors. 8. An unusually steep structure−activity relationship for analogues of 4-(3-Bromoanilino)-6,7-dimethoxyquinazoline (PD 153035), a potent inhibitor of the epidermal growth factor receptor. *Journal of Medicinal Chemistry* **1996,** *39* (1), 267-276.

83. Warren, C. M.; Landgraf, R., Signaling through ERBB receptors: Multiple layers of diversity and control. *Cellular Signalling* **2006,** *18* (7), 923-933.

84. Tian, F.; Debler, E. W.; Millar, D. P.; Deniz, A. A.; Wilson, I. A.; Schultz, P. G., The effects of antibodies on stilbene excited-state energetics. *Angewandte Chemie International Edition* **2006,** *45* (46), 7763-7765.

85. Wood, E. R.; Truesdale, A. T.; McDonald, O. B.; Yuan, D.; Hassell, A.; Dickerson, S. H.; Ellis, B.; Pennisi, C.; Horne, E.; Lackey, K.; Alligood, K. J.; Rusnak, D. W.; Gilmer, T. M.; Shewchuk, L., A unique structure for epidermal growth factor receptor bound to GW572016 (Lapatinib): relationships among protein conformation, inhibitor off-rate, and receptor activity in tumor cells. *Cancer Research* **2004,** *64* (18), 6652-6659.

86. Sarno S.; de Moliner E.; Ruzzene M.; Pagano MA.; Battistutta R.; Bain J.; Fabbro D.; Schoepfer J.; Elliott M.; Furet P.; Meggio F.; Zanotti G.; Pinna LA.; Biochemical and three-dimensional-structural study of the specific inhibition of protein kinase CK2 by [5-oxo-5,6-dihydroindolo-(1,2-a)quinazolin-7-yl]acetic acid (IQA). *Biochemical Journal* **2003,** *374*, 639–646

87. Emerson, E. S.; Conlin, M. A.; Rosenoff, A. E.; Norland, K. S.; Rodriguez, H.; Chin, D.; Bird, G. R., The geometrical structure and absorption spectrum of a cyanine dye aggregate. *The Journal of Physical Chemistry* **1967,** *71* (8), 2396-2403.

88. Le Breton, H.; Bennetau, B.; Létard, J. F.; Lapouyade, R.; Rettig, W., Nonradiative twisted intramolecular charge transfer state in polar stilbenes: Photophysical study of 4-perfluorooctylsulfonyl-4′-N,N-dimethylamino stilbene and two bridged derivatives. *Journal of Photochemistry and Photobiology A: Chemistry* **1996,** *95* (1), 7-20.

89. Huse, M.; Kuriyan, J., The conformational plasticity of protein kinases. *Cell 109* (3), 275-282.

90. Ocaña, A.; Amir, E., Irreversible pan-ErbB tyrosine kinase inhibitors and breast cancer: Current status and future directions. *Cancer Treatment Reviews 35* (8), 685-691.

91. Fabbro, D.; Ruetz, S.; Buchdunger, E.; Cowan-Jacob, S. W.; Fendrich, G.; Liebetanz, J.; Mestan, J.; O'Reilly, T.; Traxler, P.; Chaudhuri, B.; Fretz, H.; Zimmermann, J.; Meyer, T.; Caravatti, G.; Furet, P.; Manley, P. W., Protein kinases as targets for anticancer agents: from inhibitors to useful drugs. *Pharmacology & Therapeutics* **2002,** *93* (2–3), 79-98.

92. Stamos, J.; Sliwkowski, M. X.; Eigenbrot, C., Structure of the epidermal growth factor receptor kinase domain alone and in complex with a 4-anilinoquinazoline inhibitor. *Journal of Biological Chemistry* **2002,** *277* (48), 46265-46272.

93. Krueger, A. T.; Lu, H.; Lee, A. H. F.; Kool, E. T., Synthesis and properties of size-expanded DNAs: Toward designed, functional genetic systems. *Accounts of Chemical Research* **2006,** *40* (2), 141-150.

94. Secrist, J. A.; Barrio, J. R.; Leonard, N. J.; Villar-Palasi, C.; Gilman, A. G., Fluorescent modification of adenosine 3',5'-monophosphate: spectroscopic properties and activity in enzyme systems. *Science* **1972,** *177* (4045), 279-280.

95. Sinkeldam, R. W.; Greco, N. J.; Tor, Y., Fluorescent analogs of biomolecular building blocks: Design, properties, and applications. *Chemical Reviews* **2010,** *110* (5), 2579-2619.

96. Hawkins, M. E.; Pfleiderer, W.; Jungmann, O.; Balis, F. M., Synthesis and fluorescence characterization of pteridine adenosine nucleoside analogs for DNA incorporation. *Analytical Biochemistry* **2001,** *298* (2), 231-240.

97. Marenich, A. V.; Cramer, C. J.; Truhlar, D. G., Universal solvation model based on solute electron density and on a continuum model of the solvent defined by the bulk dielectric constant and atomic surface tensions. *The Journal of Physical Chemistry B* **2009,** *113* (18), 6378-6396.

98. Pitter, D. R. G.; Wigenius, J.; Brown, A. S.; Baker, J. D.; Westerlund, F.; Wilson, J. N., Turn-on fluorescent nuclear stains with live cell compatibility. *Organic Letters* **2013,** *15* (6), 1330-1333.

99. Reichardt, C., Empirical parameters of solvent polarity as linear free-energy relationships. *Angewandte Chemie International Edition in English* **1979,** *18* (2), 98-110.

100. Danielsson, L.-G. r.; Zhang, Y.-H., Methods for determining n-octanol-water partition constants. *Trends in Analytical Chemistry* **1996,** *15* (4), 188-196.

101. Yun, C.-H.; Boggon, T. J.; Li, Y.; Woo, M. S.; Greulich, H.; Meyerson, M.; Eck, M. J., Structures of lung cancer-derived EGFR mutants and inhibitor complexes: Mechanism of activation and insights into differential inhibitor sensitivity. *Cancer Cell 11* (3), 217-227.

102. Ban, H. S.; Tanaka, Y.; Nabeyama, W.; Hatori, M.; Nakamura, H., Enhancement of EGFR tyrosine kinase inhibition by C–C multiple bonds-containing anilinoquinazolines. *Bioorganic & Medicinal Chemistry* **2010,** *18* (2), 870-879.

103. Karaman, M. W. H., S.; Treiber, D. K.; Gallant, P.;Atteridge, C. E.; Campbell, B. T.; Chan, K. W.; Ciceri, P.; Davis, M. I.; Edeen, P. T.; Faraoni, R.; Floyd, M.; Hunt, J. P.; Lockhart, D. J.;; Milanov, Z. V. M., M. J.; Pallares, G.; Patel, H. K.; Pritchard, S.;Wodicka, L. M.; Zarrinkar, P. P., A quantitative analysis of kinase inhibitor selectivity. *Nature Biotechnology* **2008,** *26* (1) 127−132.

104. Kleiman L.B.; Maiwald T.; Conzelmann H.; Lauffenburger D.A.; Sorger PK., Rapid phospho-turnover by receptor tyrosine kinases impacts downstream signaling and drug binding. *Molecular Cell 43* (5), 723-737.

105. Zhao, Y.; Khodorkovsky, V.; Cohen, J.; Priel, Z., UV-visible absorption and fluorescence studies of 4,4′-diamino-trans-stilbene and its protonated species. *Journal of Photochemistry and Photobiology A: Chemistry* **1996,** *99* (1), 23-28.

106. Rechthaler, K.; Köhler, G., Photophysical properties of a highly fluorescent push-pull stilbene. *Chemical Physics Letters* **1996,** *250* (1), 152-158.

107. Waldeck, D. H., Photoisomerization dynamics of stilbenes. *Chemical Reviews* **1991,** *91* (3), 415-436.

108. Leuenberger, M. G.; Engeloch-Jarret, C.; Woggon, W.-D., The reaction mechanism of the enzyme-catalyzed central cleavage of β-Carotene to retinal. *Angewandte Chemie International Edition* **2001,** *40* (14), 2613-2617.

109. Ohara, K.; Inokuma, Y.; Fujita, M., The catalytic Z to E isomerization of stilbenes in a photosensitizing porous coordination network. *Angewandte Chemie International Edition* **2010,** *49* (32), 5507-5509.